

UNIVERSITY OF CAPE COAST

DEVELOPMENT OF DOAS REMOTE SENSING SYSTEM FOR
GROUND-BASED MEASUREMENTS OF TRACE GAS EMISSIONS IN
AN INDUSTRIAL AREA

SAMUEL SONKO SACKEY

2011

UNIVERSITY OF CAPE COAST

DEVELOPMENT OF DOAS REMOTE SENSING SYSTEM FOR
GROUND-BASED MEASUREMENTS OF TRACE GAS EMISSIONS IN
AN INDUSTRIAL AREA

BY

SAMUEL SONKO SACKEY

THESIS SUBMITTED TO THE DEPARTMENT OF PHYSICS OF THE
SCHOOL OF PHYSICAL SCIENCES, UNIVERSITY OF CAPE COAST, IN
PARTIAL FULFILLMENT OF THE REQUIREMENT FOR THE AWARD
OF DOCTOR OF PHILOSOPHY DEGREE IN PHYSICS

MARCH 2011

DECLARATION

Candidate's Declaration

I hereby declare that this thesis is the result of my own original work and that no part of it has been presented for another degree in this university of elsewhere.

.....

Date:.....

Samuel Sonko Sackey

(Candidate)

Supervisors' Declaration

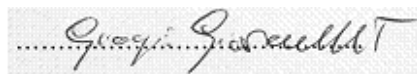
We hereby declare that the preparation and presentation of the thesis were supervised in accordance with the guidelines on supervision of thesis laid down by the University of Cape Coast.

.....

Date:.....

Prof. Paul Kingsley Buah-Bassuah

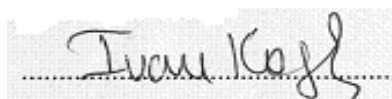
(Principal Supervisor)

.....

Date: 

Prof. Giorgio Giovanelli

(Co-Supervisor)

.....

Date: 

Dr. Ivan Kostadinov

(Co-Supervisor)

ABSTRACT

A DOAS system has been developed and deployed to determine horizontal concentrations of such pollutants as NO₂, SO₂ and O₃ in Bologna, Italy and Tema, Ghana. Measurements were conducted in Italy during the winter season of March 2005 and in Ghana during the dry harmattan season in January 2008 and raining seasons in July and August 2008. Their average line-of-sight concentrations were determined by measuring the scattered solar radiation through three optical windows in the zenith and two horizontal directions. The retrieval method was based on DOAS and a radiative transfer model. The slant column of NO₂ was retrieved within 4360-4600 Å and SO₂ and O₃ within 3120-3270 Å and 3100-3300 Å respectively. In Italy concentration values of NO₂ (in µgm⁻³) were in the range $28.21 \leq \text{NO}_2 \leq 55.51$ while in Ghana they were: $0.16 \leq \text{NO}_2 \leq 35.48$, $0.43 \leq \text{SO}_2 \leq 159.43$, $0.03 \leq \text{O}_3 \leq 764.29$ for measurements in the dry season and $0.02 \leq \text{NO}_2 \leq 25.71$, $0.15 \leq \text{SO}_2 \leq 166.37$, $1.46 \leq \text{O}_3 \leq 688.84$ for measurements in the raining season. NO₂ values were usually high during mornings, reduced towards the afternoon, due to dissociation, and increased again towards sundown. Gradual increases in SO₂ and O₃ concentrations from morning to evening indicated a build-up due to industrial and vehicular activities. Results compared with in-situ measurements carried out by the Environmental Protection Agencies in Italy and Ghana as the first method of validation showed good agreement with a correlation coefficient greater than 0.8. This DOAS technique presents an attractive approach for ground-based measurements of atmospheric trace gases in selected directions.

ACKNOWLEDGEMENTS

In writing this thesis I was indeed fortunate to receive valuable assistance in terms of suggestions and logistics from various individuals and organizations. To begin with I'll like to acknowledge the immense contributions of my supervisors Prof. Paul K. Buah-Bassuah of the Laser and Fibre Optics Center (LAFOC) at the University of Cape Coast, Ghana, and Prof. Giorgio Giovanelli and Dr. Ivan Kostadinov both of the Institute of Atmospheric Science and Climate (ISAC) in Bologna, Italy. Their painstaking supervision and useful critique culminated in this thesis write-up. The other members of the DOAS Group at ISAC: Fabrizio, Andrea, Elisa, Samuelle, Magarita and Daniele of the Geophysics Centre of the University of Evora, Portugal are duly recognized and their various inputs very much appreciated.

I am grateful to the Training and Research in Italian Laboratories (TRIL) Office and the Office of External Activities (OEA) both at the Abdus Salam International Center for Theoretical Physics (ICTP) for their support in terms of funding and sponsorship for training in Italian Laboratories. Without them this work will certainly not have been realized.

I will like to extend my sincere gratitude to my contemporaries at LAFOC: Dr. Jojo Eghan, Mr. Ebenezer Tatchie, Mr. Benjamin Anderson and indeed the entire students and staff at the Department of Physics for their unflinching motivation and support. I am indeed grateful to you all.

DEDICATION

To my Lovely wife Tiny Tina

And

Children: Stephanie, Princess and Buddy

TABLE OF CONTENTS

Content	Page
TITLE PAGE	i
DECLARATION	ii
ABSTRACT	iii
ACKNOWLEDGEMENTS	iv
DEDICATION	v
LIST OF FIGURES	xi
LIST OF TABLES	xvi
LIST OF PLATES	xviii

CHAPTER ONE

INTRODUCTION	
Why observe the earth and its atmosphere	1
How to observe the earth and its atmosphere	2
Basic components of a DOAS system	5
An overview of DOAS methodology	6
Modes of operation of DOAS systems	7
Active Mode of Operation	8
Bi-static Arrangement	10
Mono-static Configuration	11
Multi-path Configuration	11
Passive mode of operation	12
Zenith-sky arrangement	13

Concurrent Multi-Axis DOAS (CMAX-DOAS)	14
Arrangement used for data collection in this presentation	15
Merits and demerits of DOAS	16
Merits	16
Demerits	17
Applications and species measurable with DOAS	17
Volatile Organic Compounds (VOC's)	17
Photo oxidants	18
Free Radicals	20
Meteorological data	21
Objective of Work	22
Relevance of work	23
Scope of Work	23
Organization of the thesis	24

CHAPTER TWO

LITERATURE REVIEW

Overview of the DOAS Technique	26
Light attenuation in the atmosphere	27
Light Extinction due to Rayleigh scattering	28
Light Extinction due to Mie scattering	29
Absorption by other molecules in the atmosphere within the line- of-sight	29
Measuring the differential absorption	30
DOAS Measurement Parameters	33

The Ring Effect	36
Signal-to-noise ratio (SNR)	37
Determination of optical path length l	38
Description of PROMSAR model to simulate l	40
Processing of raw data to obtain slant column values	42
Data Transformation	45
Laboratory calibration procedures	46
Theoretical determination of concentration using a gas cell	46
Measured concentration calculation	46

CHAPTER THREE

EXPERIMENTAL SET UP AND MEASUREMENTS

Experimental Set up	48
Components Description	48
Light Source	48
Receiver	48
Spectrometer Unit (SU) of DOAS system	49
Description of Essential Components	50
Telescope	50
Filters	50
Stepper Motor	52
Jobin-Yvon Diffraction Grating	52
Detection system	53
Operation of Optical module O-SU	54
Electronic module E-SU	55

Assembly of instrument	58
Housing used to protect plane mirror	59
Laboratory tests carried out	61
Variation of the dark current of sensor with integration time	61
Calibration and determination of linear dispersion	62
Laboratory Calibration Using a Gas Cell	64
Polarizing effect of the sun on the sensor	66
Determination of photon path length in the atmosphere	67
Sites selected and gases monitored	69
Measurements carried out in Italy	69
Measurements carried out in Ghana	69
Images of site locations around TOR	71
Gases monitored	75
Meteorological data for Tema	75

CHAPTER FOUR

RESULTS AND DISCUSSIONS

CALIBRATION AND VALIDATION RESULTS	77
Authenticating the accuracy of sensor	77
Calibration and determination of linear dispersion of sensor	80
Laboratory Calibration Using a Gas Cell	85
Polarization Test	86
Determination of photon path length in the atmosphere	93
Results of field measurements carried out	96
Measurements carried out in Italy	96

Measurements carried out at Ghana	98
Meteorological data for Tema	98
NO ₂ Measurements in January 2008	100
All Measurements carried out in January 2008	101
Effect of wind speed and direction	109

CHAPTER FIVE

CONCLUSIONS AND RECOMMENDATIONS

Conclusions	110
Recommendations	115

REFERENCES	116
-------------------	------------

APPENDICES

Appendix 1

Raw intensity values as recorded by the sensor (in pixels) for measurements carried out in the uv spectral region.	127
---	-----

Appendix 2

Raw intensity values as recorded by the sensor (in pixels) for measurements carried out in the visible spectral region.	130
--	-----

Appendix 3

Graphical representation of concentration values measured in July 2008.	133
--	-----

Appendix 4

Graphical representation of concentration values measured in August 2008.	139
--	-----

LIST OF FIGURES

Figure		Page
1.	A typical DOAS configuration for pollution Measurements State of Queensland, 2011)	10
2.	Bi-static configuration of DOAS system (USEPA, 2007)	10
3.	Mono-static configuration of DOAS system (USEPA, 2007).	11
4.	Multi-path DOAS configuration with different transmitters and one mobile receiver (USEPA, 2007)	12
5.	Arrangement for Passive DOAS system	13
6.	CMAX-DOAS configuration with different lines-of-sight a-f.	14
7.	Passive DOAS arrangement restricted to a horizontal LOS	15
8.	The principle of absorption for spectroscopic trace gas detection	26
9.	Various light extinguishing processes within the absorbing medium (Comparative City Statistics, 2004)	28
10.	Differential absorption spectroscopy: practical example for the determination of I_o and D^1 (Platt, 1994)	31
11.	(a): Graph showing the dependence of absorption cross-section of trace gases on wavelength. (b): Graph showing the variation of intensity with wavelength for trace gases (Platt, 1999)	33
12.	A complete arrangement of the spectrometer unit of the DOAS system	49

13	The light path in a Cassegrain reflecting telescope	50
14.	Transmission characteristics for: (a) filter 1 (b) filter 3 (Schott glass filters, 1999)	52
15.	The photo-sensitivity of the sensor installed Hamamatsu Photonics, 2003)	54
16.	The complete arrangement of GASCOD-GH used for the detection of trace gases.	58
17.	Theoretical reflection of Al-MgF (Replicated mirrors, 2007)	59
18.	A 3-D representation of the housing used to protect the plane mirror	60
19.	Standard Hg lines: (a) in the uv (b) visible spectral regions.	64
20.	An organogram depicting some of the manufacturing facilities in Tema and their approximate distances from the site where the DOAS system was installed.	74
21.	A graph showing the variation of the average dark current with integration time for the various blocks on the face of the sensor.	79
22.	Graphs showing standard fine lines exhibited by Hg lamp (a) in the uv and (b) visible spectral regions (Sources of discontinuous spectra) and those observed in pixels during measurements in the (x) uv and (y) visible spectral regions using the sensor.	80

23. Graphs establishing the relationship between the wavelength and pixel-position pairs for measurements made in the (a) UV and (b) visible spectral regions. 82
24. Graphs showing the raw spectra as recorded by the sensor in pixels for measurements in the (a) uv and (b) visible spectral regions respectively. 84
25. Scatter plot and line of best fit for NO₂ as determined in the gas cell (reference concentration) and retrieved using DOAS technique (measured concentration). 85
26. Graphs showing dependence of the normalized intensities of light reaching the sensor at the various polarizing angles on wavelength for measurements in (a) the uv and (b) visible spectral regions respectively. 87
27. Graphs showing the same dependence of normalized intensities on wavelength for uv and visible spectral regions for the polarizing angles of +10⁰ and -80⁰ only measurements in (a) the uv and (b) visible spectral regions respectively. 88
28. Graphs showing transmittance at the various polarizing angles and wavelengths for the (a) uv and (b) visible spectral regions. 89
29. Graphs showing the polarizing angles against normalized intensities averaged over 100 pixels for measurements in the (a) uv and (b) visible spectral regions respectively. 91

30. Graphs showing the polarizing angles against transmittance Averaged over 100 pixels for measurements in the (a) uv and (b) visible spectral regions respectively. 92
31. Graphs showing the dependence of the photon path on SZA for simulations in the uv and visible spectral regions. 94
32. Scatter plots for NO₂ concentration between in-situ ARPA values and passive DOAS measurements in Bologna, Italy. Graphs (a-c) represent the scatter plots for March 9, 10 and 11, 2005 and (d) is the total scatter plot for all three days of measurements. 97
- 33 (a-d). Graphs showing daily variations in wind speed, wind direction, relative humidity and temperature respectively from January 10 to 23, 2008 99
34. Scatter plot for SO₂ concentration between in-situ EPA values measured at Sethi Steel Ltd. and passive DOAS measurements for measurements in January 2008 over an area in Tema. 100
35. Graph showing concentrations of NO₂ monitored in the north, south, east and west from January 10 to 23, 2008. 102
36. Graph showing concentrations of SO₂ monitored in the north, south, east and west from January 10 to 23, 2008. 103

37.	Graph showing concentrations of O ₃ monitored in the north, south, east and west from January 10 to 23, 2008.	104
38a.	Graph showing concentrations of NO ₂ monitored in the north, south, east and west from July 8 to 18, 2008.	133
38b.	Graph showing concentrations of NO ₂ monitored in the north, south, east and west from July 20 to 30, 2008.	134
39a.	Graph showing concentrations of SO ₂ monitored in the north, south, east and west from July 8 to 18, 2008.	135
39b.	Graph showing concentrations of SO ₂ monitored in the north, south, east and west from July 20 to 30, 2008.	136
40a.	Graph showing concentrations of O ₃ monitored in the north, south, east and west from July 8 to 18, 2008.	137
40b.	Graph showing concentrations of O ₃ monitored in the north, south, east and west from July 20 to 30, 2008.	138
41.	Graph showing concentrations of O ₃ monitored in the north, south, east and west from July 20 to 30, 2008.	139
42.	Graph showing concentrations of SO ₂ monitored in the north, south, east and west from August 1 to 14, 2008.	140
43.	Graph showing concentrations of O ₃ monitored in the north, south, east and west from August 1 to 14, 2008.	141

LIST OF TABLES

Table		Page
1.	A list of gases that can be detected using DOAS methodology and the wavelength interval within which they can be identified.	21
2.	Characteristics of filters used for the spectral isolation of light entering the spectrometer.	51
3.	Inputs made using the PROMSAR model to simulate the photon path lengths at various solar zenith angles	68
4.	The gases monitored and the precise wavelength interval within which they were examined.	75
5.	Mode of partitioning the 1024-pixel sensor into blocks.	77
6.	Average values of the dark current obtained at different integration times for each of the five (5) blocks on the face of the sensor.	78
7.	Wavelength positions of fixed lines exhibited by Hg lamp and their corresponding pixel spots as observed using the sensor for spectra taken in the uv and visible regions.	81
8.	The constants A and B obtained from a plot of pixel against wavelength for measurements in the uv and visible spectral regions.	83
9.	Simulated photon paths in the UV and visible regions for the lower troposphere using various values of solar zenith angle.	93

10.	The constants obtained from a plot of simulated photon path against solar zenith angle for measurements in the uv and visible spectral regions.	95
11.	Standard recommended levels of NO ₂ .	106
12.	Standard recommended levels of SO ₂ .	107
13.	Standard recommended levels of O ₃ .	108

LIST OF PLATES

Plate		Page
1a.	Picture showing the entrance window of the spectrometer unit on one side of the optical bench.	63
1b.	Picture showing the lit Hg pencil lamp on the other side of the optical bench	63
2a.	Picture showing the gas cell mounted on the movable rail on the optical bench.	66
2b.	Picture showing the gas cell covered with a black cloth to prevent the dissociation of NO ₂ .	66
3.	Picture showing the polarizer centrally installed on the angle selector and the turnable knob used to select the angles.	67
4.	A satellite photo of some townships distant from TOR (Google Earth Search, 2009)	71
5.	An aerial view of TOR showing the Administrative block and other important sites. (Google earth Search, 2009)	72
6.	Top picture - The DOAS system as it was mounted within the housing Middle picture - Constructed housing for the DOAS system Bottom picture - Administrative Block on top of which the housing was constructed	73

CHAPTER ONE

INTRODUCTION

Why observe the earth and its atmosphere

The atmosphere that surrounds and provides us with each breath we take contains a wide variety of substances like gases as well as small solid and liquid particles. These substances, to mention just a few, may include water vapor, carbon dioxide, methane, ozone, benzene and some particulate matter (PM). Some of these substances come from natural sources like the soil (through anaerobic bacteria in marshes), sea (through phytoplanktons), lightning and volcanic eruptions while others are caused by anthropogenic emissions by way of our human activities such as the use of motor vehicles, domestic businesses and industrial activities (Wang et al., 2005). An atmosphere is considered to be polluted when the environment contains these substances - water vapor, carbon dioxide, methane, ozone, benzene, particulate matter and the likes - in quantities higher than that accepted by the National Environmental Protection Agency. At such undesirable levels, they are normally present in amounts high enough to affect the comfort and health of humans and animals and also damage plants and materials. These harmful substances are labelled pollutants and may be particles, liquids or gaseous in nature.

The earth and its atmosphere need to be observed so as to fully understand the physical and chemical processes occurring on the land surface, in the polar regions, in the oceans and in the atmosphere as a whole that lead to the production of such detrimental substances.

There is also the need to monitor temporal and spatial changes due to natural and anthropogenic causes, e.g., Antarctic ozone hole, El Nino, green house effect and others. Such a careful study of the environment will in the long run enable predictions of future conditions, as in weather forecasting, and therefore assist in disaster preparedness, management and control. The ability to make such well-informed forecasts and predictions can be realized by measuring and knowing the chemical composition and amounts of substances present in the atmosphere. Making such needed measurements is complicated due to the diversity and very small mixing ratios at which many of the substances are found. Quantification methods used must therefore be very specific and sensitive to the compounds of interest.

How to observe the earth and its atmosphere

There are several techniques used in identifying the type of substances present in the atmosphere and evaluating their concentration. Some of the techniques include extractive methods that involve the collection of the samples under investigation for later laboratory analysis. This procedure is sensitive and selective to the species under consideration but gives a poor real-time monitoring. Furthermore, it has the possibility of contamination (during collection) that may lead to the loss of some of the species of interest.

Typical routines that utilize this method include the radiocarbon technique (Toyoizumi, 2001; Woo et al, 1999) and Selective Ion Chemical Ionization Mass Spectrometry (SICIMS) (Armerding et al., 1994).

There is also the in-situ technique in which direct measurements are carried-out at the location with an instrument. Such measurements result in a lower sensitivity and selectivity and give a limited spatial coverage although it ensures a good real-time monitoring. There is still the possibility of contamination of the species under investigation which may lead to the loss of some of them. A distinctive example is the Oxidation-Reduction Potentials (ORP) technique used for continuous soil pore water quality monitoring (Jang et al., 2005).

Another technique which is a remote sensing technique, generally involves the art and science of obtaining information about a phenomenon without being in contact with it. It deals with the detection and measurement of an event with devices sensitive to light (cameras), heat (thermal scanners) and radio waves (radar). The advantage with the remote sensing procedure is that it is non-invasive (consequently averts the perturbation of the samples being observed) and can be performed from many platforms (ground, balloons, aircraft, rockets, space shuttle and satellites). It is also sensitive to many samples and can provide point, column and profile data. A procedure that operates on principles based on remote sensing systems and used for identifying and quantifying the species of pollutants in the atmosphere is Differential Optical Absorption Spectroscopy (DOAS) (Noxton, 1975; Palazzi et al, 2005; Perner & Platt, 1979; Platt et al, 1979; Platt & Perner, 1980, 1983; Solomon et al, 1987).

Other procedures include Light Detection And Ranging (LIDAR) (Karger, 2000; Ravindra, 1981; USA EPA Report, 2005) and Differential Absorption Lidar (DIAL) (Nakazato et al, 2007; Weibring et al, 2003; Wolfram et al, 2008a, 2008b).

Monitoring of air pollution in Ghana is generally carried out by the Environmental Protection Agency (EPA). Their cardinal objective is the provision of an adequate assessment of the ambient atmosphere to prepare Air Quality Guidelines. Presently the EPA employs the active and high volume sampler's technique, which is an in-situ procedure, for the monitoring of air pollutants, particularly SO₂, smoke and PM₁₀ from sources such as factories, power plants, construction sites, fuel combustion on highways, open burning landfills, quarrying and surface mining operations (Jumpah, 1999).

Apart from the EPA some institutions have the technical capacity to evaluate the levels of emissions due to their activities. Tema Oil Refinery (TOR), whose activities involves the processing of crude oil, monitors its emissions using the Gravimetric Analysis of loaded filters and the Direct Reading-Gas monitor that deploys the use of diffusion barrier technology (Amoateng, 2000). The former is an extractive technique while the latter is an in-situ method. Takoradi Thermal Power Plant monitors its emissions from the combustion turbines using a Continuous Emission Monitoring System (CEMS). This is also an in-situ technique where a sample of the exhaust gas is passed through a gas analyzer and the concentration of each gas pollutant in the exhaust system displayed on an analyzer screen (Doku, 1999).

Deductively techniques employed currently in Ghana for ambient air quality monitoring are either extractive or in-situ techniques. Such techniques, as explained, are beset with their attendant handicaps and can therefore in no way be compared with remote sensing procedures. The absence of a remote sensing system in Ghana is the motivation behind this study. This thesis discusses the application of a DOAS methodology operated in a passive arrangement for the provision of a selective and sensitive on-line measurement of atmospheric constituents as a result of combustion, vehicular emissions and industrial activities.

Basic components of a DOAS system

Generally a DOAS system is made up of the following crucial parts: a telescope that will receive and focus the incoming radiation, a spectrometer and its accessories that will be used to separate and re-image radiation at different wavelengths in order to record spectral signatures, a sensor to convert spatial radiation intensity into a signal that can be transferred to a computer for further evaluation, a software for evaluation and a database for absorption cross-section of species (atoms or molecules) to be measured. In the particular arrangement in which an artificial light source is used, some optics like a transmitting telescope and a retro-reflector will be needed to arrange the light path.

An overview of DOAS methodology

DOAS methodology is a remote sensing arrangement widely used for the determination of concentrations of atmospheric species. Perner and Platt first used the technique in the late 70's and 80's (Perner & Platt, 1979; Platt et al, 1979; Platt & Perner, 1980, 1983).

It has been used for ground-based applications as well as balloon, aircraft and satellite measurements using natural or artificial light sources (Platt, 1994). In general the DOAS technique is about analyzing the broadband spectra in the UV and visible regions that have been transmitted through a long open path. Different atmospheric species will leave their absorption fingerprints in the spectra from which their concentrations could be retrieved (Platt, 2002).

This spectroscopic monitoring technique uses a modification of the well-established Beer-Lambert law for determining the average concentration of atmospheric trace gases along a light path (Plane & Smith, 1995; Platt, 1994, 2002). As light from a natural or artificial source passes through an air mass, several light extinction and attenuation processes, like absorption, scattering and reflection, take place. A raw, open-air spectrum will thus contain the imprint not only of molecular absorption but also of scattering and reflection processes. In principle the presence of such scattering and reflection processes in addition to the absorption fingerprints would prevent the application of the Beer-Lambert law for determining air pollutant concentrations. Nevertheless, a mathematical retrieval procedure allows extracting the narrow spectral features ascribed to molecular absorption contained in the spectrum.

The retrieval procedure is based on the fact that the decrease in light intensity due to molecular and aerosol scattering (Rayleigh and Mie scattering respectively) in the optical path is much less wavelength dependent in many cases than the molecular absorption features of the pollutant gases. This extracted molecular absorption spectrum can then be fitted to a reference (e.g. laboratory) spectrum which allows the calculation of the concentration of the light-absorbing species present in the observed air mass (Jiménez et al, 1999).

In UV-visible DOAS measurements, the path length has to be long enough to give a measurable absorption but also short enough to prevent saturation effects as a result of high optical depth. The best path length, therefore, is one chosen such that the signal to noise ratio is maximum and with the species having a reasonably narrow electronic transition within the UV-visible spectral regions ($250 \text{ nm} \leq \lambda \leq 700 \text{ nm}$). Path lengths of several kilometers are often needed to detect minor species. If the spectral region is extended further into the VUV ($100 \text{ nm} \leq \lambda \leq 200 \text{ nm}$) more species could be retrieved but path lengths must be reduced due to strong atmospheric attenuation (Rayleigh scattering) at these wavelengths.

Modes of operation of DOAS systems

Two clearly distinct set-ups can be identified. This depends on the use of an artificial (arc lamps or lasers) or natural light source (sun, moon or star light) for excitation (Platt, 1999; Platt & Stutz, 2008). These are categorized as the Active (artificial) and Passive (natural) modes of operation.

Active Mode of Operation

The characteristic feature about this mode of operation is the use of an artificial light source that emits in the UV-visible spectral region and gives a smooth broadband spectrum. A typical arrangement is shown in Figure 1 and consists of three major parts. These are the transmitter, receiver and analyzer (State of Queensland, 2011). The transmitter, also known as the Light Unit (LU) consists of an Optical module (O-LU) equipped with a shutter device and an Electronic module (E-LU).

The optical module (O-LU) can either be a high pressure arc lamp, for example a Xe lamp with a wide spectral range between 200-3000 nm or a broad band laser. A laser source gives a lower beam divergence and a higher spectral intensity but has the shortfall of a narrow spectral emission bandwidths or tuning range which makes it difficult to observe some molecular vibrational bands and therefore restricts the number of species that can be detected. The electronic module of the light unit (E-LU) regulates all operations of the optical unit O-LU.

The beam of light from the transmitter O-LU is sent to the receiver, also known as the Spectrometer Unit (SU), which is made up of an Optical module (O-SU) and an Electronic module (E-SU). The optical module O-SU is a central and critical component of all DOAS systems as it serves to separate the individual wavelength intervals, so that the intensity in these intervals can be measured. There are two fundamentally different approaches in use: spectrometers and interferometers. Spectrometers separate radiation of different wavelengths into different spatial directions, where the spectrum can be measured by a spatially resolving detector.

Spectrometers are based on two basic physical principles: Refraction by prisms, which rely on the dispersion in transparent optical materials such as quartz, glass, or plastic and diffraction by gratings, which make use of spatial interference effects. Interferometers make use of interferometric principles to effectively produce and record the Fourier transform (FT) of the spectral intensity distribution of the received radiation (Platt & Stutz, 2008). The Electronic module of the spectrometer unit (E-SU) remotely controls the light source shutter for background measurement. Data from the SU are transferred by means of a serial line to the Analyzer (a computer) that measures the intensity of the different wavelengths along the entire light path.

After applying a specific retrieval procedure and using the appropriate software the analyzer evaluates and converts the detected spectra into concentrations for each of the gaseous pollutants being monitored. Available on the computer is a database for absorption cross-section of species (atoms and molecules) to be measured.

With this active set-up various configurations are possible. The system can be operated in a mobile configuration with the equipment installed inside a van and allowing the use of the same instrument for measurements on different sites. It can also be functional in a static configuration for air quality measurements on fixed sites for which a number of light-path arrangements are possible. These include the Bi-static, Mono-static and Multipath arrangement.

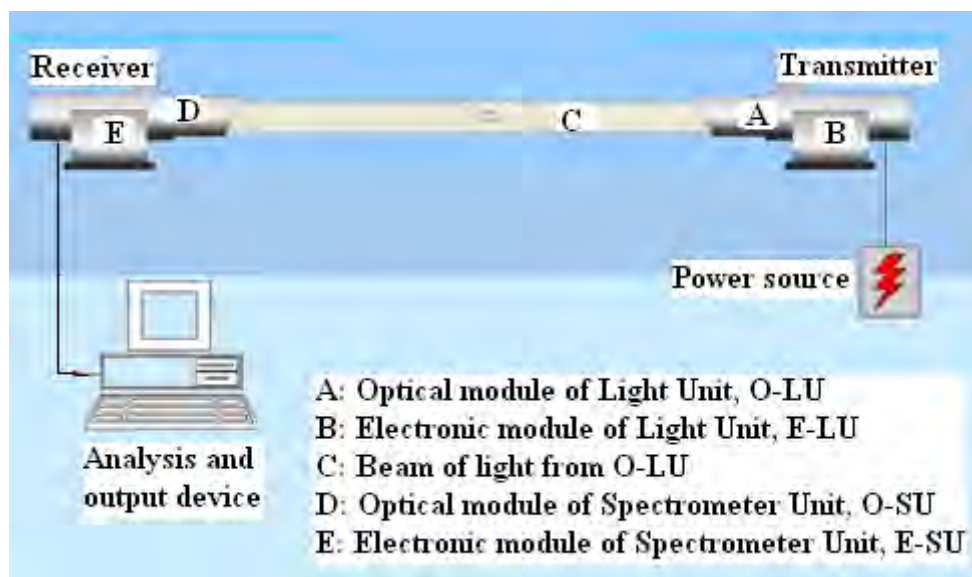


**Figure 1: A typical DOAS configuration for pollution measurements
(State of Queensland, 2011)**

Bi-static Arrangement

For this arrangement the Light and Spectrometer Units are located on either side of the measurement path as shown in Figure 2. This arrangement is also known as the non-folded optical path configuration (USEPA, 2007).

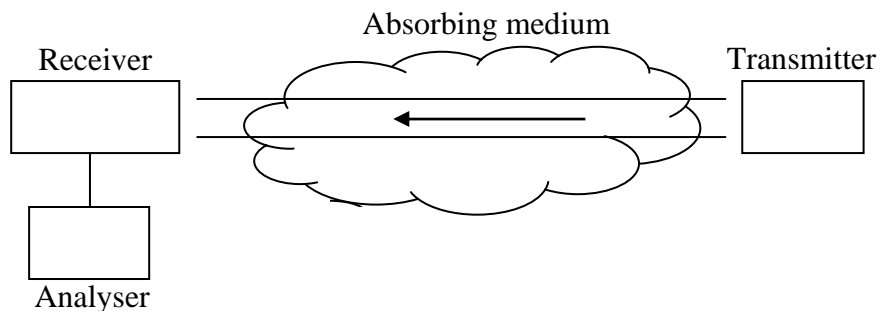


Figure 2: Bi-static configuration of DOAS system (USEPA, 2007)

Mono-static Configuration

Alternatively the system can be operated in a mono-static configuration where the Light and Spectrometer units are on the same side and the light returned to the Spectrometer unit by a retro-reflector mounted opposite the Light unit (USEPA, 2007). This is as shown in Figure 3 and is referred to as the folded optical path configuration. In contrast to bi-static systems, mono-static DOAS systems are easier to install and align and require power only at one end of the optical path.

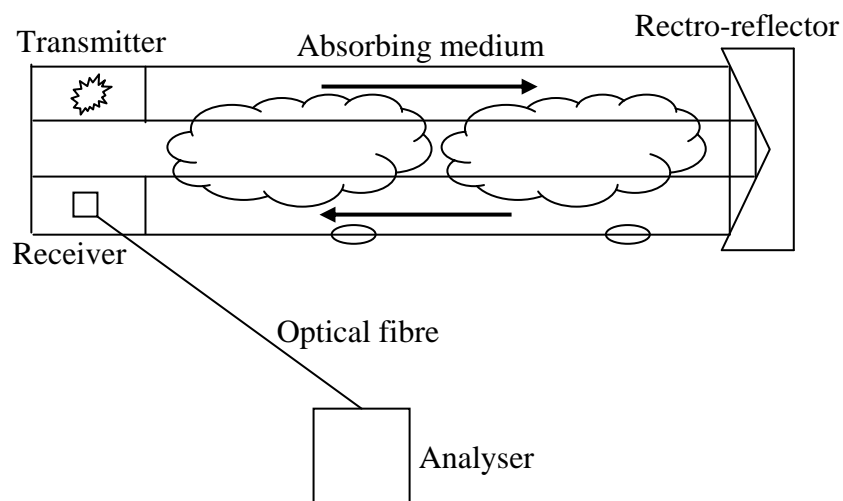
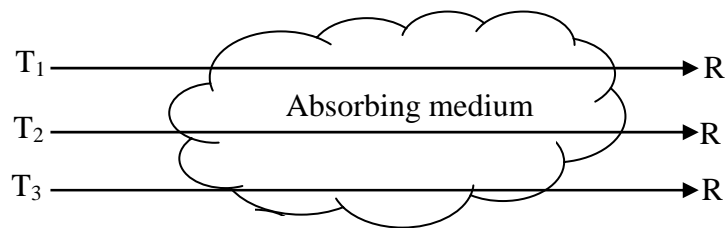


Figure 3: Mono-static configuration of DOAS system (USEPA, 2007)

Multi-path Configuration

Optionally, the equipment can be mounted and operated in a Multi-path configuration where one single receiver performs measurements on different optical paths. This is done using one transmitter for each path while the receiver, which is mobile, scans the different lines-of-sight such as T_1R , T_2R and T_3R shown in Figure 4.



T₁, T₂, T₃: Different transmitters

R: The same receiver at different lines-of-sight

Figure 4: Multi-path DOAS configuration with different transmitters and one mobile receiver. (USEPA, 2007)

Passive mode of operation

In this mode of operation natural light source from the sun, moon or stars is used. Passive techniques are used for tropospheric measurements but more commonly for big scale observations with satellites or ground-based measurements of the stratosphere where power demanding light sources are not required. One big disadvantage by using such extra terrestrial light sources is the presence of Fraunhofer lines that could affect the results through inelastic Raman scattering (Ring effect) (Krecl et al., 2006). Furthermore, measurements within the UV are difficult as radiations within this region are highly extinguished due to strong atmospheric attenuation and extinction caused by molecular and aerosol scattering. To this extent the spectrometer unit and its connecting optics would have to be made of materials very transparent to UV radiation. Two very distinct light-path arrangements can be set-up with passive DOAS operations. These are the Zenith-sky arrangement and the Concurrent Multi-Axis DOAS (CMAX-DOAS).

Zenith-sky arrangement

As characteristic of all passive arrangements, natural light from sun, moon or stars is used in zenith-sky measurements and are generally devoted to retrieving the vertical profile of gases by exploiting the effect of the progression of the sun across the sky. The Solar Zenith Angle is defined as the angle between the zenith and the sun, and varies from sunrise to sunset. The path that solar radiation takes as it passes through the atmosphere changes as the solar zenith angle changes, with the minimum path length being at solar noon. As the radiation passes through the atmosphere certain wavelengths are absorbed by different trace gases. The amount of absorption is defined by the path length and therefore calculating the change in absorption at different times of day and knowing the different path lengths that the radiation has taken through the atmosphere makes it possible to evaluate the tropospheric and stratospheric concentrations of gases. For this arrangement the receiver is installed pointing directly upwards towards the zenith as depicted in Figure 5.

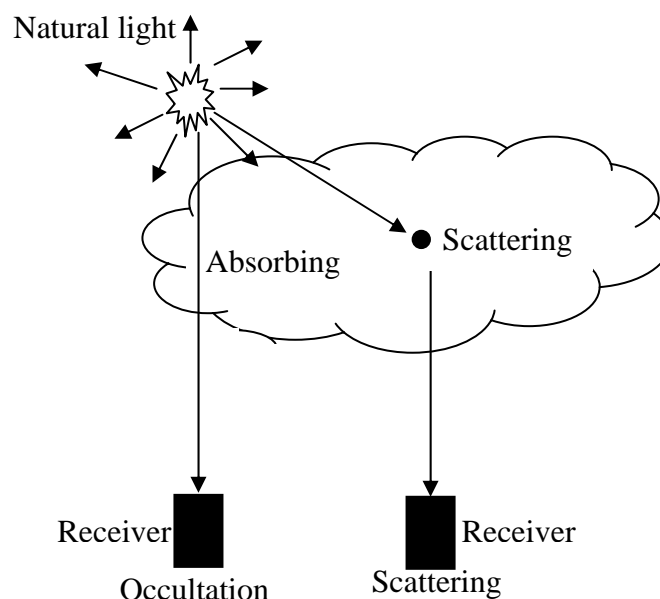


Figure 5: Arrangement for passive DOAS arrangement

Concurrent Multi-Axis DOAS (CMAx-DOAS)

This arrangement simultaneously records spectra of scattered solar radiation collected by a number of telescopes (receivers) pointing at different angles to the zenith. The additional viewing angles made available at lines-of-sight a-e, and shown in Figure 6, provide information on the vertical distribution of the gases being measured. To a rough approximation, the greater the solar zenith angle (the closer the telescope view is to the horizon) the greater the sensitivity to gases lower in the atmosphere. With the series of concurrent measurements from different viewing angles, it is therefore possible not only to calculate how much of a given gas is in the atmosphere, but also to determine its vertical distribution (Arpag et al, 1994; Fietkau et al, 2002; Sanders et al, 1993; Weaver et al, 1996).

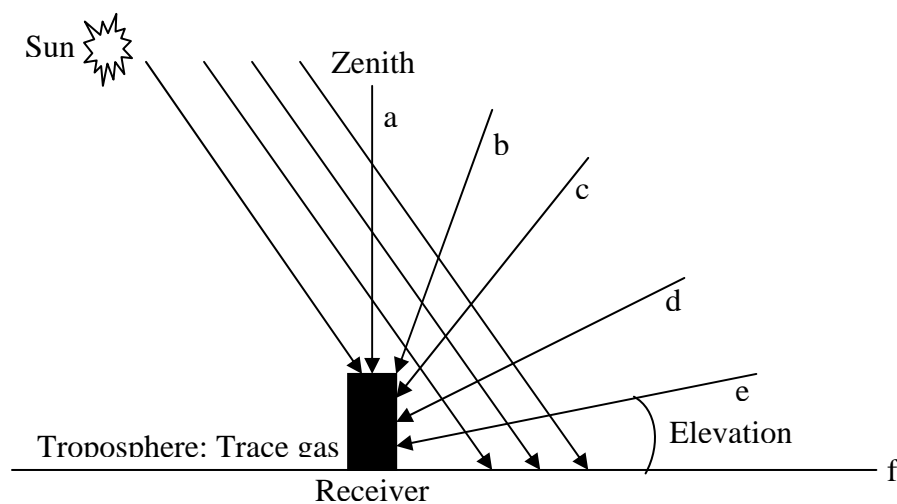


Figure 6: CMAX-DOAS configuration with different lines-of-sight a-f.

Arrangement used for data collection in this presentation

With the receiver pointing 90° off-axes in the horizontal direction (line-of-sight f) the total amount of trace gases within the horizontal line-of-sight can be determined. This arrangement is shown on Figure 7 and has been demonstrated using an airborne UV-visible spectrometer in the stratosphere (Petritoli et al, 2002). One feature, however, about this arrangement is that the presence of the gas in the stratosphere influences the measured concentration in the troposphere, i.e., within the horizontal line-of-sight (LOS). This stratospheric influence is nonetheless accounted for during measurements.

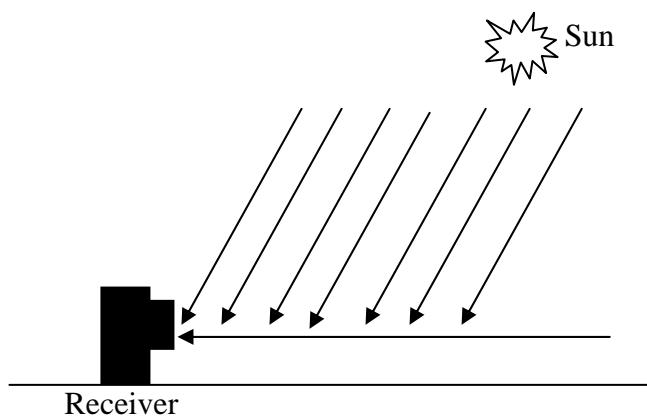


Figure 7: Passive DOAS arrangement restricted to a horizontal LOS

This passive arrangement with the receiver strictly maintained in a chosen horizontal direction (90° off-axes) and the sun as the light source was used for data collection in this presentation. Variations in the photon path length during the time of measurements were simulated using the changes in the solar zenith angle during that period.

Attempts to measure photo-chemically active gases, such as NO_2 , at larger solar zenith angles and gases with low optical depth, such as BrO and OCIO, have led to the use of this configuration to obtain a longer path and increased radiance at twilight (Petritoli et al, 2002).

Merits and demerits of DOAS

Merits:

DOAS remote sensing systems overcome some difficulties faced by conventional point monitors in several aspects. In the first place, DOAS systems offer a simultaneous real-time analysis of any light absorbing compound in the wavelength region between the near UV and the near IR. This reduces cost as one instrument can be used to measure concentrations of several species. It also gives a path-average measurement which is more representative of the concentration of pollutants in a given area than single point measurements which are easily biased by local distortions. Unlike point monitors and sampling systems, DOAS offers a “non-invasive” technique and assures the absence of wall losses by adsorption or chemical reaction which makes it well-suited for the measurement of highly reactive species such as OH (HONO) (Brandenburger et al, 1998) and nitrate radicals (NO_3) (Platt & Janssen, 1996; Platt et al, 1981). It is an absolute measurement technique where no routine gas calibration is needed. The system is automated and requires little attention. Measurements are particularly suited for fence-line monitoring of the concentration of gases and recently estimations of pollutant fluxes and budgets have been achieved by coupling DOAS with anemometric measurements (Graber et al, 1997).

Demerits

DOAS routine is sensitive to atmospheric turbulence and natural conditions like rain, snow, fog and clouds make measurements impossible. This is because such conditions induce intensity variations in the spectra which greatly affect the retrieval of concentrations of pollutants at that time.

Applications and species measurable with DOAS

Generally the DOAS approach can be used to monitor the quality of air in rural and urban areas, at airports and inaccessible regions. It can be applied for traffic and highway emission study, investigating and quantifying emissions from landfills and waste disposal sites and for perimeter and fugitive emissions monitoring. It is generally used for determining actual and typical human exposures to pollution sources. Mainly three categories of compounds can be measured using DOAS (Galle, 1999). These are Volatile Organic Compounds (VOC's like benzene, CH₂O), Photo-Oxidants (NO_x, SO_x, O₃, HNO₂, H₂O₂, CO, PAN-Peroxyacetylnitrate) and Free Radicals (BrO, OClO, IO, OH).

Volatile Organic Compounds (VOC's)

These are organic chemicals with a high vapor pressure and consequently easily form vapors at normal temperature and pressure. They are emitted as by-products of combustion and also through the evaporation of fuels and solvents. VOC's are an important health and environmental concern for several reasons. For example, benzene is toxic and a probable human carcinogen. Formaldehyde is both an irritant and a sensitizer.

VOC's from out-gassing of fabrics, building materials etc. are an important contributor to Sick Building Syndrome (SBS). Methyl tert-butyl ether (MTBE) has a high mobility in groundwater and can easily lead to the contamination of drinking water wells (USEPA, 2007; ILPI, 2009).

Photo oxidants

The primary sources of photo-oxidants is the residue of combustion processes and are capable of causing and undergoing oxidation when exposed to light of the appropriate wavelength. Some by-products that are formed due to photo-oxidation activities include the formation of O₃ in the troposphere and its destruction in the stratosphere, formation of carbon monoxide, acid rain and their undesirable adverse health implication on humans.

O₃ is a naturally occurring gas found in the troposphere and stratosphere. The major sources of natural ground-level ozone do not contribute enough to be considered a threat to the health of humans or the environment but it is the ozone that is a byproduct of human activities which is called 'bad' ozone. Tropospheric ozone is formed by the interaction of sunlight, particularly ultraviolet light, with hydrocarbons and nitrogen oxides that are emitted by automobiles, gasoline vapors, fossil fuel power plants and refineries. It damages the respiratory tissues through inhalation and has been linked to tissue decay and cell damage by oxidation. It is a particular threat to people who already have respiratory problems. Stratospheric ozone or "good ozone" is a layer of life-protecting ozone found at the top of the stratosphere that protects life on earth from the harmful effects of the sun's UV rays.

As its percentage in the atmosphere decreases, the amount of UV-B radiation reaching the surface increases. This invisible UV-B radiation has been linked to skin cancers and other biological damages. The greatest cause of the depletion of the ozone is a class of chemical compounds known as chlorofluorocarbons (CFCs). The dual ozone problems - pollution or smog in the troposphere and depletion of the ozone layer in the stratosphere - are indeed very different but have common ties in that they both are related to air pollutants that come from industry, automobiles and other gasoline powered engines.

Carbon Monoxide, CO is an inorganic compound and is usually referred to as the silent killer because it is colourless, odourless, tasteless and virtually impossible for the human senses to detect. It is generally formed as a result of incomplete oxidation with its sources including leaking chimneys and furnaces, wood and gas stoves, generators and other gasoline powered equipments. It may cause fatigue in healthy people and chest pain in people with heart disease. It may cause impaired vision, headaches, dizziness and nausea. It can cause flu-like symptoms, but ease-off when one leaves its vicinity (Borrell et al., 1997). Ozone and other photo-oxidants are secondary pollutants and are formed from the photochemical oxidation of VOC's in the presence of nitrogen and sulphur oxides (Neftel, 1999). The photo-oxidation of SO_x and NO_x is the primary origin of acid rain which causes the acidification of lakes and streams and contributes to the damage of trees and many sensitive forest soils. Additionally acid rain accelerates the decay of irreplaceable buildings, statues, and sculptures that are part of a nation's cultural heritage

Free Radicals

These are highly reactive chemical species with low chemical specificity and an unpaired electron in the valence shell of the molecule. In the upper atmosphere free radicals are produced through the dissociation of the source molecules, particularly the normally un-reactive chlorofluorocarbons, by solar ultraviolet radiation or by reactions with other stratospheric constituents. These free radicals then react with ozone in a catalytic chain reaction which destroys the ozone, but regenerates the free radical, allowing it to participate in additional reactions. They are capable of independent existence (Wisegeeck, 2008) and play an important role in biological processes such as the intracellular killing of bacteria. However, because of their high reactivity they also participate in unwanted side reactions resulting in the disruption of living cells. Many forms of cancer are the result of reactions between free radicals and DNA and with some of the symptoms of aging been attributed to the free-radical induced oxidation of many of the chemicals making up the body. Some species measurable with DOAS methodology and the wavelength interval within which they can be detected are shown on Table 1.

Table 1: A list of gases that can be detected using DOAS methodology and the wavelength interval within which they can be identified.

Species	Wavelength Range (nm)	Detection (ppt)	Path length (km)
NO	200 - 230	240	0.2
NH ₃	200 - 230	800	0.2
Benzene	250 - 290	200	2.0
p-Xylene	250 - 290	100	2.0
Benzaldehyde	250 - 290	40	2.0
Ethyl benzene	250 - 290	560	2.0
SO ₂	290 - 310	17	0.2
O ₃	300 - 330	4000	5.0
CH ₂ O	300 - 360	400	0.2
NO ₂	330 - 500	80	5.0
HNO ₂	330 - 380	40	5.0
NO ₃	600 - 670	2	5.0

Meteorological data

Any analysis of air pollution in an area should include a study of the meteorological phenomena of that area as the fate of air pollutants is greatly influenced by the movements and characteristics of the air mass into which they are emitted. The measurement of wind speed and direction, humidity, temperature and rainfall are therefore important parameters used in the study of air quality monitoring data and are necessary to enable the understanding of the chemical reactions that occur in the atmosphere.

If the air is calm and pollutants cannot disperse, then the concentration of these pollutants will build up. Conversely, if a strong and turbulent wind is blowing, any pollution generated will be rapidly dispersed in the atmosphere and will result in lower concentrations near the pollution source. The presence of water molecules in the air can attach themselves to corrosive gases such as nitrogen dioxide and sulfur dioxide which will dissolve in water and form an acid solution in the atmosphere. Temperature and sunlight play an important role in the chemical reactions that occur in the atmosphere to form photochemical smog from other pollutants to the extent that favorable conditions can lead to increased concentrations of smog. Rain has a "scavenging" effect as it washes particulate matter out of the atmosphere and dissolves gaseous pollutants such as sulfur dioxide, forming acid rain. Meteorological monitoring is by and large used to predict air pollution events such as inversions, high pollutant concentration days and areas and to simulate and predict air quality using computer models (State of Queensland, 2011).

Objective of work

The objectives of this work were as follows: The development of a DOAS system, authenticating the accuracy of the sensor installed and a study of the needed laboratory calibrations and validate its measurement capability and precision using a gas cell. After all these have been done it is part of the goal to deploy the system constructed for field measurements to detect and measure the concentrations of atmospheric trace gases in all four cardinal directions.

Relevance of work

In 1999 and 2000 two International Workshops (ICS-UNIDO International Workshop “Combustion Diagnostics and Optical Techniques”, and ICS-UNIDO International Workshop on “Monitoring of Air Pollutants due to Combustion Processes” respectively) were held at the University of Cape Coast, Ghana. It was asserted at these workshops that most of the combustion processes from industrial activities in Ghana, and indeed within the entire West-African sub region were not backed by a regular monitoring of the emitted gases into the atmosphere and therefore the absence of any environmental impact assessment program. This work will therefore package data and information on the constituents and levels of emissions from the various industrial activities based on credible measurements taken. This will enable the Environmental Protection Agency to construct pollution maps that will form the basis for a proper environmental safety management and control for the effective evaluation of the industrial community’s growing need for an accurate environmental information.

It will ultimately provide policy makers with a credible scientific data base to be used to set environmental air quality standards to regulate practices and activities that generate pollutants into the atmosphere.

Scope of work

The DOAS system was operated in a passive mode and trace gas column densities derived from the analysis of scattered and direct sunlight. For this reason data was collected only during day-light hours.

The reliability of the system was verified under different meteorological dynamics by embarking on two field campaigns with completely diverse atmospheric conditions. Firstly in Italy at the Institute of Atmospheric Science and Climate (ISAC), Bologna (44.3°N, 11.2 °E) where measurements were taken during the winter season of March 2005, and in Ghana at Tema Oil Refinery (TOR) (5°39'59.88" N, 0°00'21.26"E) Tema, where data was collected in January 2008 during the harmattan season and then in July and August 2008 during the raining season. Such diverse seasons were also deliberately chosen for measurements so as to have data from varied scenarios and subsequently draw well-informed conclusions. In both Italy and Ghana the DOAS system was installed on roof-tops at a height of about 50 m above the ground and used to quantify the amounts of selected pollutants (NO₂ in Italy, and O₃, SO₂ and NO₂ in Ghana) present in the atmosphere. The system was mounted such as to enable horizontal measurements in all four cardinal directions. This thesis will present the findings made from the two field campaigns and in all four cardinal directions.

Organization of the thesis

Chapter One involves a general prologue to the field of environmental monitoring and discusses various techniques used to observe the atmosphere. It further describes a range of modes of operation and types of arrangements of the DOAS system. It concludes with the set-up used for data acquisition in this dissertation. Chapter Two elucidates the theory behind the DOAS methodology. The configuration of the system and the entire set-up used for the data collection in this thesis is described in Chapter Three.

In Chapter Four a presentation is made of the various laboratory calibrations carried out, field measurements conducted and relevant discussions. The conclusions and necessary recommendations are captured in Chapter Five.

CHAPTER TWO

LITERATURE REVIEW

Overview of the DOAS Technique

This spectroscopic monitoring technique consists of a light source, an absorbing medium and a receiver, as illustrated in Figure 8, and makes use of the absorption of electromagnetic radiation by matter (Platt, 1994, 1999).

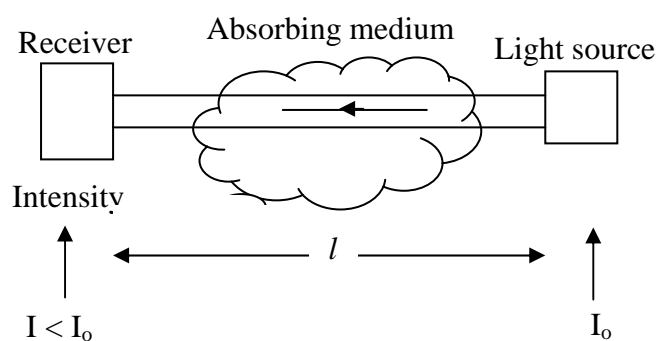


Figure 8: The principle of absorption for spectroscopic trace gas detection

Quantitatively, the fundamental principle underlying the absorption of radiation is expressed by Beer-Lambert's law which relates the quantity of light absorbed to the number of gas molecules in the light path as a function of wavelength (Plane & Smith, 1995; Platt, 1994).

This is expressed as:

$$I(\lambda) = I_o(\lambda) e^{(-l\sigma(\lambda)n)} \quad (1)$$

where

$I_o(\lambda)$ is the initial intensity emitted by the light source

$I(\lambda)$ is the radiation intensity at the receiver after passing through the absorbing medium

l is the path length [cm]

$\sigma(\lambda)$ is the wavelength dependent absorption cross-section [$\text{cm}^2 \text{molecule}^{-1}$]

n is the number density [molecules cm^{-3}]

The optical depth, τ , which is a dimensionless quantity and optical density, D can be defined as:

$$\tau = l n \sigma(\lambda) \quad (2)$$

$$D = \ln \left[\frac{I_o(\lambda)}{I(\lambda)} \right] \quad (3)$$

Combining equations (1) and (3), we have

$$n = \frac{D}{\sigma(\lambda)l} \quad (4)$$

From equation (4), theoretically, the gas number density can be determined.

Light attenuation in the atmosphere

The reduction in the intensity of a light beam by absorption due to atmospheric constituents is in principle described by equation (1). Practically, for measurements in the atmosphere this is oversimplified as it does not consider the presence of other light extinction and attenuation processes. The various extinction processes that may occur during the irradiation of matter are represented in Figure 9.

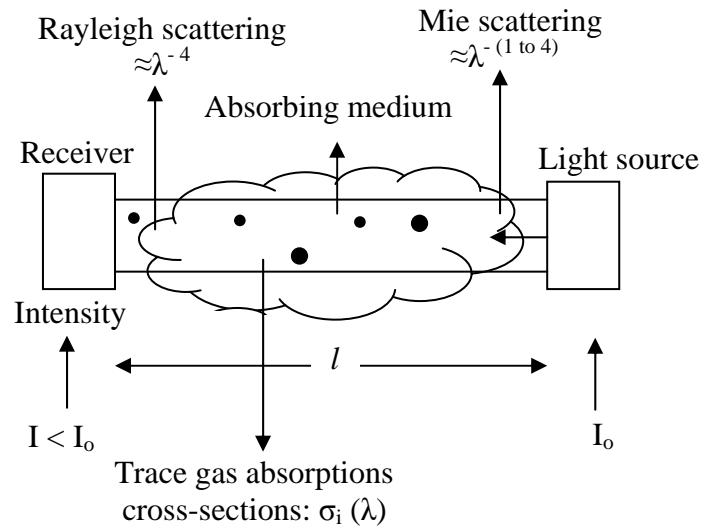


Figure 9: Various light extinguishing processes within the absorbing medium. (Comparative City Statistics, 2004)

Light Extinction due to Rayleigh scattering

This is the scattering of the light by particles smaller than the wavelength of the light, up to about a tenth of the wavelength of light. While this is not an absorption process, light scattered out of the probing light beam will normally not get directly to the detector in the single scattering approximation as a result of this phenomenon. It is consequently treated as an absorption process as it scatters light away from the line-of-sight.

Simplified, the "absorption" cross section can be written as:

$$\sigma_R(\lambda) \approx \sigma_{R0} \lambda^{-4} \quad (5)$$

where $\sigma_{R0} \approx 4.4 \times 10^{-16} \text{ cm}^2 \text{ nm}^4$ for air

Penndorf in 1957 provided a more accurate definition of the Rayleigh extinction coefficient $E_R(\lambda)$ as:

$$E_R(\lambda) = \sigma_R(\lambda)n_{air} \quad (6)$$

where n_{air} is the concentration of air molecules ($2.4 \times 10^{19} \text{ cm}^{-3}$ at 20° C , 1 atm).

Light Extinction due to Mie scattering

This is the scattering of the light by atmospheric aerosol particles. This can also be considered an absorption process with the Mie extinction coefficient, E_m , defined by the equation:

$$E_m(\lambda) = E_{m0}\lambda^{-n} \quad (7)$$

with n number density [molecules cm^{-3}] in the range 1...4 (Junge, 1963), and E_{m0} being the extinction coefficient when n is 0 (ideal situation).

Thus considering the Rayleigh and Mie extinction coefficients in the presence of a single trace gas species, equation (1) can be expressed as:

$$I(\lambda) = I_0(\lambda) \exp[-l(\sigma(\lambda)n + E_R(\lambda) + E_m(\lambda))] \quad (8)$$

Absorption by other molecules in the atmosphere within the line-of-sight

In the natural atmosphere many different molecular species will absorb light. Equation (8) can therefore be further extended to:

$$I(\lambda) = I_0(\lambda) \exp[-l(\sum(\sigma_i(\lambda)n_i) + E_R(\lambda) + E_m(\lambda))] \quad (9)$$

$\sigma_i(\lambda)$ and n_i denote the absorption cross section and concentration of the *i*th species respectively.

Measuring the differential absorption

On the contrary to laboratory spectroscopy, the true intensity, $I_o(\lambda)$, which would be received from the light source in an environment devoid of any atmospheric absorption is usually difficult to determine as it would mean removing the air from the open light path. Practically, this is achieved by measuring the supposed differential absorption, a quantity defined as the part of the total absorption of any molecule "rapidly" varying with wavelength. The absorption cross-section of a given molecule can for that reason be split into two portions:

$$\sigma_i(\lambda) = \sigma_{io}(\lambda) + \sigma_i^I(\lambda) \quad (10)$$

$\sigma_{io}(\lambda)$ varies only slowly with the wavelength (λ), denoting a general "slope", while $\sigma_i^I(\lambda)$ shows rapid variations with λ due to an absorption line. This is indicated on Figure 10.

The analysis of "rapid" and "slow" variation of the absorption cross-section is in relation to the observed wavelength interval and the width of the absorption bands detected. The extinction due to Rayleigh and Mie scattering can be considered to be slowly varying with λ . The aim of calculating differential absorption cross sections is to discriminate between narrow spectral features from unstructured absorption not useful in the DOAS method.

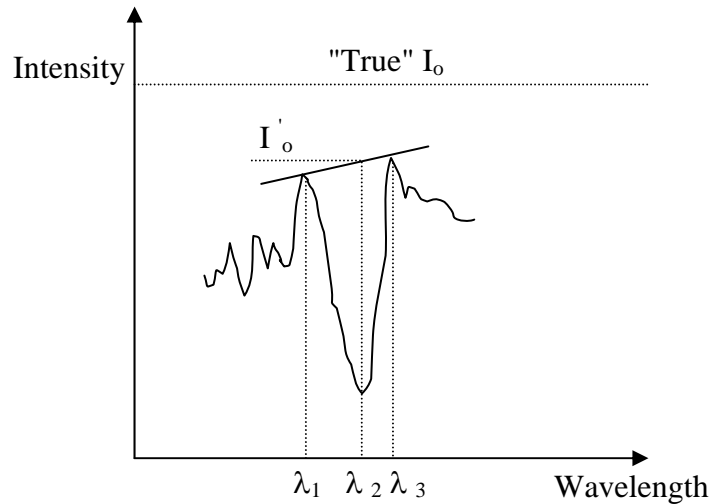


Figure 10: Differential absorption spectroscopy: practical example for the determination of I'_o and D^I (Platt, 1994)

Substituting equation (10) into equation (9) and introducing an attenuation factor $A(\lambda)$ gives:

$$I(\lambda) = I_o(\lambda) \cdot \exp[-l \sum (\sigma_i^I(\lambda) n_i)] \cdot \exp[-l (\sum (\sigma_{io}(\lambda) n_i) + E_R(\lambda) + E_m(\lambda))] \cdot A(\lambda) \quad (11)$$

The first exponential function illustrates the effect of the structured "differential" absorption of trace gas species, while the second represents the slowly varying absorption of atmospheric trace gases as well as the influence of Rayleigh and Mie scattering. The attenuation factor $A(\lambda)$ describes the slow wavelength-dependent transmission of the optical system used.

Defining I_o^I , an intensity in the absence of a differential absorption, gives:

$$I_o^I(\lambda) = I_o(\lambda) \cdot \exp[-l (\sum \sigma_{io}(\lambda) n_i) + E_R(\lambda) + E_m(\lambda)] \cdot A(\lambda) \quad (12)$$

As in figure (10), the intensity I_o^I can, for instance, be interpolated from the light intensity at either side of a sufficiently narrow absorption line of the species:

$$I_o^I(\lambda) = I(\lambda_1) + [I(\lambda_3) - I(\lambda_1)] \cdot \frac{(\lambda_2 - \lambda_1)}{(\lambda_3 - \lambda_1)} \quad (13)$$

$\sigma^I(\lambda)$ is determined in the laboratory (i.e. taken from literature data), just like $\sigma(\lambda)$. Likewise a differential optical density D^I can be defined.

$$D^I = \ln \left[\frac{I_o^I(\lambda)}{I(\lambda)} \right] = l \Sigma \left(\sigma_i^I(\lambda) n_i \right) \quad (14)$$

Atmospheric trace gas concentrations can then be calculated according to equation (4) with the differential quantities D^I and $\sigma^I(\lambda)$ substituted for D and $\sigma(\lambda)$ respectively. The trace gas concentrations are actually calculated from the amplitude of absorption structures, e.g. from differences of the absorption in the center of an absorption band or line and the spectral range between bands (Cantrell, et al, 1984; Drummond et al, 1985). Figure 11 illustrates the relationship of $\sigma(\lambda)$ and $\sigma^I(\lambda)$ and the determination of D from an actually measured spectrum. (a): Graph showing the dependence of absorption cross-section of trace gases on wavelength, (b): Graph showing the variation of intensity with wavelength for trace gases.

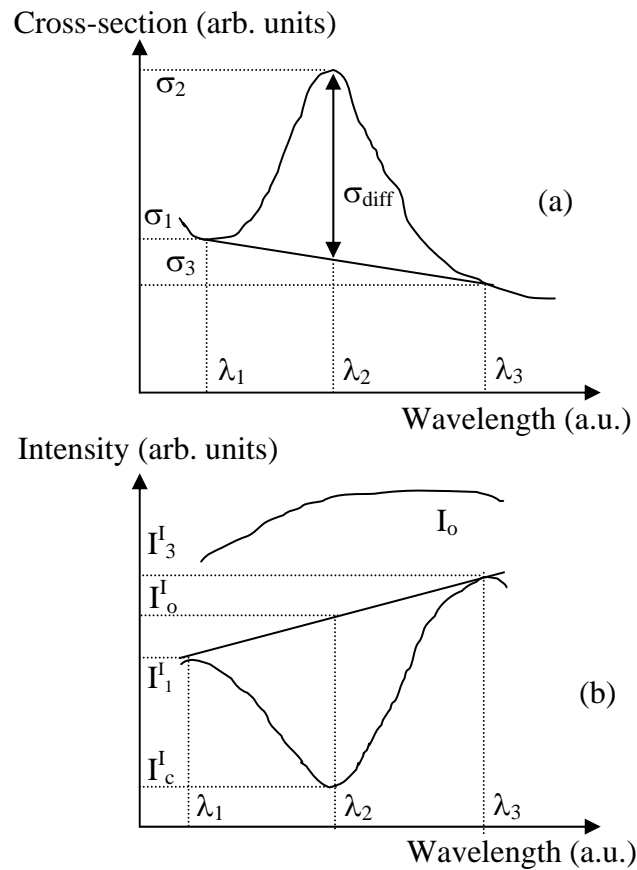


Fig. 11 (a): Graph showing the dependence of absorption cross-section of trace gases on wavelength.

(b): Graph showing the variation of intensity with wavelength for trace gases (Platt, 1999).

DOAS Measurement Parameters

The basic concept of the DOAS technique consists in the discrimination of two different contributions to the absorption spectrum obtained after the light has crossed the atmosphere.

The first absorption contribution, the interesting one containing the “fingerprints” of gases, is due to the atomic or molecular absorption of the gases present in the atmosphere and features narrow absorption bands in well defined positions of the wavelength scale. The second absorption contribution, which must be taken into account and removed in the calculations of the concentrations, is mainly due to the atmospheric scattering of the light. The absorption bands are strongly dependent on the light source’s spectral features and the instrument transfer function. The differential nature of the technique allows the removal of the instrument’s features and of the atmospheric effects, laying strong emphasis on the gas absorption contribution and therefore allowing high precision measurements of gas concentrations.

In a typical DOAS analysis a narrow spectral range is chosen and the contribution containing the “fingerprints” of gases, which is the rapidly varying part, extracted and the technique of spectral matching employed to derive the concentration of the molecular species under investigation (Sanders, 1996; Xue et al., 2000). This is achieved by first measuring a 'dark' current (by blocking the telescope entrance) for each spectra and subtracting the dark current from the sky spectrum taken in the horizontal direction (90° from zenith). This is to correct for electronic offset and dark current.

The resulting spectrum is then fitted to a reference spectrum taken almost simultaneously vertical in the zenith. The advantage of choosing the almost-simultaneous vertical measurements as reference spectra is that, to a good approximation, the slant contribution in the stratosphere cancels out.

What remains in the logarithmic ratio between the two spectra is the signal from the effective horizontal optical path, l , so that, along the line of sight, the slant column SC that is due to the gas concentration (n) integrated along the effective light path can be expressed.

This is given as:

$$SC = nl \tag{15}$$

Equation (15) represents the excess absorption along the line-of-sight with respect to the absorption in the reference spectrum (Andrea et al, 2002).

For all applications the spectra and cross-sections are high pass filtered and the differential quantities $\sigma'(\lambda)$ and D' used. A common use of a Fast Fourier Transform (FFT) is its application in finding the frequency component of a signal buried in a noisy time domain. Its essence, therefore, is to separate the effects of the low frequency or wavelength independent absorption cross-sections characteristic of the scattering and other disturbing extinction processes considered as perturbations which must be eliminated. These are the other absorption contributions due to the atmospheric scattering of the light which must be taken into account and removed in the calculations of the concentrations. Only the fast varying cross-section is responsible for the pure molecular absorption and is used to identify absorbers and quantify their integrated amounts along the light path. This technique is accordingly utilized as an effective way to filter the unwanted contents in a source spectrum (Cantrell et al, 1984).

It has been used for the purpose of enhancing the detectability of overlapping spectral bands (Baldini et al, 1975; Bonfiglioli et al, 1964; Collier et al, 1956, Dubrovkin, 1983; Giese & French, 1955; Smith, 1963). Additional advantages are the suppression of background radiation and noise, nearly total elimination of effects of instrumentally scattered radiation (Stauffer & Sakai, 1968) and suppression of atmospheric turbulence effects.

Levenberg-Marquardt multivariable minimization is used to achieve the best spectral alignment. The derived fit coefficient, α , yields the desired horizontal column density of the species (Wagner et al, 2001) and can be expressed as.

$$\left| \sum \ln(I(\lambda) - \sum I_o(\lambda) - \sum \alpha \sigma^I(\lambda) - \sum (\lambda)) \right| \rightarrow 0 \quad (16)$$

$\sigma^I(\lambda)$ denotes the differential cross-section of the species taken into account in the fitting process and $\sum \lambda$ is a polynomial used to account for all broad band features like Rayleigh and Mie scattering.

The Ring Effect

One significant limitation to the accuracy of the remote sensing of trace gas constituents in the atmosphere using UV-visible spectroscopy and scattered sunlight, and for that matter the DOAS technique, has often been a reliable knowledge of the Ring effect. This effect arises as a result of the contribution of inelastically scattered light to the total intensity of scattered sunlight observed. It leads to a modification which can be approximated as a filling-in of the Fraunhofer lines by Rotational Raman Scattering (RRS) by molecular N₂ and O₂.

It complicates the complete removal of the Fraunhofer structures and manifests itself by a broadening of the solar and atmospheric spectral features present in measured spectra (Roozendael & Fayt, 2001; Vountas et al, 1998). Only after the correction of this effect was it possible to observe 'minor atmospheric absorbers' (like BrO and OCIO) with absorptions \ll 1% (Grainger and Ring, 1962).

Usually the Ring effect can be approximately corrected by considering an additional spectrum in the DOAS fitting process, the so called Ring spectrum (Solomon et al, 1987).

Besides this 'classical' DOAS technique (fitting the optical depth) other methods are developed which directly fit the measured intensities (Chance, 1998). In such cases the Raman scattered intensity (instead of the 'classical' Ring spectrum) is included as a Ring spectrum in the fitting process. Most groups (Wagner et al, 2001) calculate Ring spectra (assuming Raman scattering as the cause of the Ring effect) by calculating the reciprocal of the measured spectrum (assuming the Raman scattered intensity is constant with wavelength) and fitting it directly to the measured spectrum during the retrieval process. Thus the Ring effect cross section is simply included as an additional pseudo-absorber (Solomon et al, 1987). This approach was used in this thesis presentation.

Signal-to-noise ratio (SNR)

Theoretically the signal-to-noise ratio is a measure to quantify how much a signal has been corrupted by noise, and therefore gives a measure of the signal strength relative to the background noise.

In less technical terms the signal-to-noise ratio compares the level of a desired signal to the level of background noise. The higher the ratio, the less obtrusive the background noise is and subsequently a ratio higher than 1:1 indicates more signal than noise. It is mathematically defined as the power ratio between a signal (meaningful information) and the background noise (unwanted signal):

$$SNR = \frac{P_{signal}}{P_{noise}} \quad (17)$$

In order to achieve the desired signal-to-noise ratios in DOAS measurements a sufficiently large number of photoelectrons needs to be recorded and must exceed the combined effects of all fixed noise sources in the set-up. Also a signal level not too much below the maximum detector signal is desirable but on the other hand, ‘overexposure’ e.g. a signal larger than the maximum allowable detector signal (e.g. due to pixel saturation) must also be avoided. Internal noise during DOAS measurements is greatly minimized by lowering the temperature of the circuitry. Such low temperatures also reduce the thermal noise as the thermal agitations of the charge carriers are then greatly reduced.

Determination of optical path length l

DOAS methodology using the sun as its source of radiation (passive mode) has proven to be one of the major tools for the determination of the slant columns of several atmospheric trace gases (Noxon, 1975; Platt, 1999; Platt et al., 1997; Solomon et al., 1987).

The columns retrieved using such technique depend not only on the amount of absorber present but also on the light path of the photons through the atmosphere. This is very important because the ability to correctly compute these slant columns depend on how well the optical path of light collected by the receiver is understood and computed by models.

Some set-ups, algorithms and models used to simulate, solve and analyse a wide range of scientific tasks including the determination of photon paths in the atmosphere include Global Ozone Monitoring Experiment (GOME-2 Measurements, 2009).

Others are the SCanning Imaging Absorption SpectroMeter for Atmospheric CHartographY (SCIAMACHY)(Gottwald et al, 2006) and PROcessing of Multi-Scattered Atmospheric Radiation (PROMSAR) (Palazzi, 2003; Palazzi et al, 2005). PROMSAR is a new radiative transfer model based on a backward Monte Carlo technique that considers scattering for the evaluation of scattered radiation measurements. This model has been validated by comparison with other radiative transfer models (Palazzi, 2003; Palazzi et al, 2004) and data available in the report of Hendrick (Hendrick et al, 2003) has also been used to perform some validation. The PROMSAR approach ensures a more realistic description of the radiation transport in the atmosphere than that given by single scattering models (Giovanelli et al., 1989, 1990, 1992). Consequently, it allows for a more accurate interpretation of zenith sky and off-axis measurements from DOAS spectrometers measuring diffuse UV-visible solar radiation.

Description of PROMSAR model to simulate I

As mentioned, it is very necessary to correctly simulate and compute the optical path of light collected by the receiver as the ability to accurately work out the slant columns depend, to a large extent, on how well the optical path of light is understood.

To simulate the optical path length collected by the receiver, an input data library is accessed by PROMSAR to build-up the appropriate probability distributions. For this purpose the radiance-transmittance code, MODTRAN (MODerate resolution TRANSmittance) (Abreu and Anderson, 1996; Berk et al, 2000) is adapted to exploit the large variety of atmospheric scenarios and climatologic choices it offers. It makes provision for six reference atmospheres. These are the tropical model, mid-latitude summer model, mid-latitude winter model, sub-arctic summer model, sub-arctic winter model and Standard U.S 1976 model. Each of these reference atmospheres is defined by temperature, pressure, molecular density and mixing ratios of major radiating atmospheric gases all as a function of altitude. The altitude increments are 1 km between 0 and 25 km, 2.5 km between 25 and 50 km and 5 km between 50 and 120 km. Representatives of atmospheric aerosol, cloud and rain models are provided within the MODTRAN code with the option of replacing them with user-modelled or measured values. With regard to aerosol, the variation of their optical properties with altitude is modelled by dividing the atmosphere into four regions of height each having a different type of aerosol. These regions are the boundary or mixing layer (0 to 2 km), the upper troposphere (2 to 10 km), the lower stratosphere (10 to 30 km), and the upper atmosphere (30 to 100 km).

A different atmospheric model with differing wavelength dependencies is used for each of these four altitude regions. The MODTRAN package includes several parameters to define aerosol profiles in the atmosphere. The most important of these are the type of aerosol and the visibility. There are several types of aerosol available based on common aerosol mixtures that are found in most terrestrial conditions. These generate the following aerosol models: rural, urban, maritime, tropospheric, fog and wind dependent desert. The rural model, for instance, represents the aerosol conditions one finds in the continental areas where the atmosphere is not directly influenced by urban and/or industrial aerosols sources. For this scenario the aerosols are assumed to be composed of 70% water-soluble substance (ammonium, calcium sulphate and organic compounds) and 30% dust-like aerosols. For an urban area the rural aerosol background is modified by the addition of aerosols from combustion products and industrial sources. The urban aerosol model is therefore taken to be a mixture of the rural aerosol and carbonaceous aerosols. The second important aerosol parameter, visibility, is used to define the amount of aerosol in the atmosphere. The data supplied by MODTRAN code has been adapted to build up a series of input data libraries for different aerosols, seasonal and latitude models to be read and processed by PROMSAR. Each of these input libraries contain the number of atmospheric layers and the values of the altitude increments for every atmospheric layer. It also contains the Mie phase functions, the aerosol scattering and absorption coefficients, the absorption and scattering coefficients of the gas compounds and the refraction indexes.

Moreover, certain parameters that are not included in the input library describing the atmospheric scenario can be set out by the user at the beginning of the simulation. These include the number of photons to be processed, the altitude where the instrument is placed (as it is possible to simulate a ground-based spectrometer or a spectrometer installed on board an aircraft) and its line of sight, the photon weight threshold, the range of the solar zenith angles and the surface albedo value.

Based on the gas of interest, simulations can be performed using the required input parameters to compute the mean photon paths at various solar zenith angles. Equipped with these data a graph of solar zenith angle can be plotted against the simulated photon paths and a general equation obtained in the form:

$$y = y_0 A e^{x/t} \quad (18)$$

with x : the solar zenith angle

y : the corresponding photon path

y_0 , A and t are constants.

Thus with the established equation, PROMSAR can be used to work out the mean path of the photons for each value of the solar zenith angle.

Processing of raw data to obtain slant column values

The raw data as recorded by the DOAS system for each of the readings taken is made-up of an array of numbers having 10 columns and 103 rows with the last row having only 4 numbers.

Thus the total count of numbers in each raw data collected is 1024, corresponding to the number of illuminated pixels on the ccd sensor. Values of these raw data recorded fall within $0 \leq \text{number} \leq 9999$ depending on the intensity recorded by the ccd at the time of measurement. '0' depicts very low sun intensity while '9999' gives a picture of high sun intensity at the time of measurement. Appendix 1 and 2 are typical examples of raw data collected in the uv and visible spectral regions respectively showing the characteristic details associated with each data collected. These details are the date and time of data collection, wavelength interval within which measurements were taken, cell and filter positions selected and the integration time for the measurement.

With the raw data collected a retrieval procedure is followed to obtain the slant columns of the gases being measured using an appropriate software installed on the computer.

The procedure involves:

1. "Preparing" the differential absorption cross-sections of gases to be measured
2. "Preparing" the reference sky spectrum
3. "Preparing" the reference from a measurement taken in zenith position
4. Verifying if the prepared reference spectrum is good for analysis
5. Processing of data to retrieve the slant columns of gases

All these processes involve the running of a customized visual basic program.

Preparing the absorption cross-sections of gases - The general absorption cross-section of the gas being captured is retrieved from a data base and modified to suit the particular measurements being made.

This modification involves the selection of the appropriate wavelength interval within which the detection is made, the choice of a fitting variant (based on the resolution of the instrument) to be used as a filter so as to match-well what was taken from literature and that measured using the instrument.

Finally the differential cross-section is prepared by choosing an appropriate off-set value such that all low frequency signals in the spectrum (those due to Rayleigh scattering, Mie scattering etc) are eliminated leaving just high frequency signals which are due to the absorption of gases.

Preparing the reference sky spectrum – The preparation of the reference sky spectrum follows the same procedure as the preparation of the absorption cross-section of the gases. Firstly the standard sky spectrum is retrieved from a data base, filtered and then its differential cross-section prepared.

Preparing the reference from a measurement taken in zenith position – The spectrum captured by the DOAS system is recorded in pixels while the standard sky spectrum (from literature) is recorded in nanometers. A comparison is therefore made between these two spectra (within the operative wavelength interval) to match the pixel position in the measured spectrum to wavelength in the standard solar reference spectrum. This procedure is carried out to achieve this matching.

Verifying if the prepared reference spectrum is good for analysis – After matching the pixel position in the measured spectrum to wavelength in the standard solar reference spectrum there is the need to mathematically investigate the quality of alignment made. A correlation coefficient, x , within the range $0.7 \leq x \leq 1$ is considered to be acceptable for analysis.

Processing of data to retrieve the slant columns of gases – This is the final step carried out to obtain the slant column values of the gases considered. It involves the selection of the prepared absorption cross-section of the gases and the prepared reference sky spectrum in addition to the selection of the raw data to be analyzed. At the end of the entire process the slant column values of the gases selected are saved in a results folder.

Data Transformation

The slant column value due to the gas concentration as measured by the DOAS system has its units in *molecules cm⁻²*. The concentrations of the gases measured will later be reported in *molecules/cm³*, *ppbv* and *μgm⁻³* using the following conversion equations:

$$\text{molecules / cm}^3 = \frac{\text{molecules / cm}^2}{l} \quad (19)$$

$$\text{ppbv} = (1.38E - 10) \left(\text{molecules / cm}^3 \right) \left(\frac{T}{P} \right) \quad (20)$$

$$\mu\text{g / m}^3 = (10E12) \left(\text{molecules / cm}^3 \right) \left(\frac{N_{\text{gas}}}{N_A} \right) \quad (21)$$

where *l* is the optical path length, *T* is the temperature in Kelvin, *P* the atmospheric pressure in millibars, *N_{gas}* is the molecular weight of the trace gas under consideration and *N_A* is the Avogadro's number.

Laboratory calibration procedures

Theoretical determination of concentration using a gas cell

In the laboratory, the exact concentration of gas contained in a cell, C_{cell} , can be determined using the equation:

$$C_{cell} = \frac{P_{cell}(mb)}{1013.25(mb)} * C_g(ppmv) \quad (22)$$

where P_{cell} is the pressure in the cell which is read on a manometer connected to the cell.

1013.25 mb is the atmospheric pressure and

C_g is the certified concentration of the NO₂ in the cylinder bottle when initially filled. For NO₂ C_g has a standard value of 950 ppmv.

In DOAS analysis C_{cell} is the 'reference concentration'. As the pressure in the cell P_{cell} is reduced (by allowing some of the trapped gas to escape into the atmosphere) the corresponding concentration of gas left is determined using equation (22). Thus with this equation the reference concentrations of the gas at the various pressures can be determined.

Measured concentration calculation

The concentration of NO₂ present in the gas cell at the various pressures mentioned above can also be retrieved using DOAS technique from the various intensities (I_s) recorded by the system. This is done with reference to the intensity of a pristine spectrum recorded, I_0 . Concentration values obtained from such measurements are the 'measured concentrations'.

Using the reference measurements as the first method of validating the DOAS technique, the two concentration values (reference and measured concentrations) can be compared by plotting a scatter graph of the reference (x) against the measured (y) and a line of best fit drawn. A good correlation coefficient between the two data sets will indicate how well the DOAS system will perform when used for field measurements.

CHAPTER THREE

EXPERIMENTAL SET UP AND MEASUREMENTS

Experimental Set up

Components Description

The DOAS system used for this study was assembled by me, and for that reason custom-built and labeled GASCOD-GH (Gas Analyzer Spectrometer Correlating Optical Differences-GHana). When in operation two main components namely Light Source and Receiver can be identified.

Light Source

GASCOD-GH was operated in a passive mode meaning that it used a natural light supply; specifically sunlight, as its source of light. Sunlight emits a wide range of wavelengths ranging from gamma rays to radio waves but measurements were restricted to wavelengths within the ultra-violet and visible spectral regions. This is because the gases of interest to be detected could be captured within these spectral regions.

Receiver

The receiver, also known as the Spectrometer Unit SU, consists of an optical module O-SU and an electronic module E-SU.

Spectrometer Unit (SU) of DOAS system

A detailed representation of the spectrometer unit is provided in Figure 12.

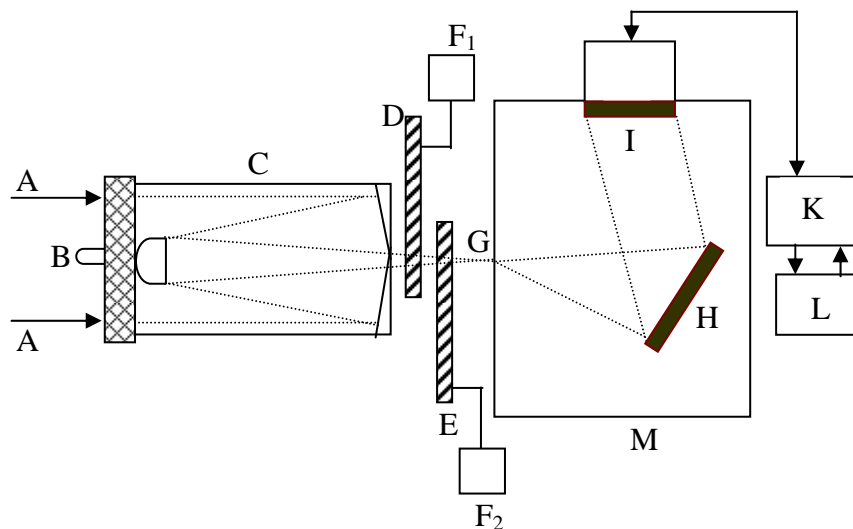


Figure 12: A complete arrangement of the spectrometer unit of the DOAS system

A - Light rays from the sun

B - Hg lamp

C - Telescope

D - Cell wheel

E - Filter wheel

F₁ and F₂ - Stepper motors (Type 103H548-04500)

G - Entrance slit

H - Jobin-Yvon diffraction grating

I - Detection system (with linear image sensor ccd)

K - Microprocessor system (Electronic Module E-SU)

L - MS-DOS computer

M - Monochromator

Description of Essential Components

Telescope

A 25-cm $f/5$ Cassegrain telescope was used and its function was to collect light from the sun as the system was operated in a passive mode. For its design, reflecting elements, i.e. mirrors (reflectors) were chosen due to the absence of chromatic aberrations in the formation of its images. Reflectors also need fewer large optical surfaces, which are expensive to manufacture. The Cassegrain design was chosen as it is much more compact. Its light path is given in Figure 13.

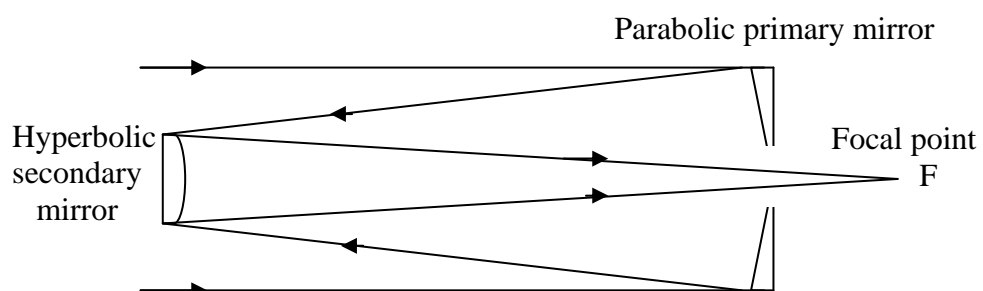


Figure 13: The light path in a Cassegrain reflecting telescope

Filters

The filter wheel installed has the capacity to accommodate 8 optical filters but was fitted with two unique types (filters 1 and 3), one of which is selected at a time based on measurements being made. The filters mounted were Oriel coloured glass band-pass interference filters which are generally ideal for the spectral selection and isolation of light (Oriel Instruments, 2005). Their function in this set-up was to block unwanted spectral orders and also reduce stray light in the spectrometer by limiting the spectral bandwidth of radiation entering the instrument.

The two filters used for this study were fixed at positions 1 and 3 on the filter wheel. Their characteristics are given in table 2 and their representative percentage transmission curve shown on Figure 14 (a) and (b) respectively. During measurements the filter of choice is positioned directly in the light path in front of the entrance slit restricting wavelengths entering the spectrometer to the bandwidth of the preferred filter.

Filter 1 with a peak transmission at a wavelength of 345 nm was chosen when readings were to be taken in the UV region while filter 3, with a peak transmission at 445 nm was chosen when readings were to be taken in the visible region.

Table 2: Characteristics of filters used for the spectral isolation of light entering the spectrometer.

Filter Position	Model No.	Refractive index	Wavelength of maximum transmission (nm)
1 (a)	BG24	1.51	345
3 (b)	BG28	1.52	445

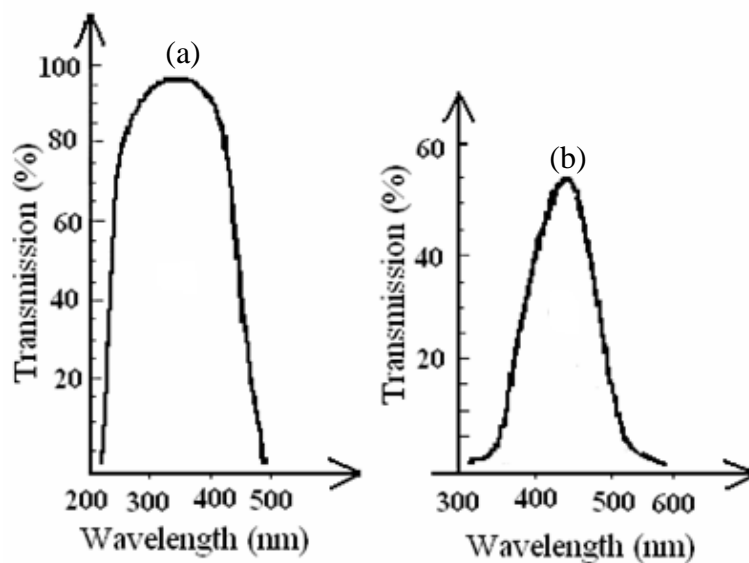


Figure 14: Transmission Characteristics for:
(a) filter 1 (b) filter 3 (Schott glass filters, 1999)

Stepper Motor

The stepper motors F_1 and F_2 were used to move the cell and filter wheels respectively in precisely known increments. The specifications of these stepper motors are as follows: Type 103H548-04500, 1.8 Ω , Lot No.: 02517F and manufactured by Sanyo Denki.

Jobin-Yvon Diffraction Grating

This advanced optical component was used to disperse the different wavelengths arriving at its surface. It has 1200 grooves/mm, a focal length of 0.30 m and a spectral dispersion of 2.4 nm/mm at 300 nm.

Detection system

The sensor installed was a solid state C4845 Hamamatsu diode array that has a CCD with 1024 pixels, all of which are illuminated during measurements. It has the competence to collect data within the wavelength range 200-1000 nm and incorporates a thermoelectrically-cooled NMOS linear image sensor, low noise driver/amplifier circuit and highly stable temperature control circuit. It was operated in the charge-accumulation mode and consequently the resulting voltage output signal is the sum of a dark signal, which is dependent on both temperature and integration time, and a signal that is proportional to the amount of light exposure. It operates from simple external signal inputs and is cooled to a preset temperature as soon as the power is turned on. Should the cooler fail and the device overheat, the built-in protection circuit automatically shuts off the power. The optimum use of the sensor calls for its ambient temperature to be low and constant and for this reason the entire system was installed in a 'housing' with the temperature maintained at 10 °C using an air-conditioner. The operation of the sensor within a low-temperature environment made it possible for a reduction in thermal noise, dark current and avoided nonlinear effects in the sensor. The photo sensitivity characteristic of the sensor is given in Figure 15.

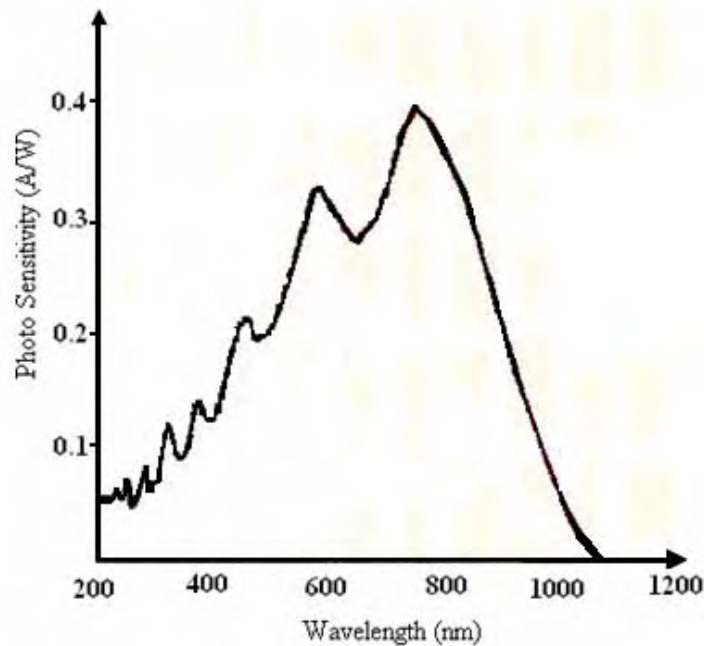


**Figure 15: The photo-sensitivity of sensor installed
(Hamamatsu Photonics, 2003)**

Operation of Optical Module O-SU

An exhaustive representation of the optical module of the spectrometer unit is given in Figure 12. The receiving telescope 'C' focuses the incoming light 'A' from the sun onto a fixed-precision type entrance slit 'G' with dimensions 0.1 mm wide by 2 mm. The cell wheel 'D' and filter wheel 'E' are each being driven by separate stepper motors ' F_1 ' and ' F_2 ' respectively. The cell wheel can accommodate five different cells represented by positions 0 – 4 out of which three (positions 1, 2 and 4) are used to make a distinction between the different lines-of-sight (vertical, horizontal left and horizontal right directions respectively) of the spectrometer.

One particular filter is chosen at a time depending on measurements being conducted.

The radiation flux emerging from the telescope onto the entrance slit is focused onto the diffraction grating '*H*' which spectrally disperses the radiation towards a detector '*T*' made up of a CCD with 1024 pixels. The grating '*H*' can be moved by another stepper motor and therefore the monochromator '*M*' by means of this movable dispersion element can analyze a 2500-8000 Å spectral range. With regards to the exactitude required to align the system, the entrance slit and detector positions were set so as to have the maximum amount of light passing through them, thereby producing an image with the strongest intensity on the detector. A Hg calibration lamp '*B*' is placed on top of the telescope and used for automatic wavelength calibration before any measurement is taken each time the spectral range is changed or is used periodically if the spectral range is not changed.

Electronic module E-SU

'*K*' is a Z80 microprocessor system. It was chosen because it is very compatible with many other systems and has features that allow peripheral components to be built with fewer support chips. This Z80 microprocessor system makes up the electronic model of the spectrometer unit and controls the operating mode of all the components of the spectrometer unit. This microprocessor controls the scanning of the diode array at programmable integration times, the reading of its 1024 output signals and their analog-to-digital conversion.

It also drives the spectrometer's moving parts (cell and filter wheels and the grating), calibration and auto-ranging procedures and data transmission to an MS-DOS PC through an RS-232 serial channel.

The auto-ranging procedure is designed to calculate the most suitable integration time for measurements depending on the intensity of incoming optical radiation at the time. The software operates the computer (Pentium 4) as a video terminal until the final 1024-pixel spectrum is received. After this the RS-232 channel is disabled, then the calibration spectrum and the source light spectrum displayed and saved on disk in a daily file in a data format and the serial channel again enabled. In totality the system is automated and unattended spectral readings taken and stored by the computer 'L' as per predefined measurement inputs using the programme ENEA1024. 1024 is indicative of the number of pixels in the CCD linear image sensor installed. When the programme is engaged an interactive dialog box pops-up on the screen from which the specific activity to be taken can be selected. The dialog box displayed appears as follows:

Selection Options:

1. Automatic Calibration
2. Spectra Acquiring
3. Auto-ranging of Tint
4. Dark Current
5. Test gratings motor
6. Positioning of windows and filters
7. Set integration time
8. Measurement (Dark current included)

Automatic Calibration: This is done using the Hg calibration lamp 'B' (in Figure 12) placed on top of the telescope. It is used for automatic wavelength standardization before any measurement is taken each time the spectral range is changed or is used periodically if the spectral range is not changed.

Spectra Acquiring: This option is chosen for manual operations when a spectrum is desired to be captured, i.e., when readings are to be taken in a non-automatic mode. Before doing this some background information will have to be provided. Firstly the wavelength interval within which the spectrum is to be taken will have to be indicated and this will dictate the type of filter to be chosen. Secondly the line-of-sight of the spectrometer unit will also have to be indicated using cell positions. Cell wheel position 1 is used for vertical readings, cell position 2 for horizontal left readings and cell position 4 for horizontal right readings.

Auto-ranging of Tint: This procedure calculates the best integration time depending on the environmental condition of the sun at the time. After calculation the obtained value is automatically uploaded and used for acquiring the next spectrum.

Dark Current: This activity is used to determine the dark current within a selected wavelength interval at the time of measurement.

Test gratings motor: This option is used during calibration procedures to move the grating either towards the UV or visible regions of the electromagnetic spectrum in order to move a particular spectral line to a desired position.

Positioning of windows and filters: This activity is used to verify the accuracy of response of the cell and filter wheels during measurements.

Set integration time: This is used to set a constant integration time for measurements to be taken, especially during trials and manual operations.

Measurement (Dark current included): Just like option “2”, this option is used in the acquisition of spectra, but with the added consideration and inclusion of the dark current during measurements. The wavelength interval, filter to be used and the line-of-sight of the spectrometer unit will have to be indicated before measurements are taken. Either this option (8) or option (2) can be selected at a time.

Assembly of instrument

The complete diagram for GASCOD-GH is shown in Figure 16.

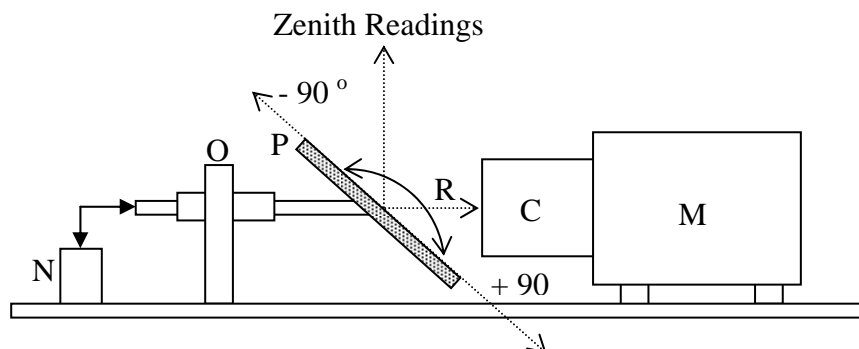


Figure 16: The complete GASCOD-GH arrangement used for the detection of trace gases.

N - Stepper motor (Type 103H548-04500)

O - Support

P - Plane mirror rotatable at $\pm 90^\circ$ w.r.t the zenith

R - Reflected light from mirror

C - Telescope

M - Monochromator

The stepper motor '*N*' is connected to a back-reflecting plane mirror '*P*' which is mounted in front of the telescope '*C*'. The mirror with dimensions 21.2 cm x 30.0 cm is rotatable at $\pm 90^\circ$ with respect to the zenith and has Al-MgF used as coating for reflection. Its reflection characteristics are shown in Figure 17.

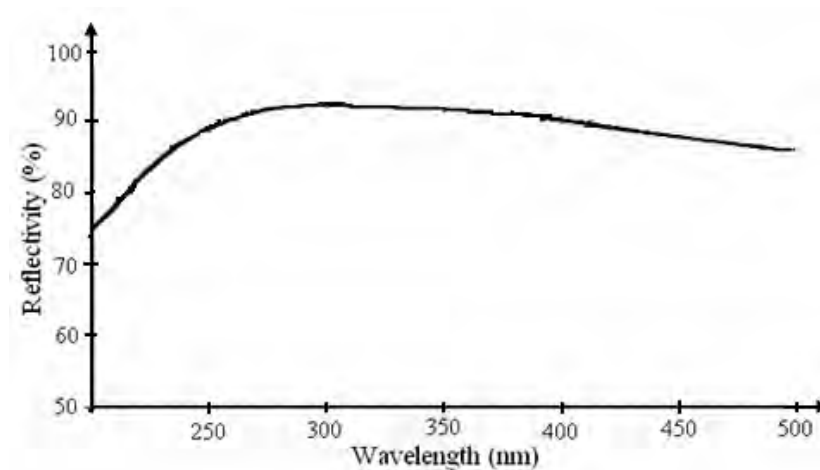


Figure 17: Theoretical reflection of Al-MgF (Replicated mirrors, 2007)

All reflections, '*R*', from the mirror are directed to the spectrometer unit, which is made up of the telescope and monochromator '*M*'. By rotating the mirror the spectrometer unit could change its line-of-sight from the zenith to the horizontal left or right directions. For protection the mirror was enclosed in a metallic 'housing' (Figure 18).

Housing used to protect plane mirror

Figure 18 is a 3-D visual of the housing used as an enclosure for the protection of the plane mirror. It has a dimension of 21.7 cm by 30.5 cm by 22.2 cm.

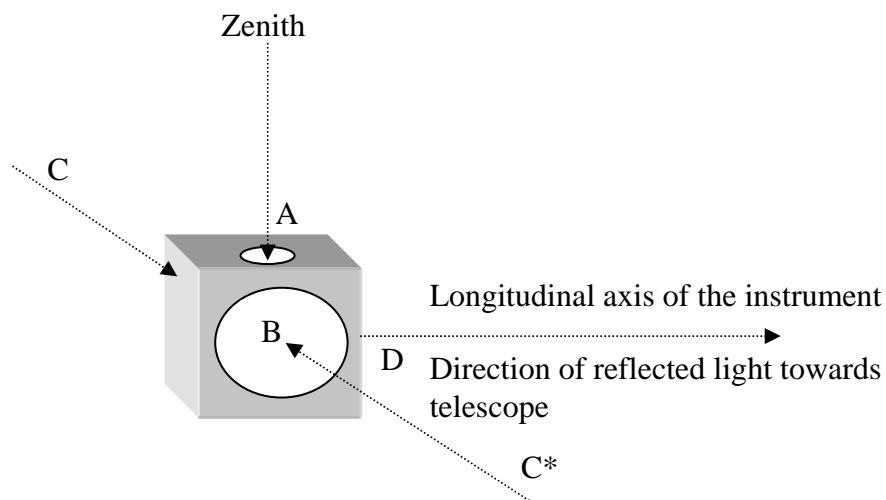


Figure 18: A 3-D representation of housing used to protect the plane mirror

Provision was made for 4 optical windows during the construction of the 'housing' for the mirror. Three of these windows 'A', 'C' and 'C*' serve as openings through which light is admitted into the telescope.

In that order these windows allowed in light straight down from the zenith and from the horizontal left and right directions respectively. The windows in the vertical 'A' and two horizontal directions 'C' and 'C*' facilitated the almost simultaneous measurements of the scattered solar radiation in these directions. The longitudinal axis of the instrument is parallel to a front window 'D' (fourth window) but perpendicular to the vertical and horizontal windows. The position of the front window enabled all light reflected from the mirror to be received along the longitudinal axis into the spectrometer unit. All reflections from the mirror fell within the field of view of the telescope.

Laboratory tests carried out

In all DOAS procedures it is prudent and essential to carry-out some laboratory tests of the spectrometer unit to ascertain its accuracy and efficiency before field measurements are carried out. The assessments carried out involved the following:

1. Confirmation of the suitability of the sensor installed by studying the variation of its dark current with integration time.
2. Calibration and determination of the linear dispersion of the sensor for the wavelength interval within which the system was operated.
3. Laboratory calibration of the DOAS system using a 100-cm gas cell.
- 4: Studying of the polarizing effect of the sun on the sensor as the sun migrates between sunrise and sunset.

For all these procedures the spectrometer unit was mounted on an optical bench.

Variation of the dark current of sensor with integration time

The ability of the DOAS system described to assess accurately the concentration of a trace gas depends very much on the performance and accuracy of its detection device. The suitability of the ccd sensor installed, therefore, had to be established by studying the variation of its dark current with integration time. During the measurement of the dark current all lights in the laboratory were switched-off while the cell and filter wheels were set in 'shutter' positions thereby preventing the entry of light into the spectrometer unit. The dark current was then measured at different integration times from 500 ms to 240,000 ms.

Calibration and determination of linear dispersion

The sensor installed took its measurements in pixels. For this reason there was the need to compare its output measure to a standard having known measurement characteristics. i.e., there was the need for the sensor to be calibrated against a known standard to guarantee accuracy, validate it and its measurement technique and determine the wavelength scale that is mapped onto the CCD. This entails measuring the spectral dispersion (\AA per pixel) of the spectrometer. The standard used for this calibration was the discrete and fixed lines exhibited by Hg pencil-lamp. The standard wavelength positions of the Hg lamp (in \AA) were compared to the corresponding pixel-positions observed using the spectrometer. To determine these pixel positions the spectrometer unit was mounted on one side of the optical bench while on the other side was the low-pressure 6035-Hg pencil lamp which was used as a reference lamp.

Plate 1a is a picture of the spectrometer unit on one side of the optical bench while plate 1b is a picture of the lit Hg pencil lamp on the other side at a distance of 8 m from the spectrometer unit.

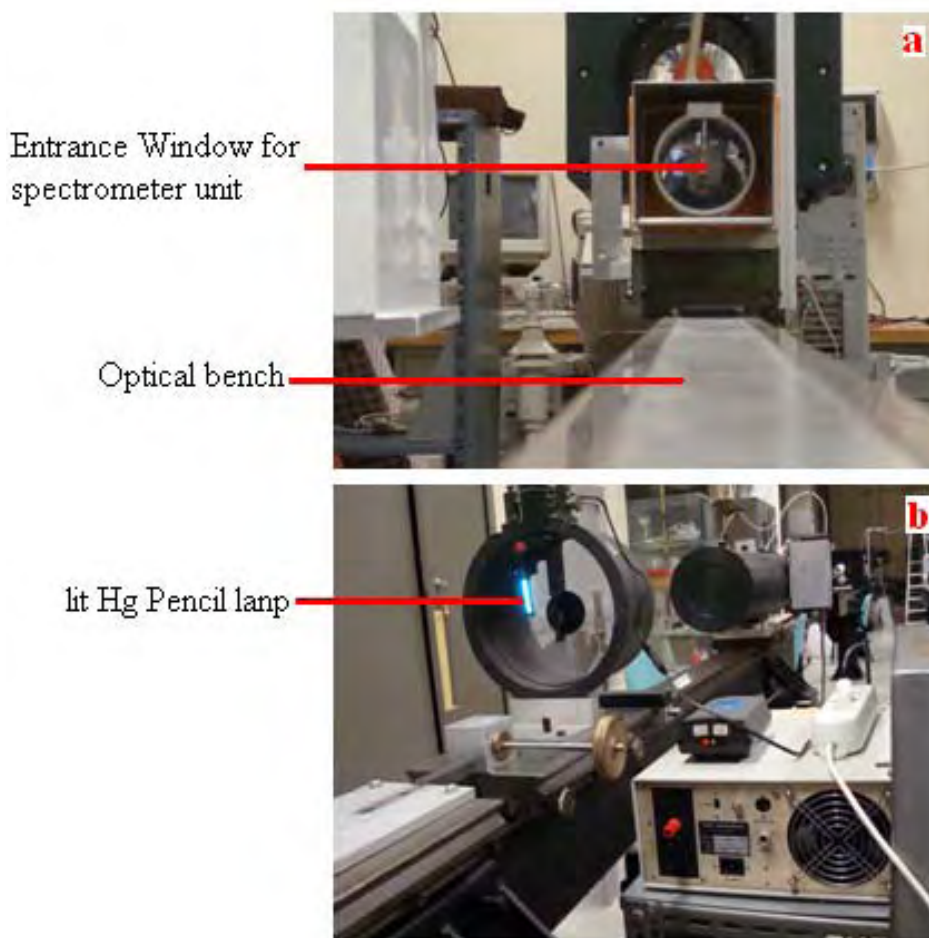


Plate 1a: Picture showing the entrance window of the spectrometer unit on one side of the optical bench.

1b: Picture showing the lit Hg pencil lamp on the other side of the optical bench.

The Hg pencil lamp is useful as an intense and efficient UV source as it exhibits observable fine, discrete, narrow and fixed lines at resonant gas wavelengths. These visible lines were used to align, calibrate and determine the linear resolution of the sensor.

The standard fixed lines exhibited by Hg lamp in the UV and visible regions are given in Figures 19 (a) and (b) respectively. These standard lines were then compared to the spectra obtained when the Hg lamp was used to illuminate the entrance slit of the spectrometer.

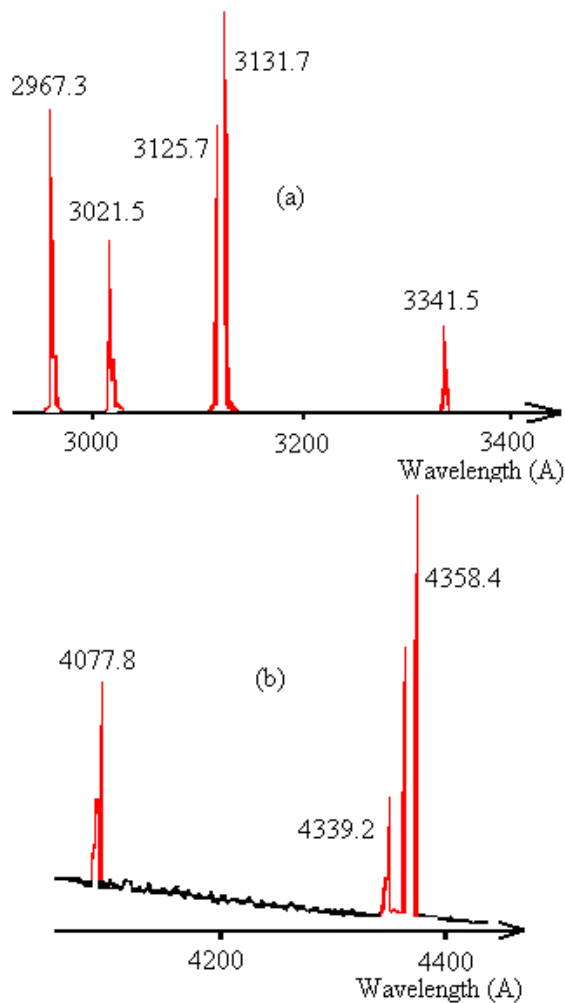


Figure 19: Standard Hg lines: (a) in the uv (b) visible spectral regions

Laboratory Calibration Using a Gas Cell

In the laboratory a critical validation of the measurement precision of the system was conducted by using it to confirm the known concentrations of NO_2 in a-100 cm gas cell.

The spectrometer unit was maintained on one side of the optical bench while on the other side was a lit Xe lamp. The gas cell was arranged on a movable rail on the optical bench such that it could be positioned either directly within or away from the light path between the spectrometer and the Xe lamp. The other items used during this procedure were a vacuum pump and NO_2 stored in a gas cylinder.

Procedure: Two specific concentration measurements were carried out. The spectrum of the Xe lamp was initially captured by the spectrometer when the path between the lit Xe lamp and spectrometer was free. This gave I_0 , the intensity of the pristine Xe spectrum. The gas cell was then evacuated of air using the vacuum pump, filled with NO_2 to an initial pressure P_1 and the spectrum I_1 captured. The concentration of gas in the cell is then determined using the theoretical equation (reference) and the concentration again determined using DOAS technique (measured). The pressure was then continuously changed (lowered) and for each new pressure P_s the corresponding spectral intensity, I_s , was recorded. NO_2 dissociates in the presence of light and therefore the gas cell was covered with a black cloth (to prevent dissociation) as it was filled with the NO_2 . Plate 2a is a picture of the gas cell mounted on a movable rail on the optical bench while plate 2b is a picture of the black cloth covering the gas cell when the cell was filled with NO_2 and readings taken.

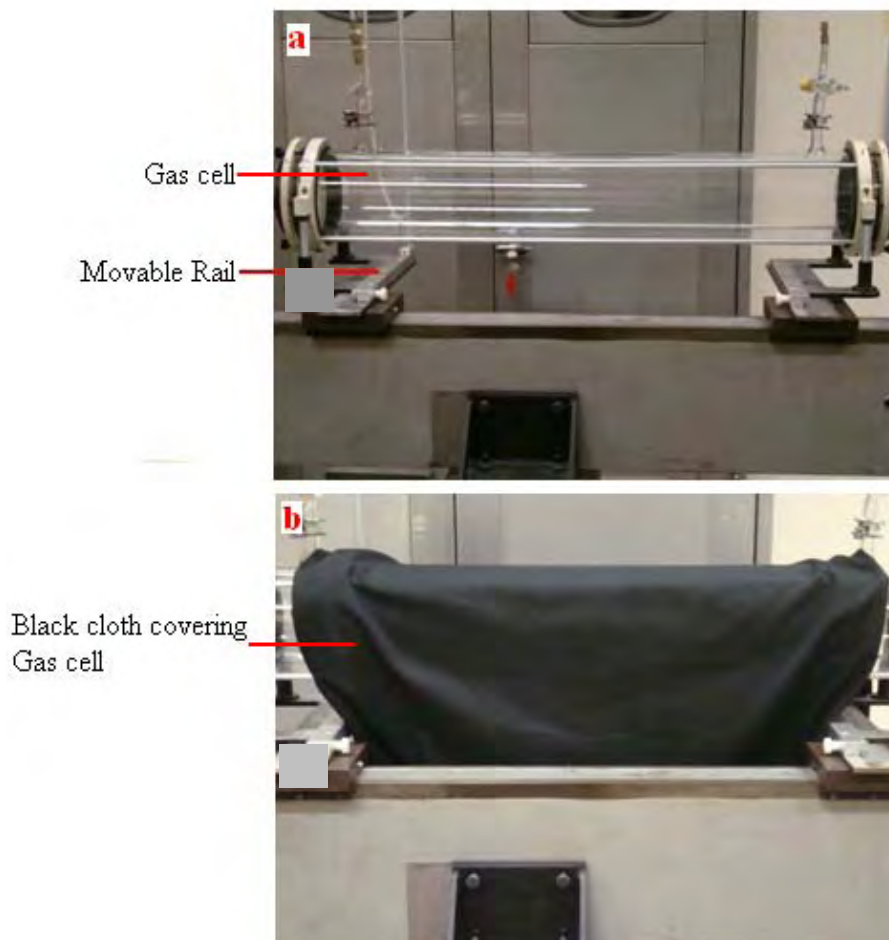


Plate 2a: Picture showing the gas cell mounted on the movable rail on the optical bench.

2b: Picture showing the gas cell covered with a black cloth to prevent the dissociation of NO₂.

Polarizing effect of the sun on the sensor

The migration of the sun between sunrise and sunset brings about changes in the solar zenith angle which consequently polarizes the diffraction grating, which is the dispersion element of the system. This effect was studied using a halogen lamp (continuous light source), polarizer and a rotatable angle selector.

Procedure: The polarizer was centrally set on the angle selector while the mirror of the DOAS system was positioned to receive light from the zenith position. With the halogen lamp installed on top of the polarizer, the polarizing angle was varied in steps of 10^0 within the range $-90^0 \leq \theta \leq +90^0$. For each angle selected the intensity of light reaching the sensor was recorded between the spectral windows 2823 \AA and 7677 \AA . During the entire process, it was ensured that the voltage and current readings of the power supply remained fixed at 12 V and 1.79 A respectively.

Plate 3 is a picture of the polarizer centrally fixed on the angle selector and the turnable knob used to select the angles.

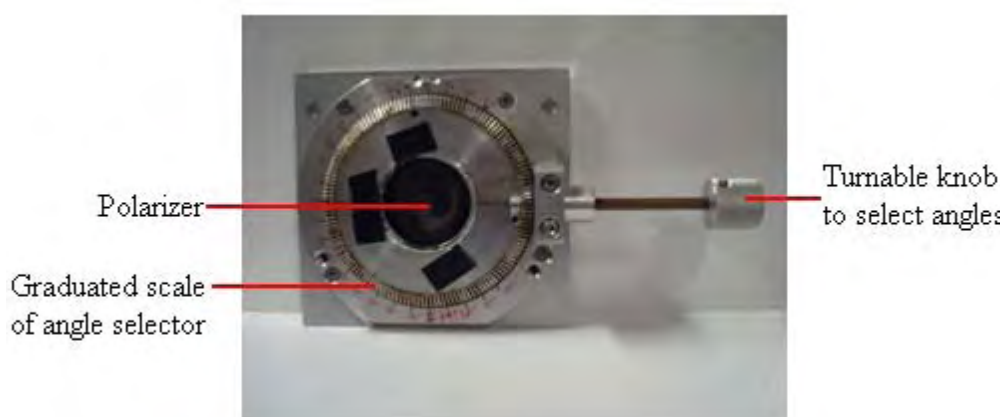


Plate 3: Picture showing the polarizer centrally installed on the angle selector and the turnable knob used to select the angles.

Determination of photon path length in the atmosphere

Aside the laboratory tests carried out to verify the suitability of the system before field measurements are carried out, the accuracy of every passive DOAS technique depends significantly on how well the optical path of light collected by the receiver is understood and computed by the model used.

Simulations using PROcessing of Multi-Scattered Atmospheric Radiation (PROMSAR) model within a well defined grid were therefore performed to determine the optical paths at various solar zenith angles. Inputs made for the simulations are given in Table 3.

Table 3: Inputs made using the PROMSAR model to simulate the photon path lengths at various solar zenith angles.

Input Parameter	Type or Factor Used
	Mid-latitude summer model
Reference Atmospheres	(For measurements in Italy)
	Tropical model (For measurements in Ghana)
	Mixing layer or lower troposphere
Region of Atmosphere	(0 – 2 km above ground)
Aerosol model	Urban extinction type
Visibility	5 km
Wavelength: Visible Region	440 nm
UV Region	330 nm
Solar Zenith Angle (S.Z.A.)	10° – 80°
Surface Albedo Value	0.3
Relative azimuth angle	0°
Line-of-Sight	90°

After the simulation values for the photon path lengths were obtained for the solar zenith angles from 10° – 80°.

Sites selected and gases monitored

Measurements carried out in Italy

Location: Institute of Atmospheric Science and Climate (ISAC) (44.3°N, 11.2 °E), Bologna. Concentration of NO₂ was monitored at this site. Measurements were carried out in March 2005 on 9th, 10th and 11th and concentration values obtained compared with values provided by the ARPA in-situ analyzer as they were used as the first method of validation. ARPA is the National Environmental Protection Agency of Italy and has a station located about 500 m away from ISAC where in-situ concentration measurements are carried out on some trace gases.

Measurements carried out in Ghana

Location: Tema Oil Refinery (TOR), Tema (5°39'59.88" N, 0°00'21.26"E). For this site concentration values of NO₂, SO₂ and O₃ will be presented for two different periods and in the four cardinal directions (north, south, east and west). The periods in question are January 2008 during the harmattan season and July and August 2008 during the rainy season. Such diverse seasons for measurements were chosen so as to have data from varied scenarios to draw well-informed conclusions. Tema is Ghana's leading seaport and industrial center with industries producing aluminum and steel products, chemicals, detergents and food products, textiles and building materials and petroleum products (Ghana City Tema, 2009).

TOR is a petroleum refinery plant that refines crude oil to turn out varied petroleum products. Its activities over the years have involved the production of liquid petroleum gas (LPG), motor gasoline and kerosene, aviation turbine kerosene (ATK), gas oil (diesel) and residual fuel oil. The potential atmospheric releases due to the various stages of this production process, particularly combustion and flaring of fuel oil and gas, include gaseous emissions such as volatile organic compounds and atmospheric particulate. In compliance with National guidelines, statutory requirements and in pursuance of TOR's environmental policy, a programme was drawn to develop the refinery's capacity for environmental air quality assurance. The DOAS instrument was accordingly installed on its premises to monitor and measure the concentration of gases emitted into the atmosphere due to its activities and also due to the operations of other industries within its environs. In addition, the installation at TOR was in line with an established collaborative research understanding between TOR and the Laser and Fibre Optics Centre (LAFOC) of the University of Cape Coast, Cape Coast. At TOR the roof-top of the Administrative Block, which is at a height of about 50 m from the ground, provided a suitable location for the construction of the housing for the system and was provided with four (4) optical viewing windows in all the four cardinal directions (north, south, east and west). Gases monitored were NO_2 , SO_2 and O_3 and their concentration retrieved within an average optical path length of 3 km. These gases, been the criteria compounds, were monitored due to the important roles they play in the chemical dynamics of the atmosphere.

Images of site locations around TOR

Knowledge of the townships bordering TOR, which is the site where measurements were carried out, is of importance as meteorological factors will influence the dispersion of pollutants to these townships. Plates 4 is a satellite picture of some of the townships in the vicinity of TOR.



Plate 4: A satellite photo of some townships distant from TOR (Google Earth Search, 2009)

Plate 5 is an aerial view of TOR showing the Administrative Block (AB), the building on which the DOAS system was installed and measurements carried out.

The refinery plants are represented by ‘*RFCC*’ (Residue Fluid Catalytic Cracking Unit), and ‘*CDU*’ (Crude Distillation Unit) while ‘*PL*’ represents the Pay load, the precinct where the heavy-duty tankers are loaded with the various finished petroleum products.



Plate 5: An aerial view of TOR showing the Administrative block and other important sites. (Google Earth Search, 2009)

The top picture in plate 6 shows the DOAS system as it was mounted within the housing. The middle picture shows the ‘housing’ which accommodated the DOAS system.

The housing was provided with four (4) optical viewing windows in all four cardinal directions with the photograph showing the window in the east. The bottom picture shows the Administrative Block on top of which the housing was constructed.



Plate 6: Top picture - The DOAS system as it was mounted within the housing

Middle picture - Constructed housing for the DOAS system

Bottom picture - Administrative Block on top of which the housing was constructed

Figure 20 is an organogram depicting some of the manufacturing facilities in Tema and their approximate distances from the DOAS site, the point where the DOAS system was installed and data collected.

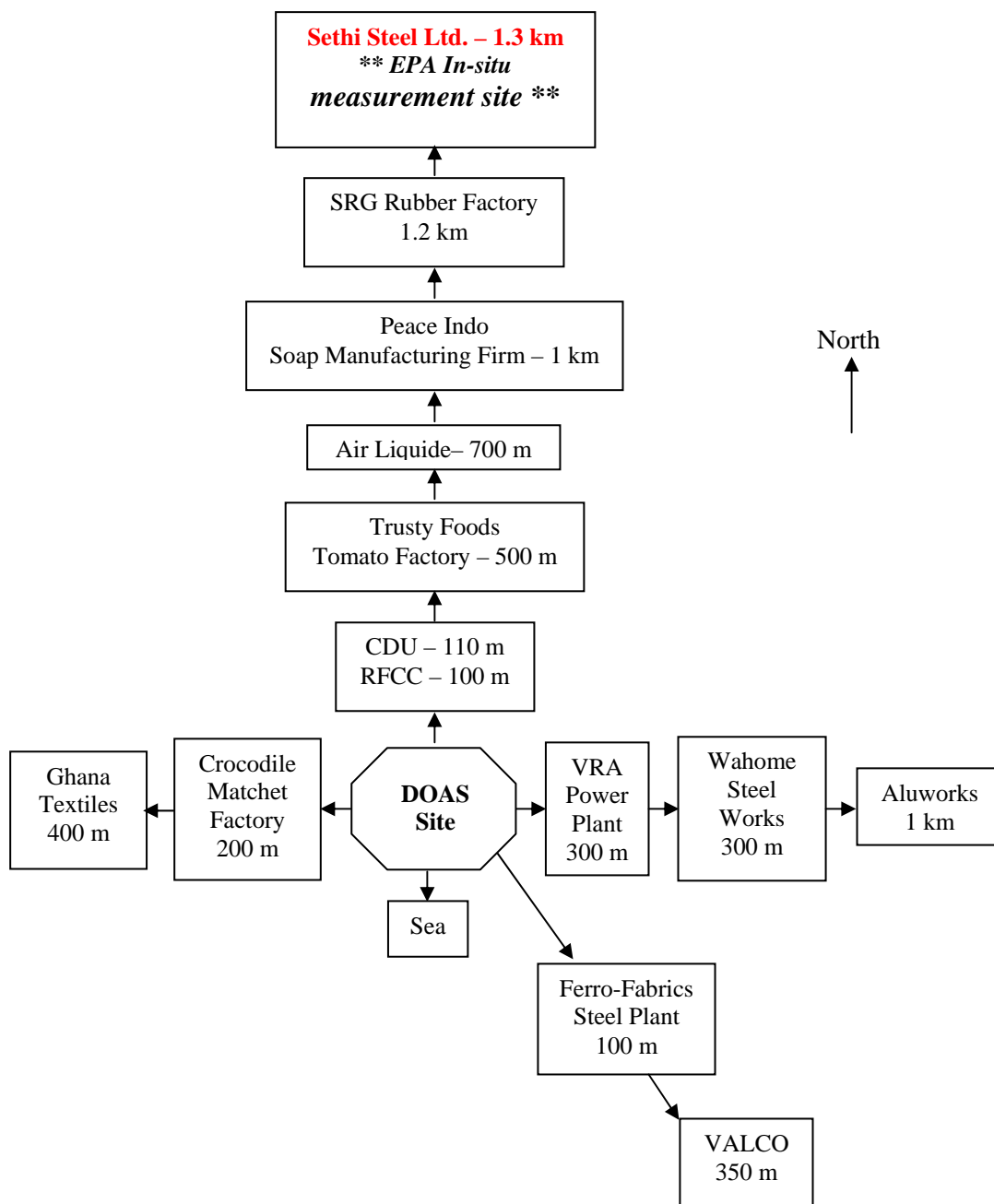


Figure 20: An organogram depicting some of the manufacturing facilities in Tema and their approximate distances from the site where the DOAS system was installed.

The Environmental Protection Agency (EPA), Ghana, carried out in-situ concentration measurements of SO₂ at Sethi Steel Ltd., a steel processing plant located in the north with respect to the DOAS site. The measurements at Sethi Steel were used as reference values during the analysis of data and used as the first method of validation.

Gases monitored

The gases monitored were NO₂, SO₂ and O₃. NO₂ was monitored within the visible region while SO₂ and O₃ were monitored in the uv region. Table 4 mentions the exact wavelength intervals within which these gases were observed.

Table 4: The gases monitored and the precise wavelength interval within which they were examined.

Gas	Wavelength Interval (nm)
NO ₂	4360 Å – 4600 Å
SO ₂	3120 Å – 3270 Å
O ₃	3100 Å – 3300 Å

Meteorological data for Tema

There was the need to critically examine the meteorological dynamics of Tema as the fate of released air pollutants are greatly influenced by the nature of the air mass into which they are released. The prevailing wind direction for Tema municipality is in the south-west for most part of the year.

Between January and March, however, there is a change in this dominant direction as a result of the influence of the north-east trade winds that blow from the Sahara desert towards the equator. This results in the wind changing its course unpredictably and blowing virtually in all directions.

Meteorological data on wind speed, wind direction, relative humidity and temperature for the month of January 2008 are presented.

CHAPTER FOUR

RESULTS AND DISCUSSIONS

This Chapter will have two (2) sets of results: Firstly, calibration and validation results of the DOAS system after it had been development, and secondly, results of field measurements conducted in Italy and Ghana.

CALIBRATION AND VALIDATION RESULTS

Authenticating the accuracy of sensor

This test was conducted to determine the suitability of the sensor installed and was done by studying the variation of its dark current with integration time. The entire 1024-pixel sensor was divided into five (5) blocks using the pixel positions as reference points. Table 5 illustrates how this partitioning was done while Table 6 gives the average values of the dark current obtained for each of the blocks of the sensor at the different integration times.

Table 5: Mode of partitioning the 1024-pixel sensor into blocks.

Pixel Position	1-205	206-410	411-615	616-820	821-1024
Block	1	2	3	4	5

Table 6: Average values of the dark current obtained at different integration times for each of the five (5) blocks on the face of the sensor.

Integration Time (ms)	Average dark current values for various Blocks (a.u.)				
	1	2	3	4	5
100	156.8	155.0	154.4	154.0	154.4
500	157.7	155.6	155.4	155.2	156.7
1000	163.6	160.0	157.7	158.4	162.0
2000	167.9	164.0	162.8	162.7	164.1
5000	181.7	178.6	176.0	174.5	177.5
10000	206.9	201.1	197.4	196.1	197.5
15000	228.5	223.7	220.2	220.4	218.9
20000	251.2	245.9	240.4	240.7	241.0
30000	296.7	289.6	283.7	283.2	285.2
60000	438.3	425.7	410.5	411.0	416.4
90000	577.0	555.9	537.5	538.5	544.4
120000	715.7	688.0	665.1	664.5	673.5
180000	990.6	950.4	914.4	916.1	930.1
210000	1125.6	1081.9	1038.7	1041.5	1055.9
240000	1260.0	1211.1	1162.8	1163.3	1182.7

Figure 21 shows graphs obtained for each of the five blocks on the face of the sensor. A top quality sensor is supposed to show a linear dependence of the dark current on integration time at each of the blocks of the sensor.

The scatter graph for each block showed a good linear variation between the dark current and integration time with a correlation coefficient value $R^2 = 0.9999$ for all the blocks. This characteristic property meets the design criterion for ideal sensors and thus validates the aptness of the sensor installed.

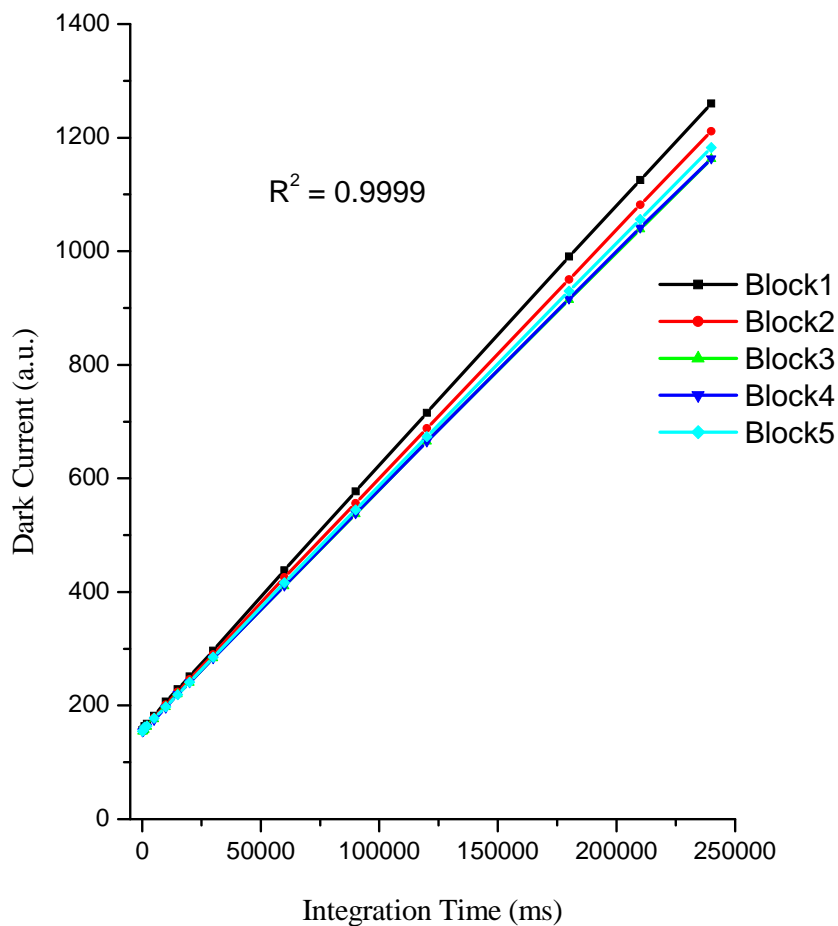


Figure 21: A graph showing the variation of the average dark current with integration time for the various blocks on the face of the sensor.

Calibration and determination of the linear dispersion of sensor

This test was conducted to calibrate the sensor against a known standard to guarantee accuracy, validate it and its measurement technique and determine the wavelength scale that is mapped onto the CCD. In Figure 22 the standard detectable Hg lines in the uv and visible spectral regions are represented by (a) and (b) respectively while the observable lines recorded during measurements in the uv and visible spectral regions using the sensor are represented by (x) and (y) respectively.

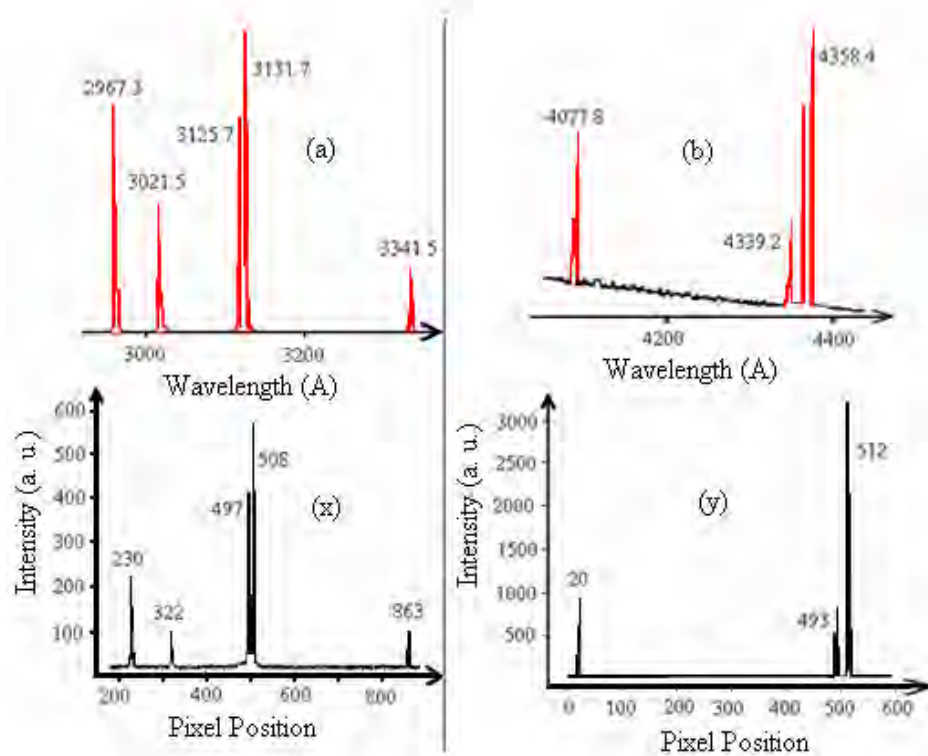


Figure 22: Graphs showing standard fine lines exhibited by Hg lamp

(a) in the uv and (b) visible spectral regions (Sources of discontinuous spectra) and those observed in pixels during measurements in the (x) uv and (y) visible spectral regions using the sensor.

From Figures 22 it will be observed that parallels can be drawn between the fixed lines exhibited by Hg lamp and the pixel positions recorded using the sensor. Table 7 gives a tabular correspondence showing the wavelength to pixel position pairs.

Table 7: Wavelength positions of fixed lines exhibited by Hg lamp and their corresponding pixel spots as observed using the sensor for spectra taken in the uv and visible regions.

UV Spectral Region		Visible Region	
Wavelength (Å)	Pixel Position	Wavelength (Å)	Pixel Position
2967	230	4077.8	20
3022	322	4339.2	493
3125	497	4358.4	512
3132	508		
3342	863		

A Plot of pixel position against wavelength gave a straight line of which the slope is the linear dispersion of the spectrometer. This is shown in Figure 23 for the uv (a) and visible (b) spectral regions respectively.

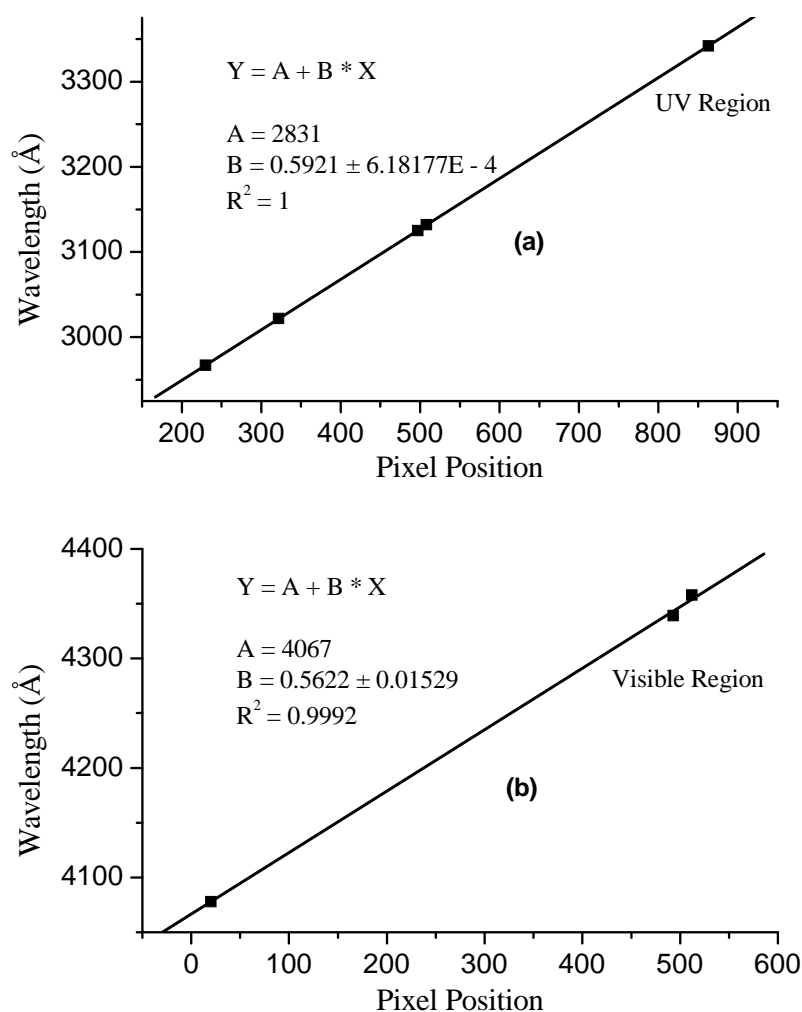


Figure 23: Graphs establishing the relationship between the wavelength and pixel-position pairs for measurements made in the (a) UV and (b) visible spectral regions.

Fitting linearly a general equation was obtained in the form:

$$Y = A + B * X \quad (23)$$

with X : pixel position

Y : corresponding wavelength

A and B are constants, with:

A : intercept on the y -axis

B : is the slope of the line

A has dimensions of wavelength while B , which is the linear dispersion of the sensor, has dimensions of Å per pixel. Their values obtained for measurements carried out in the uv and visible spectral regions are given in Table 8. The linear dispersion is a function of wavelength. Accordingly dissimilar values were obtained for the different spectral regions.

Table 8: The constants A and B obtained from a plot of pixel against wavelength for measurements in the uv and visible spectral regions.

Constant	UV Region	Visible Region
A (Å)	2831	4067
B (Å per pixel)	$0.5921 \pm 6.18177E - 4$	0.5622 ± 0.01529

The correlation established was used to determine the wavelength scale that was mapped onto the sensor, thereby converting pixels, as measured by the sensor, to wavelength in Å. Figures 24 (a) and (b) show plots of raw spectra as measured in pixels in the uv and visible spectral intervals respectively while (x) and (y) show the same graphs after conversion into wavelength in Å.

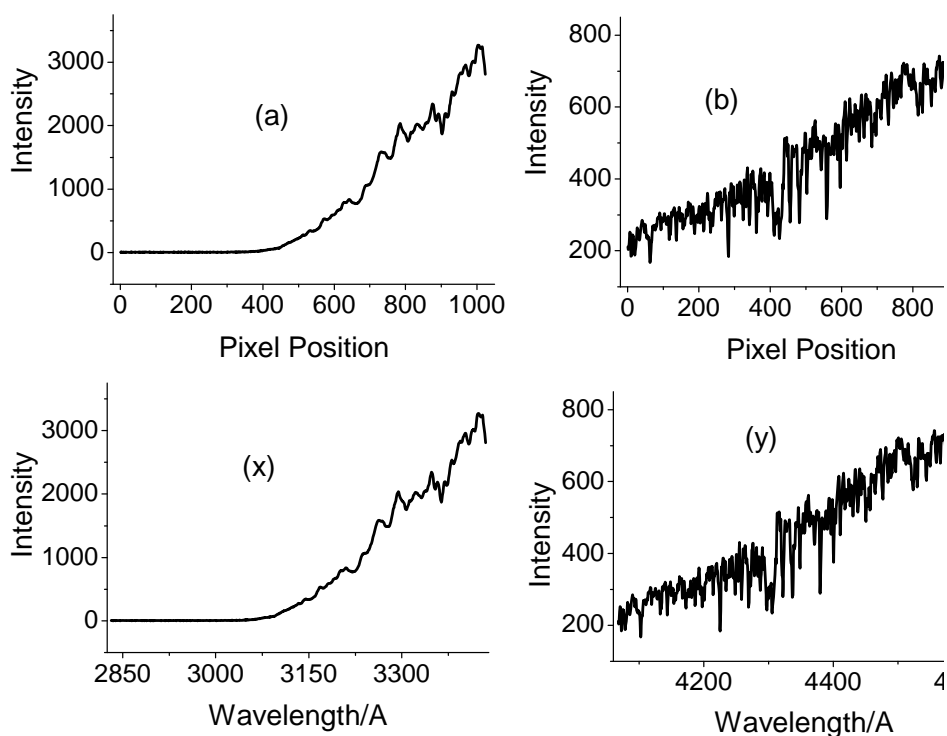


Figure 24: Graphs showing the raw spectra as recorded by the sensor in pixels for measurements in the (a) uv and (b) visible spectral regions respectively.

A typical raw data as recorded by the sensor (in pixels) for measurements carried out in the uv and visible spectral regions have been given in Appendix 1 and 2 respectively. The data is made up of a set of numbers with 10 columns and 103 rows with the last row having only four (4) numbers. This therefore gives a total of 1024 numbers, corresponding to the number of illuminated pixels in the sensor installed.

Laboratory Calibration Using a Gas Cell

A scatter graph of the two concentration values obtained (reference concentration against measured concentration) was plotted. The line of best fit was drawn and the correlation coefficient determined as shown in Figure 25. The reference measurement was thus used as the first method of validating the DOAS technique.

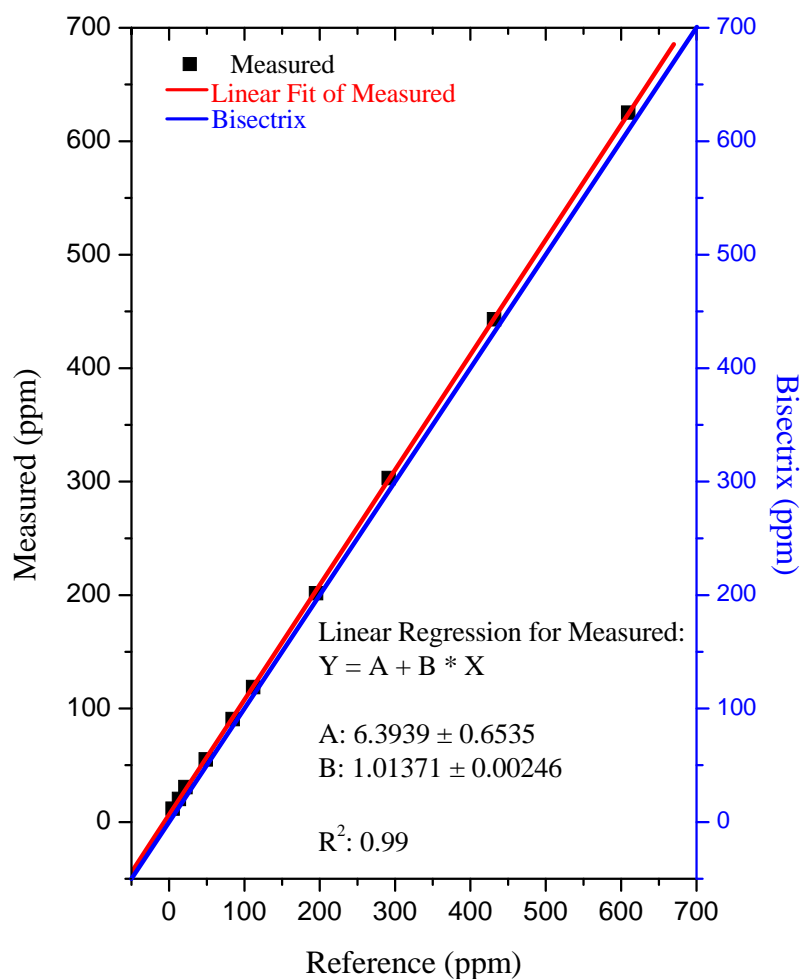


Figure 25: Scatter plot and line of best fit for NO₂ as determined in the gas cell (reference concentration) and retrieved using DOAS technique (measured concentration).

A study of the equation of best fit gives a correlation coefficient R^2 of 0.99. This signifies that the relation between the two data set is good and indicates how similar the reference and measured values are. A close look at the graph reveals a constant over-estimation of the DOAS technique relative to the theoretical calculation for both low and high concentration measurements. This is confirmed by the slope which is 1.01371, slightly greater than 1. This therefore illustrates and confirms how well the DOAS system operates and measures its concentrations.

Polarization Test

Plots illustrating the dependence of the normalized intensities of light (halogen lamp) reaching the sensor on wavelength are shown in Figure 26 (a) and (b). This has been done for the various polarizing angles and for measurements carried out in the uv and visible spectral regions respectively. The graph shows that maximum intensity of light was transmitted to the sensor at a polarizing angle of $+10^0$ while the minimum intensity was transmitted at -80^0 for both the uv and visible spectral regions. This is in agreement with theory as the angle between the maximum and minimum intensity transmitting angles should be 90^0 . Figure 27 shows the intensity variations at these two polarizing angles ($+10^0$ and -80^0) only.

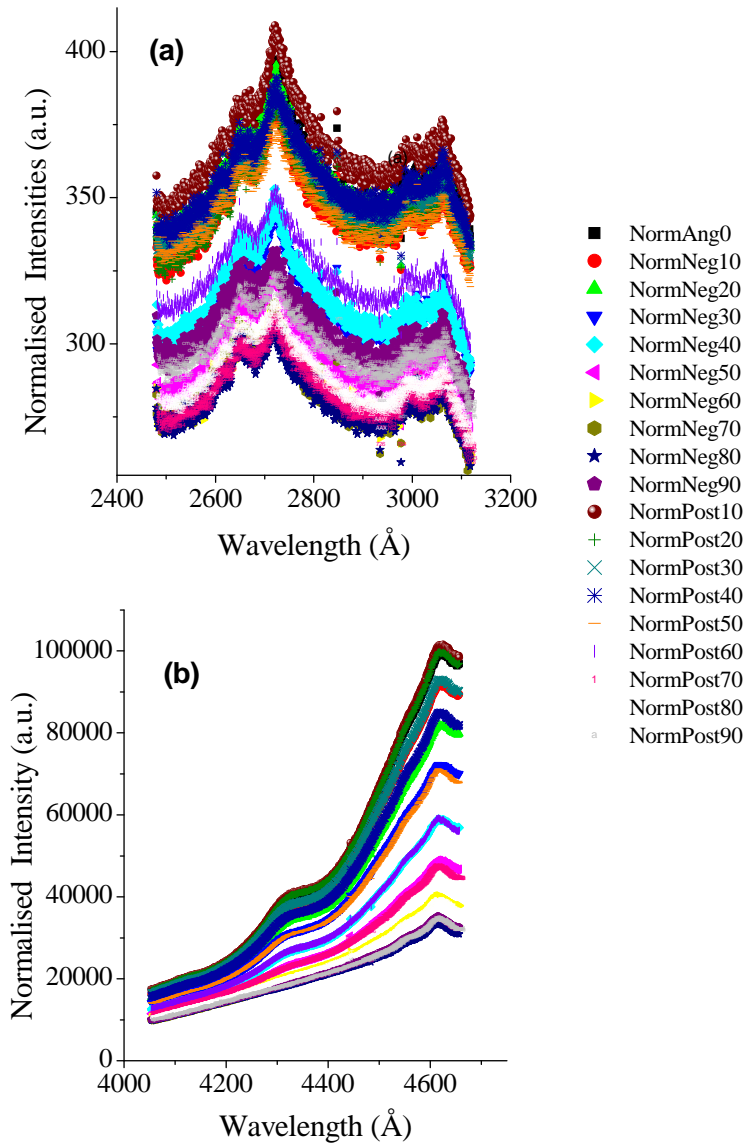


Figure 26: Graphs showing dependence of the normalized intensities of light reaching the sensor at the various polarizing angles on wavelength for measurements in (a) the uv and (b) visible spectral regions respectively.

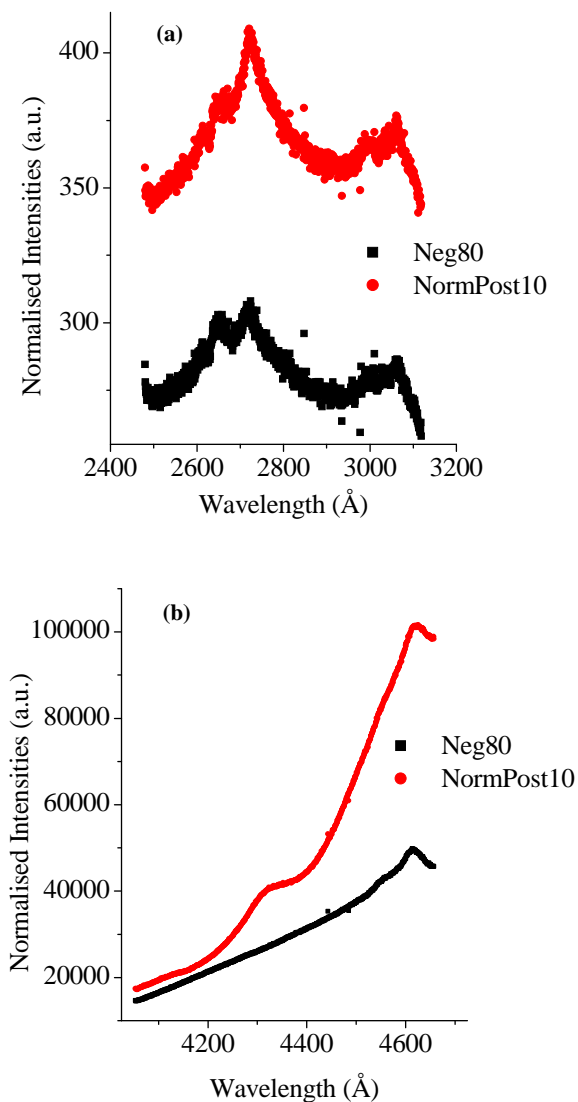


Figure 27: Graphs showing the same dependence of normalized intensities on wavelength for uv and visible spectral regions for the polarizing angles of $+10^0$ and -80^0 only measurements in (a) the uv and (b) visible spectral regions respectively.

The transmittances at the various polarizing angles and wavelengths were determined by dividing the normalized intensities with the maximum transmitted intensity (intensity at polarizing angle $+10^0$) for each polarizing angle and at each wavelength. Predictably this yielded a transmittance of 1 for the polarizing angle $+10^0$ for the various wavelengths. Figure 28 (a) and (b) show the transmittance at the various polarizing angles and wavelengths for the uv and visible spectral regions respectively.

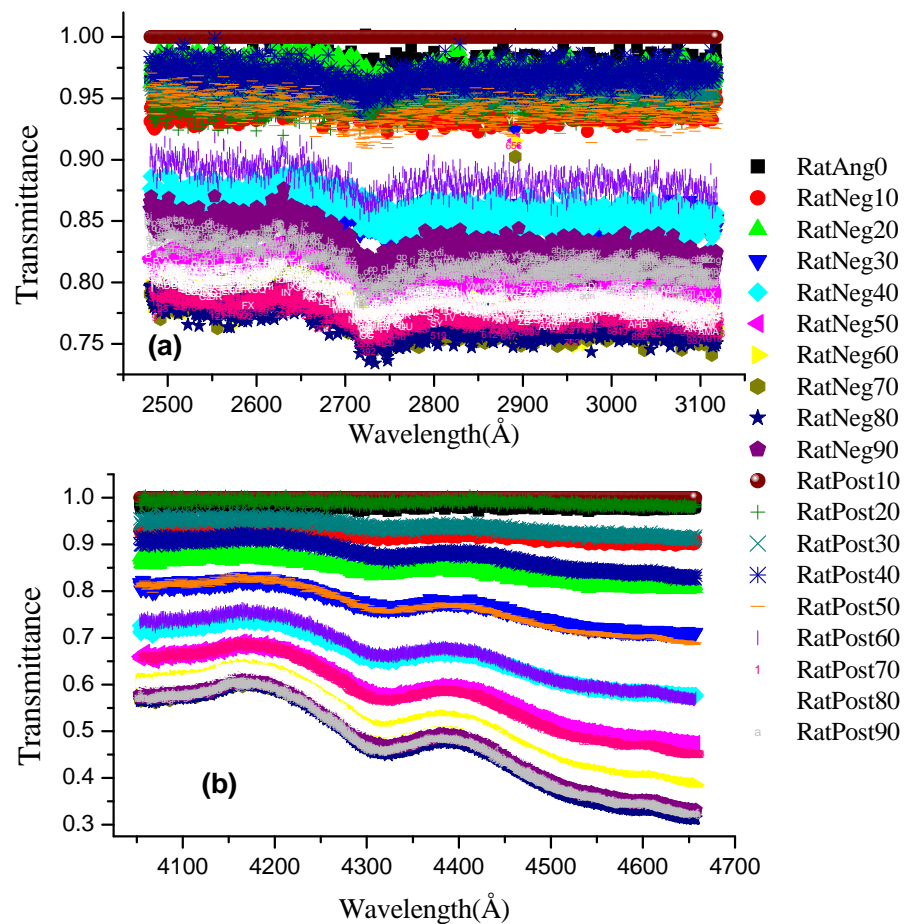


Figure 28: Graphs showing transmittance at the various polarizing angles and wavelengths for the (a) uv and (b) visible spectral regions.

Averaging over 100 pixels for each polarizing angle and plotting the averaged intensity values against the polarizing angles displayed a line of symmetry at $\theta = +10^0$, with the intensities gradually decreasing away from this line of symmetry. A line of symmetry was again displayed when the procedure was repeated using data from the transmittance. Figure 29 (a) and (b) are graphs showing the polarizing angles against the normalized intensities averaged over 100 pixels for measurements in the uv and visible spectral regions respectively. Figure 30 (a) and (b) are graphs of the polarizing angles against the transmittance averaged over 100 pixels for measurements in the uv and visible spectral regions respectively. The line of symmetry observed at $\theta = +10^0$ actually confirmed that the maximum intensity of light into the sensor was indeed transmitted at a polarizing angle of $+10^0$. With this finding the system was installed for field measurements with an orientation in which $\theta = +10^0$ was directed in the east to minimize the integration times during sunrise periods.

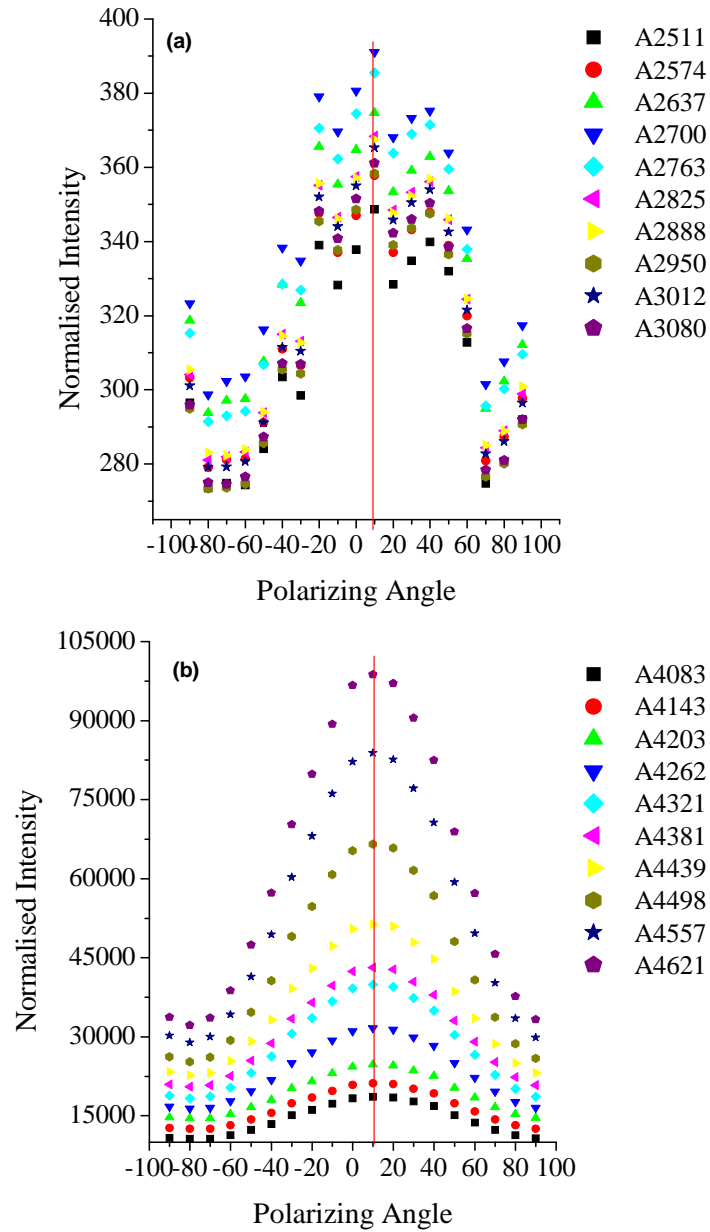


Figure 29: Graphs showing the polarizing angles against normalized intensities averaged over 100 pixels for measurements in the (a) uv and (b) visible spectral regions respectively.

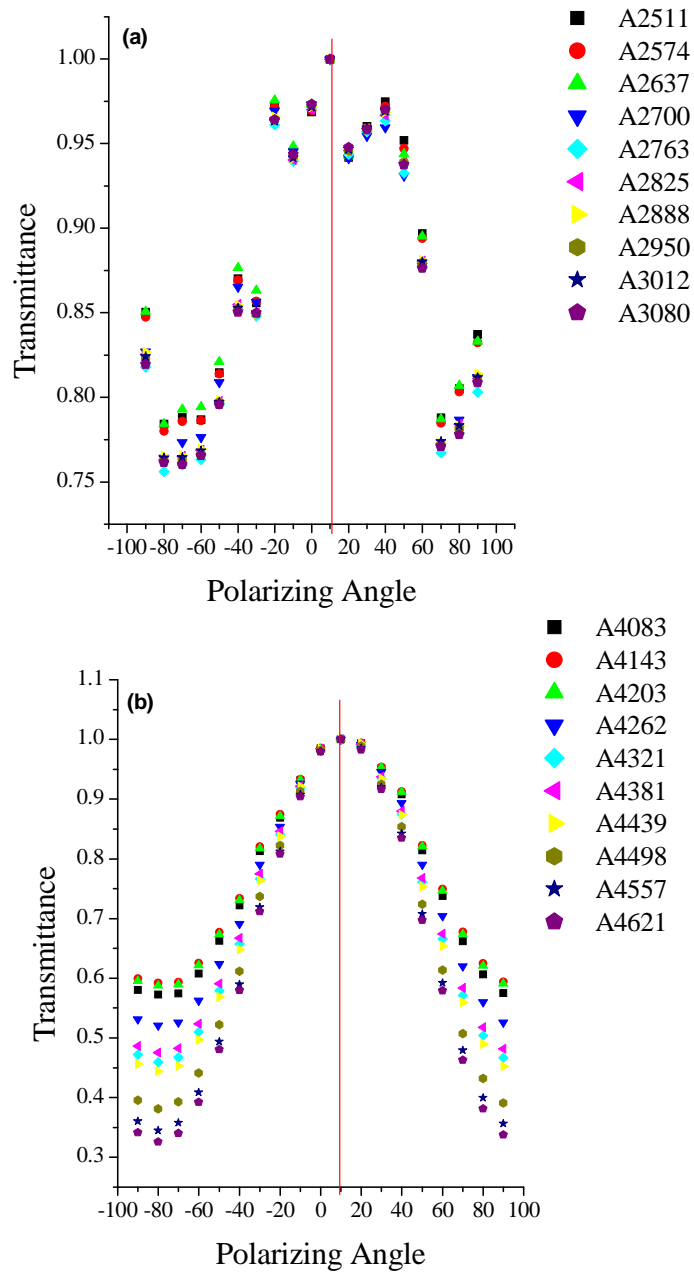


Figure 30: Graphs showing the polarizing angles against transmittance

Averaged over 100 pixels for measurements in the

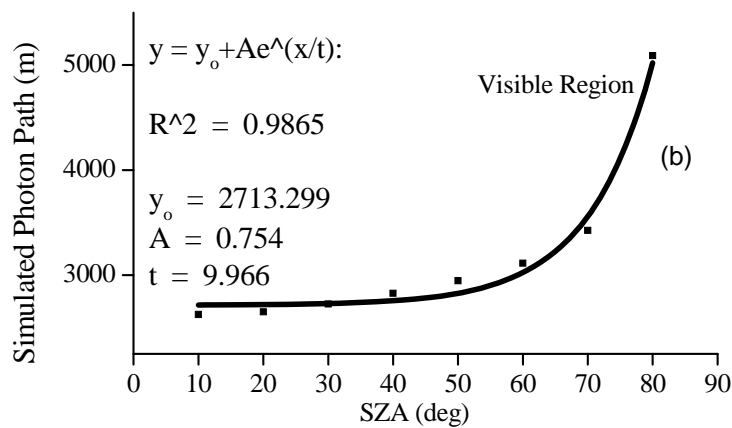
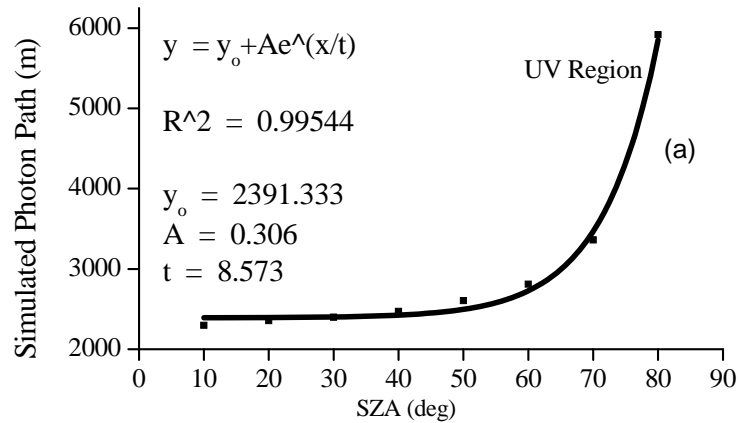
(a) uv and (b) visible spectral regions respectively.

Determination of photon path length in the atmosphere

After simulation the values obtained at the various solar zenith angles for the photon paths in the lower troposphere are presented in Table 9. A graph plotted using these values is shown in Figure 31 for measurements in the uv and visible spectral regions.

Table 9: Simulated photon paths in the UV and visible regions for the lower troposphere using various values of solar zenith angle.

S.Z.A	Photon Paths (km)	
	UV Region	Visible Region
10.0	2.296281507	2.624121080
20.0	2.357229497	2.649631774
30.0	2.397109779	2.723953768
40.0	2.469431032	2.827529574
50.0	2.603752596	2.946262290
60.0	2.810429982	3.114745413
70.0	3.362066233	3.426602394
80.0	5.915731598	5.089503127



Figures 31: Graphs showing the dependence of the photon path on SZA for simulations in the uv and visible spectral regions.

Using the best fits for the graphs (exponential growth) a general equation was obtained in the form:

$$y = y_0 + Ae^{\left(\frac{x}{t}\right)} \quad (24)$$

with x : the solar zenith angle (independent variable)

y : the corresponding photon path (dependent variable)

y_0 , A and t are constants.

The values of these constants obtained for the uv and visible spectral regions are given in Table 10.

Table 10: The constants obtained from a plot of simulated photon path against solar zenith angle for measurements in the uv and visible spectral regions.

Constant	UV Region	Visible region
y_0	2391.333	2713.299
A	0.306	0.754
t	8.573	9.966

With these constants substituted into the general established equation (24), PROMSAR was used to work out the mean path of photons for each value of the solar zenith angle in the uv and visible spectral regions.

Results of field measurements carried out

As already hinted field measurements were carried out at two different locations: firstly in Italy, then in Ghana.

Measurements carried out in Italy

Location: Institute of Atmospheric Science and Climate (ISAC) (44.3°N, 11.2 °E), Bologna. Concentrations of NO₂ were monitored at this site with measurements carried out in March 2005 on 9th, 10th and 11th. The concentration values obtained compared with values provided by the ARPA in-situ analyzer which was used as the first method of validation.

ARPA is the National Environmental Protection Agency of Italy and has a station located about 500 m away from ISAC where in-situ concentration measurements are carried out on some trace gases, including NO₂. Figure 32 is a scatter plot between the in-situ data released by ARPA and the outdoor concentrations of NO₂ as measured by the passive DOAS with a 3-km optical path length. The first three graphs (a-c) represent the scatter plots for measurements on March 9, 10 and 11, 2005 while the fourth (d) is the total scatter plot for the entire three days of measurements. Despite the difference in measurement techniques the two data set showed a good agreement. Considering the examined days singularly a correlation coefficient R^2 value of 0.9279, 0.9383 and 0.9029 were respectively obtained and based on the full data set ($N = 25$) a correlation coefficient of 0.9177 was obtained. The intercept of the linear fit for all the graphs is always positive underlying the constant over estimation of the passive DOAS technique with respect to the ARPA data set.

This constant over estimation can be attributed to the fact that the DOAS system, through out the measurement period, was focused towards a highway and therefore depicted the true averaged-path concentration value of NO₂ within that LOS.

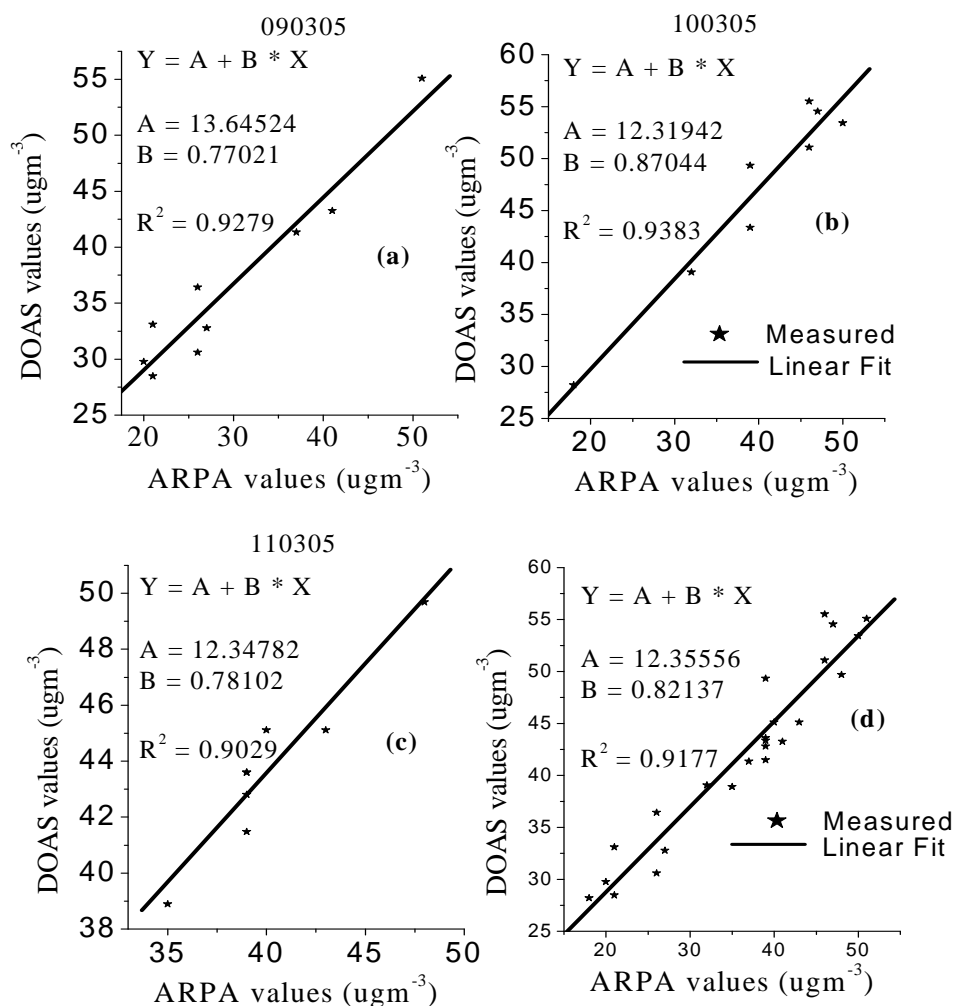


Figure 32: Scatter plots for NO₂ concentration between in-situ ARPA values and passive DOAS measurements in Bologna, Italy. Graphs (a-c) represent the scatter plots for March 9, 10 and 11, 2005 and (d) is the total scatter plot for all three days of measurements.

Measurements carried out at Ghana

Location: Tema Oil Refinery (TOR), Tema ($5^{\circ}39'59.88''$ N, $0^{\circ}00'21.26''$ E). For this site concentration values of NO_2 , SO_2 and O_3 will be presented for two different periods and in the four cardinal directions (north, south, east and west). The periods in question are January 2008 during the harmattan season and July and August 2008 during the rainy season.

Meteorological data for Tema

There was the need to critically examine the meteorological dynamics of Tema as the fate of released air pollutants are greatly influenced by the nature of the air mass into which they are released. The prevailing wind direction for Tema municipality is in the south-west for most part of the year.

Between January and March, however, there is a change in this dominant direction as a result of the influence of the north-east trade winds that blow from the Sahara desert towards the equator. This results in the wind changing its course unpredictably and blowing virtually in all directions. Meteorological data on wind speed, wind direction, relative humidity and temperature for the month of January 2008 are presented in Figure 33 (a-d) respectively.

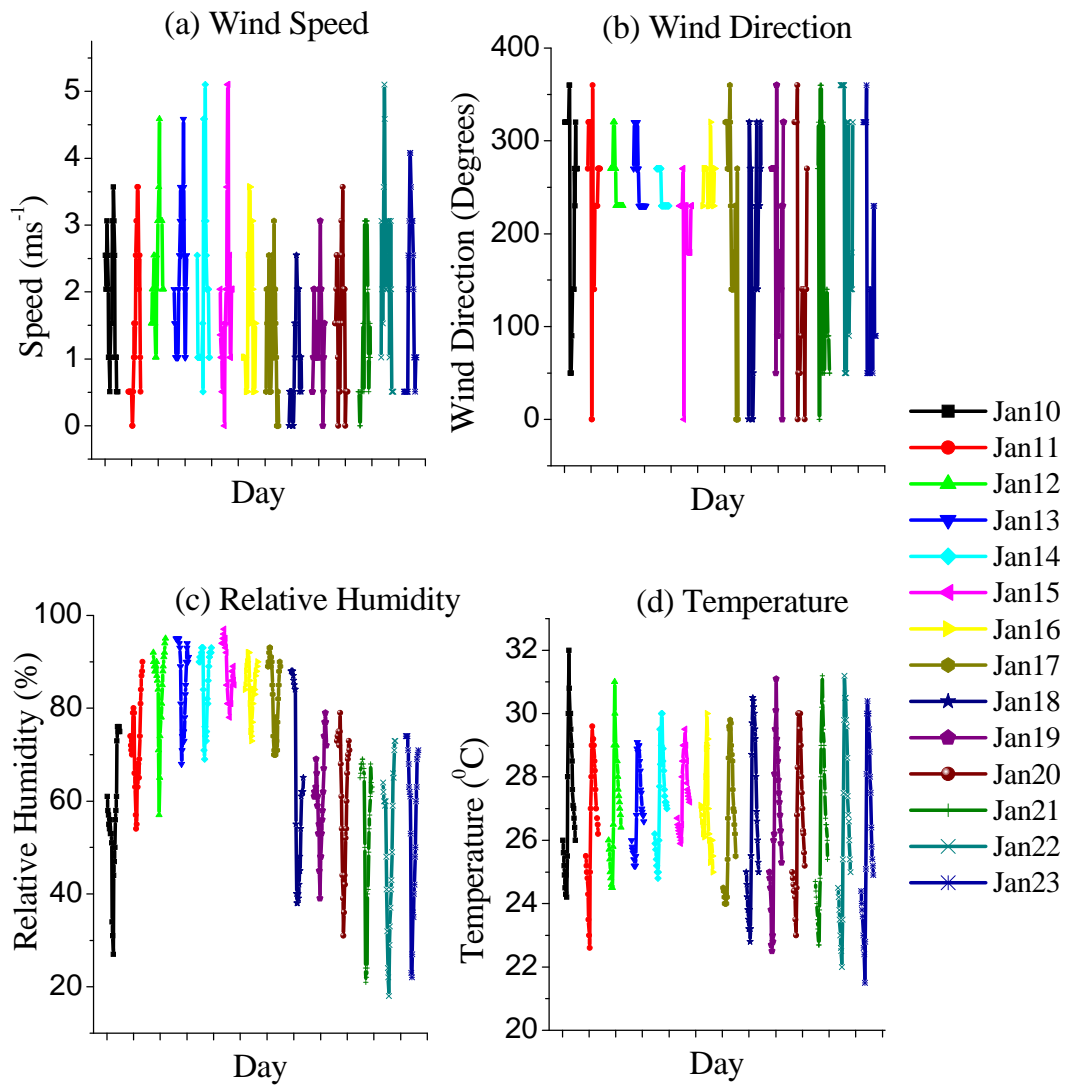


Figure 33 (a-d): Graphs showing daily variations in wind speed, wind direction, relative humidity and temperature respectively from January 10 to 23, 2008

NO₂ Measurements in January 2008

Comparison with measurements carried out by EPA-Ghana

Between December 2007 and January 2008 the Environmental Protection Agency of Ghana carried out concentration measurements of SO₂ at Sethi Steel Ltd, a steel processing plant in Tema. This plant is at a distance of about 1.3 km from TOR and falls directly in the northern line-of-sight of the DOAS system. Results obtained in January using the DOAS system were compared with measurements from the in-situ instruments carried out by EPA in the same month. This was used as the first method of validation. Figure 34 is a scatter plot between the concentration values of SO₂ released by EPA-Ghana and that measured using the passive DOAS technique with a 3-km optical path length. The graph is the scatter plot for measurements carried out from January 10 to 23, 2008.

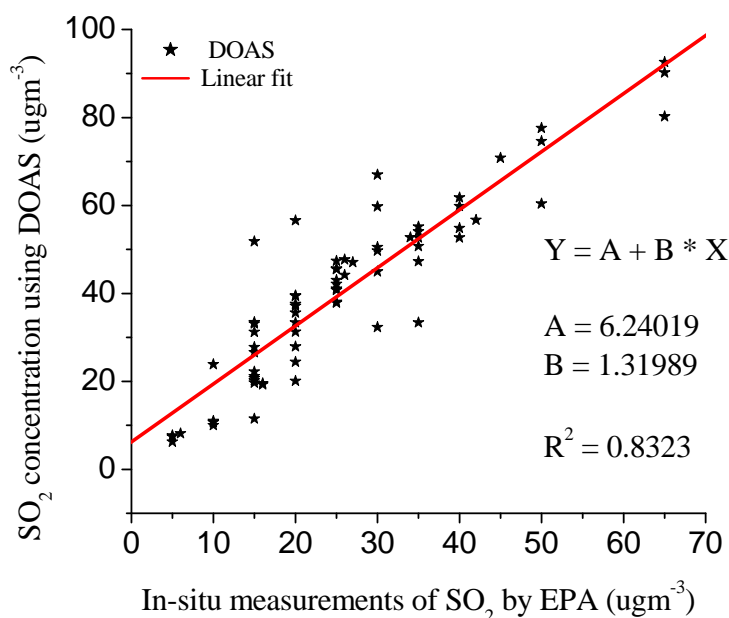


Figure 34: Scatter plot for SO₂ concentration between in-situ EPA values measured at Sethi Steel Ltd. and passive DOAS measurements for measurements in January 2008 over an area in Tema.

Here again regardless of the difference in measurement techniques – in-situ and long path passive DOAS – the two data set showed a good agreement with a correlation coefficient of 0.8323 considering the full data set ($N = 70$). The intercept of the linear fit for all the graphs is always positive underlying the constant over estimation of the passive DOAS technique with respect to the EPA data set. This constant over estimation can be attributed to the fact that there are a number of factories within that line-of-sight, as depicted on the organogram in Figure 19, and therefore the increase in the average concentration values of SO_2 , which in actual fact is a true reflection of the concentration in that direction. These facts confirm that the DOAS system measures the concentration of gases accurately.

All Measurements carried out in January 2008

In January 2008 measurements were carried out not only for the retrieval of SO_2 concentrations but also for the concentrations of NO_2 and O_3 . Figures 35, 36 and 37 respectively give a graphical representation of all these concentrations for measurements taken in the north, south, east and west directions from January 10 to 23.

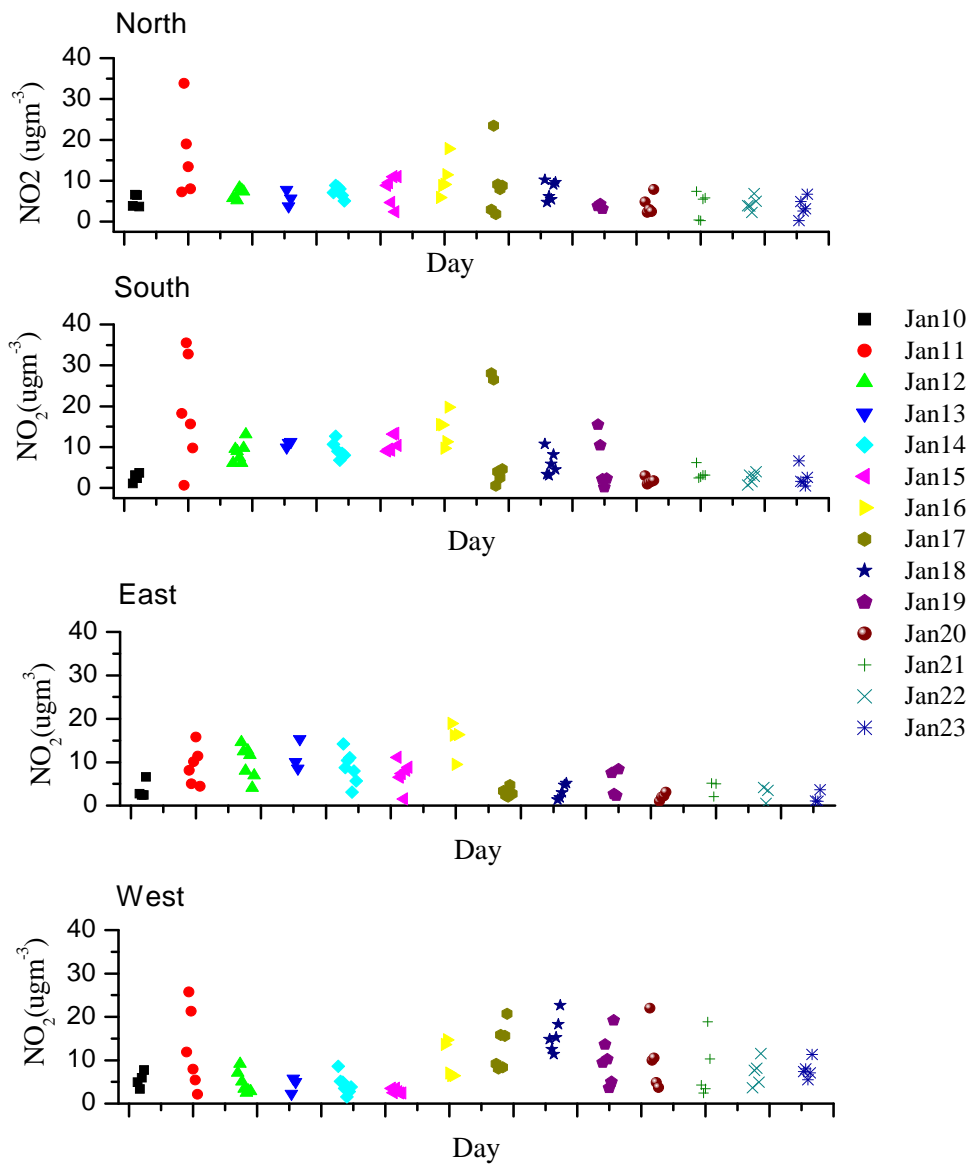


Figure 35: Graph showing concentrations of NO₂ monitored in the north, south, east and west from January 10 to 23, 2008.

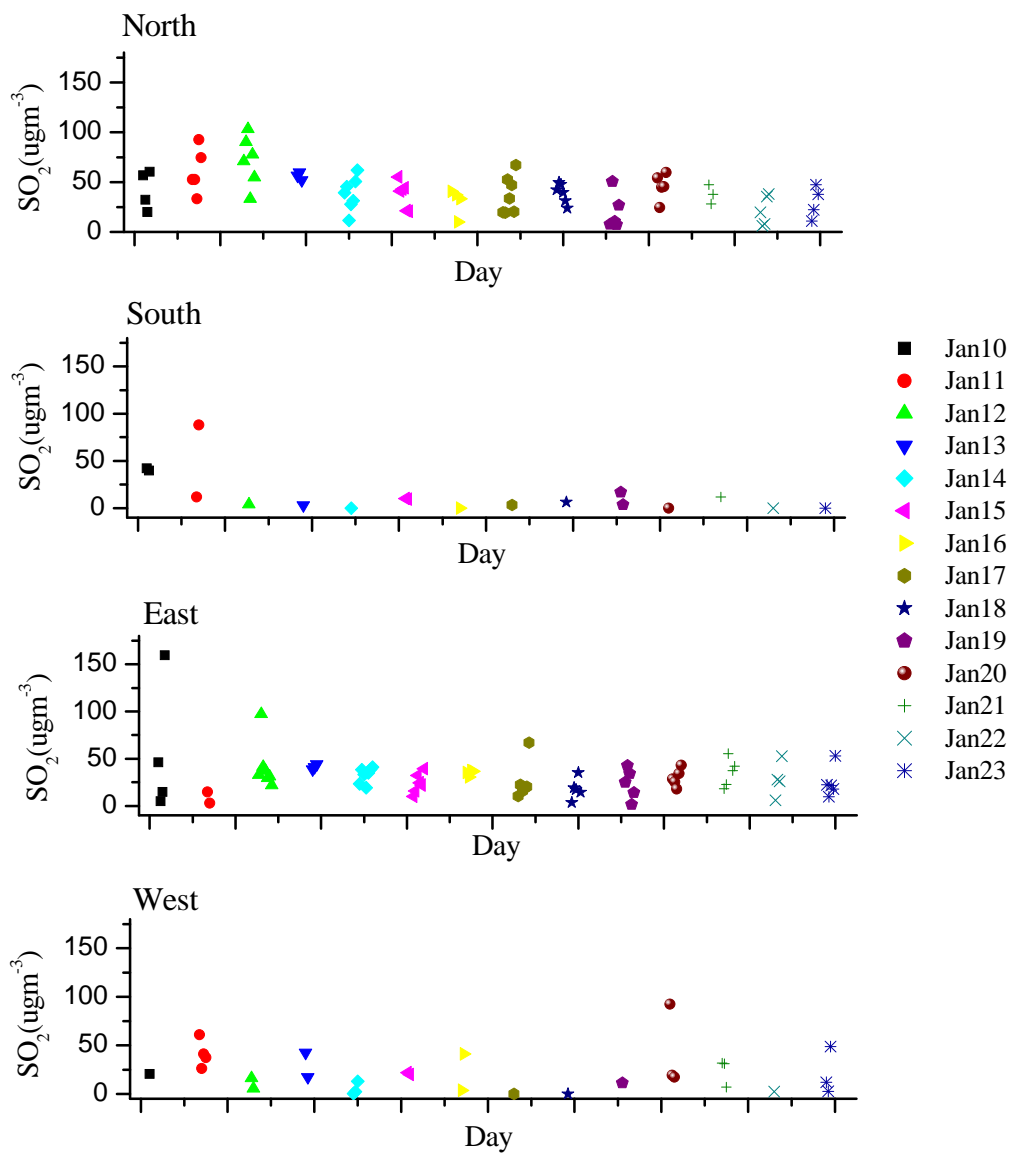


Figure 36: Graph showing concentrations of SO_2 monitored in the north, south, east and west from January 10 to 23, 2008.

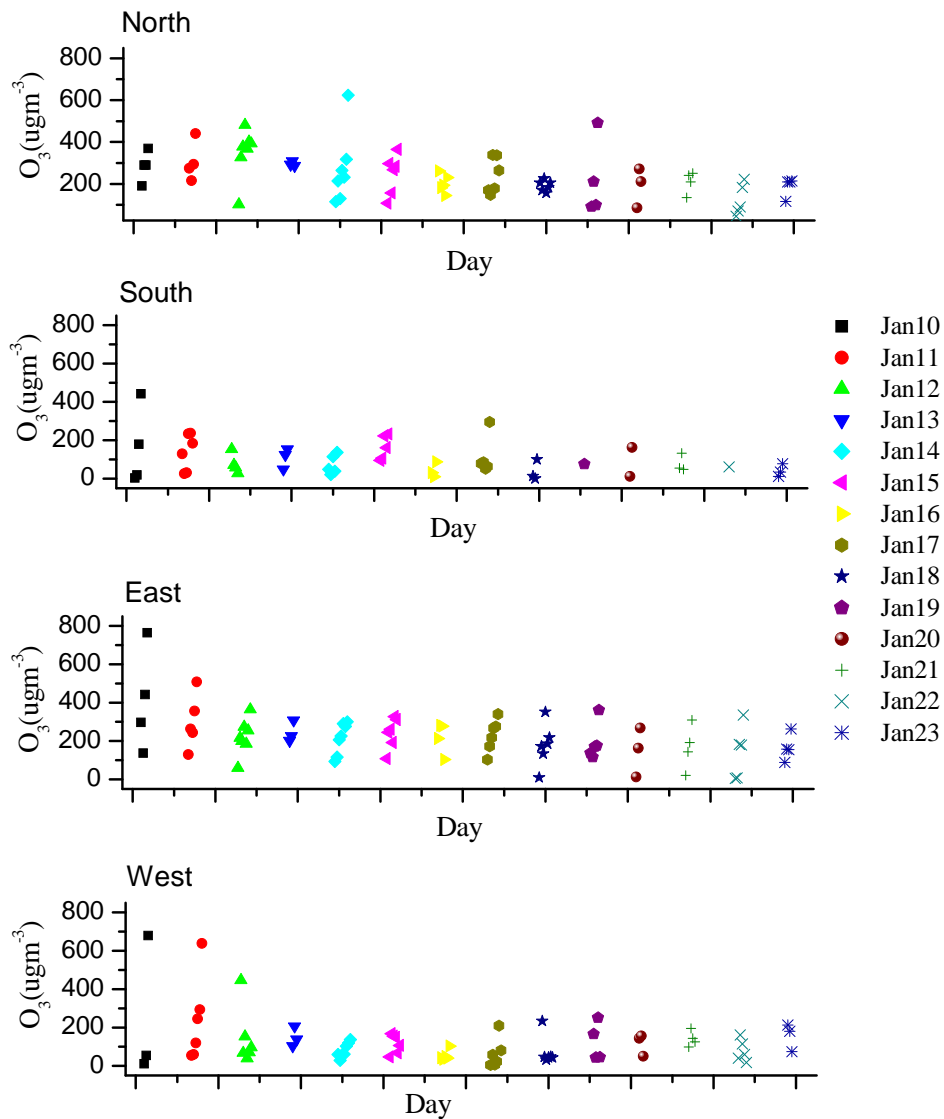


Figure 37: Graph showing concentrations of O_3 monitored in the north, south, east and west from January 10 to 23, 2008.

Graphical representation of concentration values measured in July and August in the north, south, east and west directions have been provided in Appendix 3 and 4 respectively.

The concentrations values of gases retrieved were compared to standard values as recommended by the Environmental Protection Agency (EPA) of Ghana, the European Union (EU), World Health Organization (WHO) and the Canadian Agency for Environmental Protection. Tables 11, 12 and 13, in that order, give the standard recommended levels of NO_2 , SO_2 and O_3 for an environment safe for habitation. Comparing the retrieved concentration values to the recommended levels it will be observed that for NO_2 and SO_2 concentrations measured in the cardinal directions were below the approved levels, meaning that pollution levels were within the approved limits as far as these pollutants were concerned. The findings were however not the same for O_3 as measured concentrations were above recommended values. Further investigation needs to be conducted to establish the source of such high levels of tropospheric ozone. This is because although the majority of tropospheric ozone formation occurs when its precursors, nitrogen oxides (NO_x), carbon monoxide (CO) and volatile organic compounds (VOC's) like fuels and xylene, react in the atmosphere in the presence of sunlight, there is also the occasional migration of stratospheric ozone down into the troposphere. Among its precursors only NO_2 was measured in this project and therefore the need to conduct the further study to ascertain the cause (s) of such high levels of O_3 .

Table 11: Standard recommended levels of NO₂.

	Standard Values (μgm^{-3})					
	Canada Guidelines			WHO	EU	EPA
	Des.	Acpt.	Tol.			Ghana
1 hr.	na [*]	394	985	389	200	
24 hrs.	na [*]	196	296	148	na [*]	
Annual	59	98	na [*]	na [*]	40	
Ind. 1 hr.						400
Resd. 1 hr.						200
Ind. 24 hrs.						150
Resd. 24 hrs						60
Ind. 1 yr.						na [*]
Resd. 1 yr.						na [*]

Ind. – Industrial

Resd. – Residential

Des. – Desirable

Acpt. – Acceptable

Tol. – Tolerable

na^{*} - data for these not available

Table 12: Standard recommended levels of SO₂.

	Standard Values (μgm^{-3})					
	Canada Guidelines			WHO	EU	EPA
	Des.	Acpt.	Tol.			Ghana
1 hr.	442	858	na*	334	350	
24 hrs.	147	296	785	98-150	125	
Annual	29	60	na*	39-60	20	
Ind. 1 hour						900
Resd. 1 hr.						700
Ind. 24 hrs.						150
Resd. 24 hrs.						100
Ind. 1 yr.						80
Resd. 1 yr.						50

Ind. – Industrial

Resd. – Residential

Des. – Desirable

Acpt. – Acceptable

Tol. – Tolerable

na* - data for these not available

Table 13: Standard recommended levels of O₃.

Ozone	Standard Values (μgm^{-3})					
	Canada Guidelines			WHO	EU	EPA
	Des.	Acpt.	Tol.			Ghana
1 hr.	98	158	294	96-193	120	
24 hrs.	29	48	na*	na*	na*	
Annual	na*	29	na*	na*	na*	
Ind. 1 hr.						na*
Resd .1 hr.						na*
Ind. 24 hr.						na*
Resd .24 hrs.						na*
Ind. 1 yr.						na*
Resd. 1 yr.						na*

Ind. – Industrial

Resd. – Residential

Des. – Desirable

Acpt. – Acceptable

Tol. – Tolerable

na* - data for these not available

Effect of wind speed and direction

Using the Beaufort Wind Force Scale (an empirical measure for describing wind speed), calm, light air, light breeze and gentle breeze are expressions that can be used to describe the nature of wind in Tema. This is because wind speeds range from 0 to 5.2 ms^{-2} , as shown in figure 29 (a), resulting in a categorization between 0 and 3 in terms of Beaufort numbers. Wind speeds this low result in the laminar flow of pollutants, thereby restricting pollution movements specifically in the wind direction. The path of the produced pollutants can then be traced specifically to the wind direction at the time.

For Tema the dominant wind direction for most part of the year is in the south-west direction. Considering the geography of Tema, as depicted in Plate 4, it will be realized that settlements in this direction begin from Sakumono extending to Lashibi and Nungua. These settlements are at least 10 km from Tema and therefore pollution levels will have reduced even further before reaching there due to dispersion. The immediate residential areas in Tema are dotted in all the other directions. On the other hand, between January and March when there is a change in the prevailing wind direction due to the influence of the north-east trade winds that blow from the Sahara desert towards the equator, there is a change in the prevailing wind direction, resulting in the wind changing its course unpredictably and blowing virtually in all directions. This means that during such periods pollutant gases are dispersed in all directions and subsequently all over the townships in and around Tema, exposing all communities to the effects of pollution.

CHAPTER FIVE

CONCLUSIONS AND RECOMMENDATIONS

CONCLUSIONS

A Differential Optical Absorption Spectroscopy (DOAS) system that exploits the capacity to utilize sunlight for the detection of gases has been developed and used for the measurement of the concentrations of NO₂, SO₂ and O₃. Its spectrometer unit consisted of an optical and electronic unit. The optical unit was made up of a Cassegrain telescope that focused the incoming sunlight through a cell, an optical filter (to minimize extraneous scattered light in the monochromator), an entrance slit and finally onto a solid state ccd sensor with 1024 pixels whose dark current was decreased to negligible levels by reducing its operating temperature to about 10 °C. The slit and detector positions were set to produce an image with the strongest intensity because they were positioned to have the maximum amount of light passing through them. The grating could be moved by a stepper motor and as a result the spectrometer unit, by means of this movable dispersion element, could analyze a 2500-8000 Å spectral range. The electronic unit controlled the operating mode of all the components of the optical unit by running a custom-built program.

A mirror was fixed in front of the spectrometer unit and the provision of a stepper motor to rotate this mirror facilitated measurements of scattered solar radiation from the three entrance windows in the vertical (for reference measurements) and horizontal left and right directions.

Using Beer-Lambert's law the acquired spectra were processed to extract the optical depth differences of the measured spectra with respect to the reference spectrum. The obtained values were correlated with the spectral "fingerprints" or absorption cross sections of the gases to calculate the slant column amounts. NO_2 was retrieved within the interval 4360-4600 Å while SO_2 and O_3 were retrieved within the interval 3120-3270 Å and 3100-3300 Å respectively. Levenberg-Marquardt multivariable minimization was used to achieve the best spectral alignment to fit the measured spectra to the reference spectrum. Applying differential spectroscopy the effects of low frequency absorption cross-sections characteristic of scattering and other extinction processes considered as perturbations were eliminated leaving just the fast varying cross-section responsible for pure molecular absorption. The technique of eliminating the ring effect by including a ring effect cross section as an additional pseudo-absorber was used. This was done by calculating the reciprocal of the measured spectrum and fitting it directly to the measured spectrum during the retrieval process which significantly improved the detection limit. The radiative transfer model PROMSAR was used for the simulation of the photon path length to work out the mean path of photons for every solar zenith angle. Dividing the slant column amounts by the photon path length gave the concentration required.

The accuracy of the instrument was confirmed in two field measurements: Firstly at the Institute of Atmospheric Science and Climate (ISAC), in Bologna (44.3°N, 11.2 °E), Italy for the measurement of NO₂ during the winter season of March 2005.

It was then used in Ghana at Tema Oil Refinery (TOR), Tema (5°39'59.88" N, 0°00'21.26"E) where data was collected and analyzed for NO₂, SO₂ and O₃ in January 2008 during the harmattan season and then in July and August of 2008 during the raining seasons.

For all measurements the system was operated in the passive mode at a height of about 50 m above the ground and concentrations retrieved within an average optical path length of 3 km. For measurements in Italy concentration values of NO₂ (in µgm⁻³) were in the range $28.21 \leq \text{NO}_2 \leq 55.51$ while in Ghana concentration values were: $0.16 \leq \text{NO}_2 \leq 35.48$, $0.43 \leq \text{SO}_2 \leq 159.43$, $0.03 \leq \text{O}_3 \leq 764.29$ for measurements in the dry season and $0.02 \leq \text{NO}_2 \leq 25.71$, $0.15 \leq \text{SO}_2 \leq 166.37$, $1.46 \leq \text{O}_3 \leq 688.84$ for measurements in the raining season. NO₂ values were usually high in the mornings, reduced towards the afternoon, due to dissociation in sunlight and increased again towards sundown. Gradual increases in the concentrations of SO₂ and O₃ from morning to evening indicate a build-up in their concentration as a result of industrial and vehicular activities. Concentration values of NO₂ and SO₂ measured were below the approved levels whereas those for O₃ were above recommended values. These concentration values obtained were then compared with measurements from in-situ instruments carried out by the Environmental Protection Agencies in Italy (ARPA) and Ghana (EPA) as the first method of validation.

A correlation coefficient greater than 0.8 obtained for both field measurements established the good agreement between the two-data sets and confirmed the suitability of the DOAS system for the retrieval of concentrations of atmospheric trace gases.

An additional study of some meteorological parameters like wind speed and direction, relative humidity and temperature were carried out for the local area of Tema as the fate of air pollutants released into an area is greatly manipulated by the activities and uniqueness of the air mass into which they are emitted. From this study it came out that the prevailing wind direction for Tema is in the south-west. What's more, the geography of Tema shows that settlements in this direction are at least 10 km away from Tema, beginning from Sakumono and extending to Lashibi and Nungua. Pollution levels will have reduced before reaching these settlements due to dispersion. The very immediate residential areas in Tema are dotted in all the other directions. Between January and March each year, however, there is a change in the dominant wind direction due to the influence of the north-east trade winds that blow from the Sahara desert towards the equator. This results in the wind blowing virtually in all directions and dispersing pollutant gases all over the townships in and around Tema, exposing communities such as Ashiaman in the north; Harbor Area and Tema New Town in the south; Kpong in the east and Communities 7 and 8 in the west to harmful effects of pollution.

It is said that the brain is the largest oxygen consumer in our body and therefore inhaling polluted air decreases its oxygen supply, bringing about a decrease in its efficiency. One of the greatest challenges humanity is facing today is the understanding of the complex issues of environmental change. Our efforts to understand the fundamental physical and chemical process that control occurrences in the atmosphere are not only motivated by scientific curiosity and inquisitiveness, but more importantly by the desire to assess and mitigate our anthropogenic activities that impact negatively on the atmosphere leading to the production of such pollutant gases. Such a DOAS spectroscopic technique being robust and affordable has a great potential to become an industrially well-established technology that can help us in quantifying our atmospheric releases and subsequently enable us monitor and protect our environment.

RECOMMENDATIONS

The DOAS system developed was operated in the passive mode with an average optical path length of 3 km. Concentrations measured were therefore restricted within the 3 km range with pollutant gases beyond this 3 km radius escaping detection by the DOAS system. It is recommended that a mobile system be obtained so as to enable measurements virtually at all places.

Measurements were limited in the north, south, east and west and in the horizontal line-of-sight. A system should be obtained such that measurements could be taken in all directions and at different angles relative to the zenith. This will provide a complete 3-D map of the concentrations of the minor gases present in the atmosphere.

In Ghana, between January and March the wind direction becomes unpredictable blowing virtually in all directions. Consequently pollutants are dispersed in all directions affecting communities, especially those located within the immediate environs of Tema. The EPA should be announcing daily safe sunshine exposure hours to the public so as to prevent the incidence of sunburns which is mainly caused by ultraviolet radiation, commonly from the sun's rays.

REFERENCES

- Abreu, L. W. & Anderson, G. P. (1996). The Modtran 2/3 report and Lowtran 7 model. Philips Laboratory, Geophysics Directorate. PL/GPOS, Hascom AFB, MA 01731-3010.
- Amoateng, C. A. (2000). "Gas Emissions in Crude Oil Refinery Processes". Proceedings, Monitoring of Air Pollution due to Combustion, Publication of LAFOC, University of Cape Coast, Ghana, 2000.
- Andrea P, Fabrizio R, Giorgio G, Danielle B, Ubaldo B, Ivan, K. and Alexey O. (2002). Off-axis measurements of atmospheric trace gases by use of an airborne uv spectrometer. Applied Optics, Vol. 41, (27), 5593-5599.
- Armerding, W., Spiekermann, M., and Comes, F. J. (1994). OH Multipass absorption: Absolute and In-situ Method for Local Monitoring of Tropospheric Hydroxyl Radicals. J. Geophys. Res., 99, 1225-1230.
- Arpag, K. H., Johnston, P. V., Miller, H. L., Sanders R. W., and Solomon, S. (1994). Observation of stratospheric BrO column over Colorado, 40 °N. J. Geophys. Res. 99, 8175-8181.
- Baldini, G., Grilli, E., and Guzzi, M. (1975). Simple derivative optical spectrometer. Appl. Opt. 14, 2687-2690.
- Berk, A., Anderson, G. P., Acharya, P. K., Chetwynd, J. H., Bernstein, L. S., Shettle, E. P., Matthew, M. W., and Adler-Golden, S. M. (2000).: MODTRAN4 USER's MANUAL. Hanscom AFB: Air Force Research, Space Vehicles Directorate, Air Force Command, MA 01731-3010.

- Bonfiglioli, G., and Brovotto, P. (1964). Principles of Self-Modulating Derivative Optical Spectroscopy. *Appl. Opt.* 3, 1417-1424.
- Borrell, P., Bultjes, P., Grennfelt, P., and Hov, O. (1997). *Photo-oxidants, Acid and tools: Policy Applications of EUROTRAC Results*. Springer.
- Brandenburger, U., Brauers, T., Dorn, H. P., Hausmann, M., and Ehhalt, D. H. (1998). Measurements of tropospheric hydroxyl radicals by folded long-path laser absorption during the field campaign POPCORN. *J. Atmos. Chem.* 31, (1-2).
- Cantrell, C. A., Stedman, D. H., and Wendel, G. J. (1984). Measurement of atmospheric peroxy-radicals by chemical amplification, *Anal Chem.* 56, 1496-1502.
- Chance, K. (1998). Analysis of BrO measurements from the Global Ozone Monitoring Experiment, *Geophys. Res. Lett.*, 25, 3335-3338.
- Collier, G. L., and Singleton, F. (1956). Infra-Red Analysis by the Derivative Method. *J. Appl. Chem.*, 6, 495.
- Comparative City Statistics, (2004), State of the Environment in Riga 2001, Retrieved August 28, 2009 from http://www.ceroi.net/reports/riga/air_things/what_is_doas.htm.
- Doku, S. K. (1999). "Case Study on Combustion Processes in Thermal Plant and Energy Generation–Takoradi Thermal Power Plant", Proceedings of Workshop on Combustion Diagnostics and Optical techniques, ICS-UNIDO and University Of Cape Coast, Laser and Fiber Optics Center.
- Drummond, J. W., Volz, A. and Ehhalt, D.H. (1985). An optimized chemiluminescence detector for tropospheric NO measurements. *J. atmos. Chem.* 2, 287–306.

- Dubrovkin, I. M. (1983). Spectrometry by recording derivatives. *J. of App. Spect.* Vol 39, (6), 1341-1353.
- Fietkau, S., Medeke, T., Adukpo, D. C., Ladstatter-Weibenmayer, A., Lowe, A. G., Oetjen, H., Richter, A., Wittrock, F., and Burrows, J. P. (2002). Multi-axis DOAS observation of atmospheric trace gases in Nairobi and Bremen. IGAC meeting. Retrieved June 12, 2009, from http://www.iup.uni-bremen.de/doas/posters/igac_0209_fietkau.pdf.
- Galle, B. (1999). *Development and application of methods based on DOAS and FTIR absorption spectroscopy for atmospheric research*. Ph.D. thesis, Dep. of Experimental Physics, Chalmers University of technology, Sweden.
- Ghana City Tema: Retrieved August 4, 2009, from <http://www.ghanaweb.com/GhanaHomePage/geography/tema.php>.
- Giese, A. T., and French, C. S. (1955). The Analysis of Overlapping Spectral Absorption Bands by Derivative Spectrophotometry. *Appl. Spectrosc.* 9, 78-96.
- Giovanelli, G., Bonasoni, P., and Evangelisti, F. (1989). Measurements of stratospheric gas absorption in UV and visible spectral regions, in: Colacino, M., Giovanelli, G., Stefanutti, L. (Eds), 1st Workshop, Italian Research on Antarctic Atmosphere. SIF Conference Proceedings, 20, 197-214.
- Giovanelli, G., Bonasoni, P., and Evangelisti, F. (1990). O₃ and NO₂ Ground-based measurements at Terra Nova Bay, Antarctica, in: Colacino, M., Giovanelli, G., Stefanutti, L. (Eds), 2nd Workshop, Italian Research on Antarctic Atmosphere. SIF Conference Proceedings, 27, 255-268.

- Giovanelli, G., Bonasoni, P., and Evangelisti, F. (1992). Determination of gas column amount by solar zenith radiation measurements, in: Colacino, M., Giovanelli, G., Stefanutti, L. (Eds), 4th Workshop, Italian Research on Antarctic Atmosphere. SIF Conference Proceedings. 35, 453-467.
- GOME-2 Measurements. Retrieved September 1, 2009 from <http://www.iup.uni-bremen.de/doas/gome-2.htm>.
- Google Earth Search (2009). Retrieved March 15, 2010.
- Gottwald, M., Bovensmann, H., Lichtenberg, G., Noel, S., Von-Bargen, A., Slijkhuis, S., Piders, A., Hoogeveen, R., Von-Savigny, C., Buchwitz, M., Kokhanovsky, A., Richter, A., Rozanov, A., Holzer-Popp, T., Bramstedt, K., Lambert, J. C., Skupin, J., Wittrock, F., Schrijver, H., and Burrows, J. P. (2006). SCIAMACHY, Monitoring the Changing Earth's Atmosphere: Published by DLR.
- Graber, W. K., Furger, M., and Poggio, L. (1997). DOAS and scintillation anemometry for the determination of trace gas fluxes and budgets. Proceedings of Envirosense, Munich, (SPIE 1997 3106, 128-136).
- Grainger, J. F., and J. Ring. (1962). Fraunhofer line profiles, Nature, 193762.
- Hamamatsu Photonics, 2003. Retrieved June 16, 2011 from http://jp.hamamatsu.com/products/sensor-ssd/pd101/pd105/pd106/S3904-512Q/index_en.html.
- Hendrick, F., Van Roozendaal, M., Kylling, A., Wittrock, F., Von Friedeburg, C., Sanghavi, S., Petritoli, A., Denis, L., and Schofield, R. (2003). Report on the Workshop on Radiative Transfer Modelling, IASB-BIRA, Brussels, Belgium, Report of the QUILT project (EVK2-2000-00545), European Commission, Brussels.

- Interactive Learning Paradigms, Incorporated (ILPI), June, 2009 Retrieved January 6, 2009, from <http://www.ilpi.com/msds/ref/voc.html>.
- Jang, A., Kapur, R., Adams, T., Giuliano, K. A., and Mrksich, M. (2005). Miniaturized Redox Potential Probe for In Situ Environmental Monitoring. *Environ. Sci. Technol.*, 39, (16), 6191-6197.
- Jiménez, R., Van den Bergh, H., and Calpini, B. (1999). *DOAS as an Analytical Tool for Effective Air Pollution Management*. Air Pollution Laboratory Report (LPAS), Swiss Federal Institute of Technology (EPFL) CH-1015 Lausanne, Switzerland.
- Jumphah, D. T. (1999). "Combustion Processes Monitoring by Environmental Protection Agency in Ghana", Proceedings of Workshop on Combustion Diagnostics and Optical techniques, ICS-UNIDO and University Of Cape Coast, Laser and Fiber Optics Center.
- Junge, C. E. (1963). *Air Chemistry and Radioactivity*. Int. Geophys. Ser., Vol. 4. Academic Press, New York and London.
- Karger, A. (2000). Report on Environmental Monitoring: *Compact Raman LIDAR System Utilizing APD Array Detectors*. USEPA.
- Krecl, P., Haley, C. S., Stegman, J., Brohede, S. M., and Berthet, G. (2006). Retrieving vertical distribution of stratospheric OCIO from Odin/OS IRIS lomb-scattered sunlight measurements. *Atmos. Chem. Phys.*, 6, 1879-1894.
- Nakazato, M., Nagai, T., Sakai, T., and Hirose, Y. (2007). Tropospheric ozone differential-absorption lidar using stimulated Raman scattering in carbon dioxide. *Appl Opt.* 46, (12), 2269-79.

- Neftel, A. (1999). Examples of the importance of trace gas measurements in the Milan ozone plume ANALYSIS, 27, (4). EDP Sciences, Wiley-VCH.
- Noxon, J. F. (1975). Nitrogen dioxide in stratosphere and troposphere measured by ground- absorption spectroscopy. *Science*, 189, 547-549.
- Palazzi, E. (2003). Sviluppo di modelli a supporto della metodologia DOAS per la determinazione degli inquinanti in troposfera. Tesi di laurea, Università di Bologna.
- Palazzi, E., Premuda, M., Petritoli, A., Giovanelli, G., Kostadinov, I., Ravegnani, F., and Bortoli, D. (2004). A multiple scattering atmospheric radiative transfer model for diffuse solar radiation measurements along slant polar trajectories, in: Colacino, M. (Eds), 10th Workshop, Italian Research on Antarctic Atmosphere. SIF Conference Proceedings, 89, 41-58.
- Palazzi, E., Petritoli, A., Giovanelli, G., Kostadinov, I., Bortoli, D., Ravegnani, F and Sackey, S. S. (2005). PROMSAR: A backward Monte Carlo spherical RTM for the analysis of DOAS remote sensing measurements. *Advances in Space Research (COSPAR publication)*, 36, 1007-1014.
- Penndorf, R. J. (1957). Tables of Refractive Index for Standard Air and the Rayleigh Scattering Coefficient for the Spectral Region between 0.2 and 20.0 μm and their Application to Atmospheric Optics. *Optic. Soc. Am. J.*, 47, 176 - 182.
- Perner, D., and Platt, U. (1979). Detection of nitrous acid in the atmosphere by differential optical absorption. *Geophys. Res. Lett.*, 6, 917-920.

- Perner, D., Platt, U., Trainer, M., Hübler, G., Drummond, J., Junkermann, W., Rudolph, J., Schubert, B., Volz, A., Ehhalt, D. H., Rumpel, J. and Helas, G. (1987). Measurement of tropospheric OH concentrations: a comparison of field data with model predictions. *Journal of Atmospheric Chemistry*, 5, 185–216.
- Petritoli, A., Giovanelli, G., Ravegnani, F., Bortoli, D., Kostadinov, I., and Oulanovsky, A. (2002). Off-axis measurements of atmospheric trace gases from an airborne uv-vis spectroradiometer. *Applied Optics: Lasers, Photonics, and Environmental Optics*, 41, (27), 5593-5599.
- Plane, J. M. C., and Smith, N. (1995). Atmospheric monitoring by differential absorption spectroscopy. *Spectroscopy in Environmental Science*, R. J. H Clark and R. E. Hester, Eds., Wiley, Chichester, 223-262.
- Platt, U. (1994). *Differential optical absorption spectroscopy (DOAS)*, In: *Air monitoring by Spectroscopic Techniques*. M. W. Sigrist, Edition, Chemical Analysis series, Vol. 127. John Wiley & Sons, Inc. 27–84.
- Platt, U. (1999). Modern methods of the measurement of atmospheric trace gases. Invited Lecture. *Phys. Chem. Chem. Phys.*, 1, 5409 – 5415.
- Platt, U. (2002). Probing the Atmosphere with Differential Optical Absorption Spectroscopy. Abstract of oral presented papers, 4th International Symposium on Advanced Environmental Monitoring, Jeju, Korea.
- Platt, U. and Perner, D. (1980). Direct measurements of atmospheric CH₂O, HNO₂, O₃, NO₂ and SO₂ by differential optical absorption in the near UV. *J. Geophys. Res.* 85, 7453-7458.

- Platt, U., and Janssen, C. (1996). Observation and role of the free radicals NO_3 , ClO , BrO and IO in the Troposphere. *Faraday Discuss* 100, 175-198.
- Platt, U., and Perner, D. (1983). *Optical and Remote Sensing*. Edited by Killinger D. K., and Moorandian, A. Springer-Verlag, Berlin, 97–105.
- Platt, U., and Stutz, J. (2008). *Differential Optical Absorption Spectroscopy. Principles and Applications*. Springer Berlin Heidelberg, 495-504.
- Platt, U., Marquard, L., Wagner., and Prener, D. (1997) Corrections for zenith scattered light DOAS. *Geophys. Res. Lett.* 24, 1759-1762.
- Platt, U., Perner, D., and Patz, H. W. (1979). Simultaneous measurements of atmospheric CH_2 , O_3 and NO_2 by differential optical absorption. *J. Geophys. Res.* 84, 6329-6335.
- Platt, U., Perner, D., Schroder, J., Kessler, C., and Tonnissen, A. (1981). The diurnal variation of NO_3 . *J. geophys. Res.* 86, 11965-11970.
- Ravindra, S. (1981). Precision gimbaled mirror control in remote sensing LIDAR for environmental monitoring. Soc. of Photo-Optical Instrumentation Engineers, Bellingham, WA, ETATS-UNIS.
- Replicated mirrors, (2007). Retrieved on June 15, 2011 from <http://www.newportfranklin.com/pdfDatasheet/ReplicatedMirrorsSpectroscopy.pdf>
- Roozendael, M. V., and Fayt, C. (2001). WinDOAS 2.1 Software User Manual.
- Sanders, R. W. (1996). Improved analysis of atmospheric absorption spectra by including the temperature dependence of NO_2 . *J. Geophys. Res.* 101, 20945-20952.

- Sanders, R. W., Solomon, S., Smith, J. P., Perliski, L., Miller, H. L., Mount, G. H., Keys, J. G., and Schmeltekopf, A. L. (1993). Visible and near-ultraviolet spectroscopy at McMudro Station, Antarctica. Observations of OCIO from April to October 1991. *J. Geophys. Res.* 98, 2719-c 7228.
- Schott glass filters, 1999. Retrieved June 16, 2011 from <http://www.noao.edu/kpno/filters/sgt.html>
- Smith, R. C. (1963). Resolution in the derivative recording of absorption spectra. *Rev. Sci. Instrum.*, Vol. 34, (3), 296-297.
- Solomon, S., Schmeltekopf, A. L., and Sanders, R. W. (1987). On the interpretation of zenith-sky absorption measurements, *J. Geophys. Res.* 92, 8311-8319.
- Stauffer, F. R., and Sakai, H. (1968). Derivative Spectroscopy. *Appl. Optics*, Vol. 7, (1), 61-65.
- State of Queensland, Department of Environment and Resource Management Report (2011). Retrieved February 9, 2011, from http://www.epa.qld.gov.au/environmental_management/air/air_quality_monitoring/meteorological_data/what_is_doas/.
- Székely, L. (2000). *Contribution to the Development of a Calibration System for the Measurement of Nitrous Acid (HONO) by Differential Optical Absorption Spectroscopy (DOAS)*. Environmental Engineering Diploma Work, Department of Environmental Engineering and Chemical Technology, University of Veszprém, Hungary.

- Toyozumi, H. (2001). Application of Radio-Carbon Techniques to Environmental Monitoring. Journal Proceedings: 27th International Cosmic Ray Conference (ICRC), Hamburg, Germany. 4192-4195.
- U.S.A. Environmental Protection Agency (EPA) Report. (2005). *Lidar Remote Sensing for Industry and Environmental Monitoring VI*. San Diego.
- United States EPA Report (2007). Retrieved May 16, 2009, from <http://www.clu-in.org/programs/21m2/openpath/uv-doas>.
- Vountas, M., Rozanov, V. V., and Burrows, J. P. (1998). Ring effect: Impact of rotational Raman scattering on radiative transfer in Earth's atmosphere. *J. of Quantitative Spectroscopy and Radiative Transfer*, Vol. 60, (6), 943-961.
- Wagner, T., Chance, K., Frieß, U., Gil, M., Goutail, F., Hönninger, G., Johnston, P. V., Karlsen-Tørnkvist, K., Kostadinov, I., Leser, H., Petritoli, A., Richter, A., Van Roozendaal, M., Platt, U. (2001). Correction of the Ring effect and I₀-effect for DOAS Observations of Scattered Sunlight. Proceedings, 1st DOAS Workshop, Heidelberg.
- Wang, P., Richter, A., Bruns, M., Rozanov, V. V., Burrows, J. P., Heue, K. P., Wagner, T., Pundt, I. and Platt, U. (2005). Measurements of tropospheric NO₂ with an airborne multi-axis DOAS instrument. *Atmos. Chem. Phys.*, 5, 337-343.
- Weaver, A., Solomon, S., Sanders, R. W., Arpag, K., and Miller, H. L. (1996). Atmospheric NO₃. Off-axis measurements at sunrise: estimates of tropospheric NO₃ at 40 °N. *J. Geophys. Res.* 101, 18605-18612.

- Weibring, P., Edner, H., and Svanberg, S. (2003). Versatile Mobile Lidar System for Environmental Monitoring. *Applied Optics*, 18, (42) 3583-3594.
- Williams, T. T., Dohno, C., Stemp, E. D A., and Barton, J. K. (2004). Effects of the photooxidant on DNA-mediated charge transport. *J. Amer. Chem. Soc.* 126 (26), 8148-8158.
- WisegEEK, 2008 Retrieved August I, 2009, from <http://www.wisegEEK.com/what-are-free-radicals.htm>
- Wolfram, E. A., Salvador, J., D'Elia, R., Casiccia, C., Paes-Leme, N., Pazmiño, A., Porteneuve, J., Godin-Beekman, S., Nakane, H., and Quel, E. J. (2008a). New Differential Absorption Lidar for Stratospheric Ozone Monitoring in Patagonia, South Argentina. *J. Opt. A: Pure Appl. Opt.* 10, 104021.
- Wolfram, E. A., Salvador, J., D'Elia, R., Pazmiño, A., and Godin-Beeckmann, S. (2008b). New Differential Absorption Lidar for Stratospheric Ozone Monitoring in Argentina. *AIP Conf. Proc.*, 992, 589-593.
- Woo, H. J., Cho, S. Y., Chun, S. K., Kim, N. B., Kang, D. W., and Kim, E. H. (1999). Sample treatment techniques for the determination of environmental radiocarbon in a nuclear power station area. *Journal of Radioanalytical and Nuclear Chemistry.* 3, (239), 533-538.
- Xue, Y., Niu, J., Liu, W., Kuze, H., and Takeuchi, N. (2000). Daytime monitoring of urban NO₂ column density by solar spectroscopic method, *Jpn. J. Appl. Phys.* 39, 622-627.

APPENDICES

Appendix 1

Raw intensity values as recorded by the sensor (in pixels) for measurements carried out in the uv spectral region.

Items									
1	2	3	4	5	6				
10-01-08	12:03	3132	1	1	120000				
23	23	22	15	15	22	21	20	18	20
23	24	20	18	16	19	20	21	17	17
24	25	18	18	14	21	21	19	17	24
22	22	19	16	14	18	21	21	16	16
22	23	18	18	14	21	20	20	17	17
21	21	18	15	14	19	23	17	14	17
23	19	18	16	16	18	20	22	16	19
24	23	20	19	13	21	20	21	18	18
19	20	19	15	15	22	20	22	17	17
23	24	18	18	14	21	23	19	17	18
23	26	19	15	13	23	19	23	16	19
24	23	22	17	17	23	22	22	17	21
26	22	18	18	16	19	22	23	18	21
24	27	22	16	16	20	21	21	19	19
22	23	20	18	18	25	23	23	21	16
22	24	23	17	14	23	21	20	21	19
21	24	19	19	15	22	20	22	19	20
25	22	20	18	15	22	21	20	19	21
22	24	22	18	19	21	19	21	19	18
26	28	24	22	18	25	22	24	20	19
27	29	23	24	20	24	22	25	21	21
25	28	22	23	21	25	27	25	24	27
28	26	28	23	23	27	27	31	26	27
31	30	30	26	24	30	31	33	28	32
37	36	35	27	31	38	37	39	32	35
38	42	38	35	34	42	41	43	41	45
48	49	45	39	42	47	45	45	45	49
53	56	50	52	49	56	56	56	54	52
60	61	56	57	54	62	62	66	67	63
72	75	70	67	65	74	78	80	78	81
85	94	90	89	91	95	97	96	94	93
99	101	99	103	101	110	115	115	115	119
126	135	133	132	132	143	149	150	153	157
170	178	182	186	194	205	207	212	212	212
224	226	226	224	226	232	235	242	239	247
253	265	264	265	265	266	268	271	270	273
282	295	303	314	320	334	343	349	350	353
361	360	357	350	344	353	357	360	366	378
393	405	404	401	399	401	402	397	385	383

Appendix 1 continued

392	394	404	408	421	440	455	471	484	494
506	509	510	513	518	528	535	547	562	575
591	599	605	613	613	617	623	628	636	644
657	669	673	673	673	677	681	678	675	669
661	663	654	649	653	666	672	682	687	686
695	690	681	666	656	647	640	644	645	652
676	697	724	749	774	801	831	855	875	890
906	923	939	957	977	1004	1023	1052	1085	1114
1146	1163	1173	1176	1175	1176	1176	1171	1168	1161
1162	1158	1155	1156	1162	1170	1175	1177	1176	1173
1173	1176	1177	1180	1177	1188	1203	1214	1223	1234
1244	1256	1264	1265	1268	1281	1296	1307	1315	1325
1349	1375	1389	1393	1400	1411	1407	1387	1366	1348
1337	1333	1333	1338	1355	1386	1416	1437	1450	1467
1477	1476	1465	1459	1444	1436	1425	1419	1420	1419
1422	1433	1439	1440	1430	1425	1410	1403	1391	1391
1395	1394	1390	1394	1389	1391	1390	1390	1389	1389
1402	1418	1438	1471	1513	1567	1623	1676	1718	1755
1785	1820	1842	1861	1873	1883	1884	1887	1872	1862
1846	1829	1816	1805	1797	1799	1789	1777	1772	1763
1761	1758	1747	1752	1758	1762	1764	1757	1752	1753
1753	1754	1756	1762	1766	1803	1832	1857	1884	1909
1937	1958	1968	1970	1968	1973	1963	1955	1949	1958
1987	2021	2063	2108	2157	2201	2226	2240	2251	2245
2239	2237	2217	2196	2170	2156	2152	2160	2150	2147
2145	2144	2131	2120	2106	2103	2096	2088	2073	2055
2047	2042	2045	2039	2049	2067	2091	2098	2099	2098
2105	2103	2081	2058	2051	2051	2055	2042	2036	2036
2037	2029	2021	2002	2004	2015	2020	2022	2028	2058
2104	2152	2190	2223	2271	2311	2342	2360	2375	2400
2423	2443	2454	2476	2497	2514	2520	2528	2547	2553
2562	2572	2593	2607	2606	2632	2658	2697	2727	2747
2784	2815	2843	2872	2906	2954	3002	3059	3108	3163
3198	3230	3258	3286	3320	3355	3387	3419	3468	3497
3519	3530	3530	3519	3502	3497	3491	3483	3475	3487
3508	3523	3514	3518	3529	3537	3533	3517	3494	3475
3452	3445	3427	3432	3441	3454	3465	3486	3475	3448
3428	3409	3392	3378	3392	3431	3478	3525	3562	3604
3662	3711	3745	3775	3804	3845	3887	3919	3959	3996
4061	4136	4208	4293	4359	4390	4410	4410	4390	4372
4344	4317	4273	4244	4201	4181	4159	4172	4177	4187
4198	4193	4168	4134	4078	4027	3977	3928	3908	3901
3912	3928	3957	4008	4066	4118	4174	4208	4219	4202
4179	4155	4137	4124	4128	4166	4207	4250	4283	4319
4352	4348	4327	4311	4297	4284	4272	4279	4297	4315
4330	4332	4328	4316	4302	4285	4286	4272	4249	4234
4254	4293	4305	4307	4320	4357	4388	4392	4392	4416
4439	4456	4478	4508	4520	4529	4544	4576	4607	4636
4674	4729	4781	4832	4882	4937	4982	5025	5034	5037

Appendix 1 continued

5016	4966	4875	4779	4681	4591	4522	4486	4509	4559
4620	4678	4720	4753	4763	4736	4697	4634	4519	4391
4271	4183	4110	4062	4060	4125	4221	4314	4424	4539
4660	4745	4790	4818	4825	4822	4777	4710	4673	4655
4667	4699	4741	4824	4905	5028	5125	5231	5358	5441
5481	5503	5486	5498	5474	5445	5454	5455	5465	5468
5476	5504	5567	5587	5596	5630	5704	5767	5829	5884
5942	6025	6078	6101	6151	6180	6209	6206	6194	6200
6261	6320	6380	6437	6494	6541	6557	6560	6559	6569
6594	6590	6564	6547	6479	6404	6305	6218	6186	6170
6162	6171	6199	6284	6359	6426	6499	6582	6641	6670
6657	6637	6601	6577	6546	6559	6600	6668	6754	6860
6990	7092	7191	7270	7306	7361	7375	7321	7246	7174
7163	7161	7184	7213	7268	7326	7353	7353	7328	7227
7133	7037	6915	6771						

There are six (6) 'items' on top of the appendix. These are interpreted as:

Item 1 - '10-01-08' represents the date that data was collected by the system.

Item 2 - '12:03' represents time of measurements. Measurements are carried out only during the day it means that this data was collected at 12:03 pm.

Item 3 - '3132' represents the wavelength within which the data was collected. 3132 Å is for measurements in the uv region while 4358 Å is for measurements in the visible region.

Item 4 - '1' represents the cell position chosen for the measurements. Positions 1, 2 and 4 are used to make a distinction between the vertical, horizontal left and horizontal right measurements respectively.

Item 5 - '1' represents the filter chosen for the measurements. Filter 1 is for measurements in the uv spectral region while filter 3 is for measurements in the visible spectral region.

Item 6 - '120000' represents the integration time calculated and used for that particular data collection.

Appendix 2

Raw intensity values as recorded by the sensor (in pixels) for measurements carried out in the visible spectral region.

Items									
1	2	3	4	5	6				
10-01-08	11:21	4358	2	3	30829				
2607	2706	2835	2964	3055	3114	3075	2842	2612	2572
2764	2888	2943	2980	3061	3066	2941	2772	2619	2590
2636	2687	2750	2916	3109	3261	3305	3304	3231	3150
3044	2971	2962	2989	3067	3184	3327	3437	3489	3514
3501	3472	3474	3432	3288	3253	3377	3453	3376	3294
3213	3159	3083	3074	3022	3009	3037	3021	2898	2683
2433	2295	2293	2421	2532	2665	2806	3010	3135	3215
3250	3320	3333	3340	3302	3298	3281	3314	3324	3337
3382	3498	3595	3599	3612	3694	3751	3777	3796	3738
3527	3407	3426	3489	3523	3545	3549	3580	3536	3514
3561	3688	3660	3589	3576	3561	3449	3401	3457	3479
3491	3578	3608	3415	3197	3139	3218	3154	3068	3225
3528	3684	3686	3700	3777	3867	3907	3911	3920	3962
3969	3837	3644	3391	3085	2988	3162	3332	3437	3603
3709	3733	3783	3801	3657	3553	3607	3688	3641	3619
3690	3732	3524	3339	3433	3550	3458	3379	3450	3565
3556	3631	3734	3832	3797	3760	3826	3960	4014	4000
4000	4008	3960	3975	3967	3767	3566	3575	3684	3724
3826	3891	3882	3678	3488	3295	3205	3260	3346	3427
3497	3601	3660	3566	3517	3533	3591	3674	3786	3879
3779	3640	3541	3556	3518	3536	3631	3814	3890	3793
3557	3321	3286	3311	3467	3681	3879	3854	3723	3696
3881	4028	4166	4181	4031	3824	3672	3635	3660	3575
3374	3242	3389	3497	3529	3578	3451	3373	3469	3628
3729	3790	3892	3992	4013	4015	4074	4182	4211	4162
4096	3974	3953	4046	4158	4242	4283	4303	4298	4184
3859	3624	3672	3749	3870	4007	4096	4124	4156	4316
4404	4408	4329	4237	4134	3933	3804	3645	3410	2935
2514	2406	2763	3326	3763	4029	4201	4339	4383	4426
4338	4094	3945	4058	4162	4013	3759	3634	3667	3736
3887	3932	3914	3881	3921	4171	4391	4338	4204	4089
4177	4369	4466	4522	4533	4389	4157	3986	3918	3897
3805	3595	3481	3702	4060	4338	4506	4453	4171	3916
3830	3883	4132	4512	4703	4576	4363	4212	3876	3509
3371	3529	3813	4224	4597	4700	4674	4639	4711	4813
4811	4669	4490	4404	4412	4306	4266	4045	3572	3143
3209	3513	3708	3805	3746	3671	3832	4146	4410	4619
4788	4893	4802	4512	4187	4112	4271	4361	4336	4489
4674	4707	4550	4368	4128	4040	4168	4278	4388	4247
3923	3699	3645	3751	3873	4241	4483	4659	4535	4335
2956	3203	3353	3298	3268	3338	3416	3502	3488	3513

Appendix 2 continued										3353
3588	3596	3258	2972	2843	2881	2977	3135	3241		
3440	3621	3937	4222	4317	4466	4826	5318	5640	5882	
5948	5815	5743	5806	5794	5630	5520	5562	5527	5185	
4652	4259	3980	3626	3408	3570	4025	4519	5076	5455	
5701	5720	5599	5474	5461	5555	5595	5619	5636	5642	
5662	5718	5750	5558	5144	4703	4453	4272	4072	3700	
3411	3372	3730	4234	4623	4805	4800	4913	5149	5420	
5510	5532	5487	5469	5547	5809	6004	6023	5759	5208	
4690	4382	4612	4996	5326	5437	5428	5399	5468	5660	
5848	5794	5623	5363	5299	5398	5703	5993	6118	5983	
5820	5737	5896	6130	6295	6225	6068	5721	5518	5541	
5739	5717	5709	5654	5594	5630	5755	5731	5610	5396	
5134	4972	4960	5137	5396	5656	5825	5927	5922	5886	
5802	5739	5789	5777	5297	4484	3767	3449	3554	4030	
4737	5281	5492	5519	5470	5451	5404	5349	5278	5304	
5342	5539	5729	5757	5749	5653	5465	5354	5573	5829	
6119	6264	6305	6229	6046	5768	5487	5313	5502	5902	
6097	6016	5504	4818	4543	4860	5324	5724	5846	5669	
5573	5660	5912	6162	6334	6486	6610	6739	6823	6751	
6418	5780	5360	5386	5667	5896	6108	6236	6434	6691	
6895	7018	6961	6734	6384	6148	6104	6224	6414	6429	
6391	6395	6381	6341	6425	6678	6825	6800	6498	6251	
6258	6406	6547	6574	6469	6324	6032	5767	5692	5867	
6181	6516	6786	6979	7098	7082	6942	6762	6560	6306	
6091	5995	6014	6206	6563	6900	7135	7114	6860	6642	
6685	6841	6980	6955	6848	6741	6814	6882	6916	6884	
6700	6255	5841	5668	5758	5943	6168	6241	6201	6076	
6084	6257	6340	6223	6024	6024	6264	6647	6848	6876	
6865	6906	6788	6797	6935	6979	6881	6692	6572	6529	
6636	6871	7106	7183	7268	7426	7519	7543	7444	7278	
7225	7402	7563	7693	7729	7503	7164	6822	6548	6333	
6259	6405	6744	7028	7281	7494	7572	7622	7727	7724	
7590	7413	7154	6921	6828	6865	6982	7216	7439	7631	
7635	7398	7141	7030	7060	7093	7232	7424	7594	7650	
7709	7788	7798	7630	7471	7372	7458	7669	7941	8094	
8158	8166	8160	8141	8113	8047	7945	7868	7879	7934	
8036	8129	8096	8009	7895	7800	7690	7579	7492	7558	
7669	7798	7769	7640	7565	7638	7740	7799	7895	8040	
8079	7899	7703	7626	7645	7592	7566	7503	7303	7045	
6970	6901	6713	6627	6788	6869	6877	6952	7220	7389	
7376	7282	7213	7050	6844	6788	6989	7417	7785	8094	
8251	8202	8108	7913	7758	7709	7723	7834	7999	8105	
8012	7864	7745	7702	7655	7668	7700	7741	7596	7280	
7156	7211	7362	7550	7685	7773	7774	7653	7555	7551	
7425	7386	7554	7784	7930	8071	8193	8233	8209	8210	
8282	8349	8406	8408	8251	8064	7872	7635	7507	7562	
7752	7977	8213	8301	8312	8384	8387	8253	8019	7806	
7781	7947	8127	8284	8392	8414	8360	8317	8344	8421	
8382	8322	8217	8036	7822	7610	7483	7495	7637	7665	

Appendix 2 continued

7703	7750	7792	7680	7574	7636	7750	7828	8002	8206
8345	8366	8337	8290	8097	7899	7790	7799	7885	7953
7999	7950	7857	7890	7858	7770	7865	8017	8064	7954
7854	7858	7879	7847	7893	8023	8131	8056	7968	7975
8037	8067	8087	8186	8377	8469	8533	8589	8520	8343
8280	8259	8114	8023	8121	8253	8286	8297	8326	8338
8356	8334	8258	8196	8172	8223	8283	8381	8450	8443
8431	8462	8464	8416	8393	8371	8338	8336	8392	8483
8500	8442	8344	8329	8344	8423	8474	8459	8405	8344
8283	8243	8277	8336	8374	8297	8140	8104	8129	8027
8008	8107	8240	8322	8442	8546	8513	8492	8487	8426
8318	8177	8056	7940						

The six items on top of the appendix 2 are interpreted the same way as those in appendix 1.

Appendix 3:

Graphical representation of concentration values measured in July 2008.

NO₂ concentration values in the north, south, east and west from 8th to 18th.

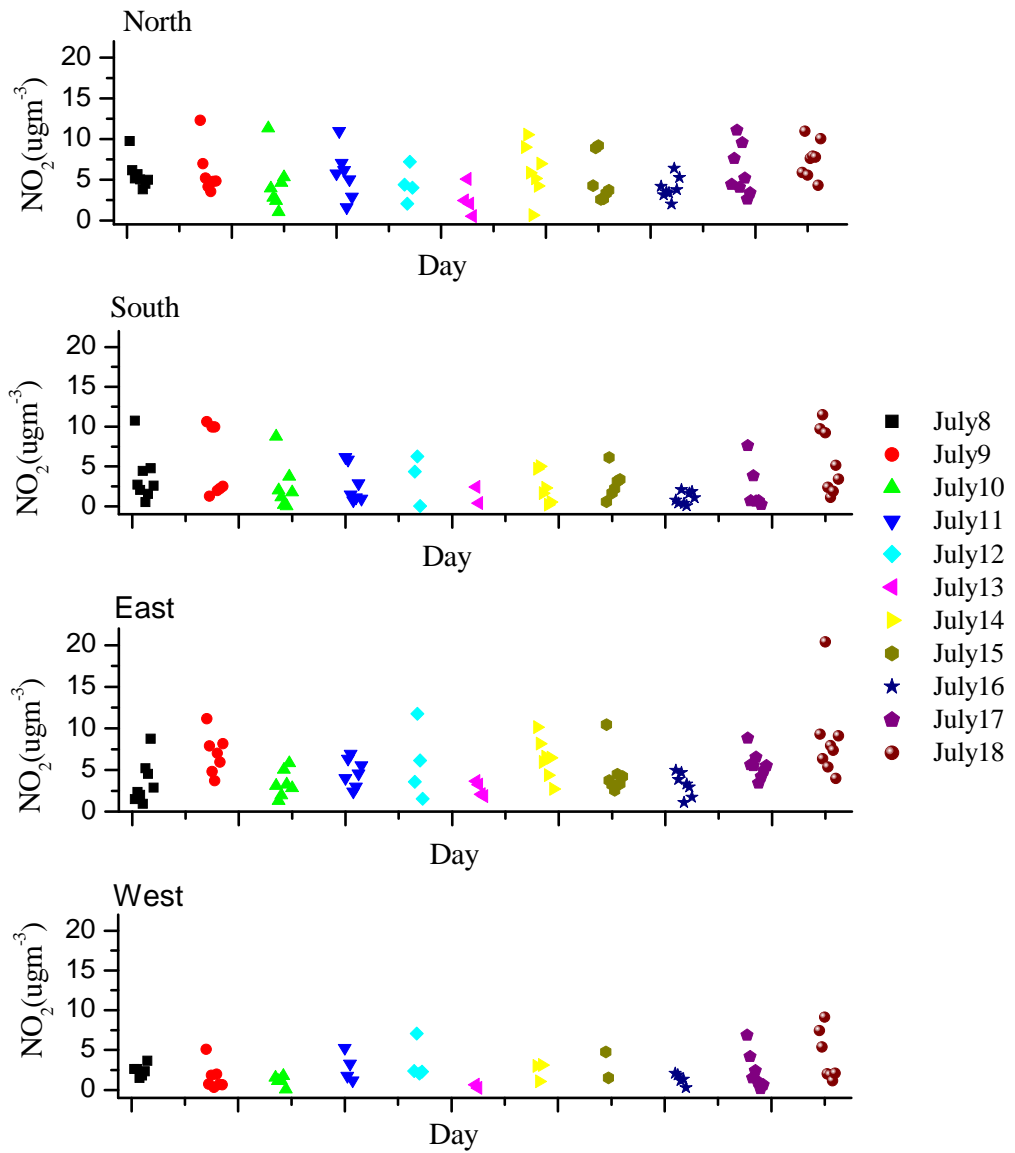


Figure 38a: Graph showing concentrations of NO₂ monitored in the north, south, east and west from July 8 to 18, 2008.

NO₂ concentration values in the north, south, east and west from 20th to 30th

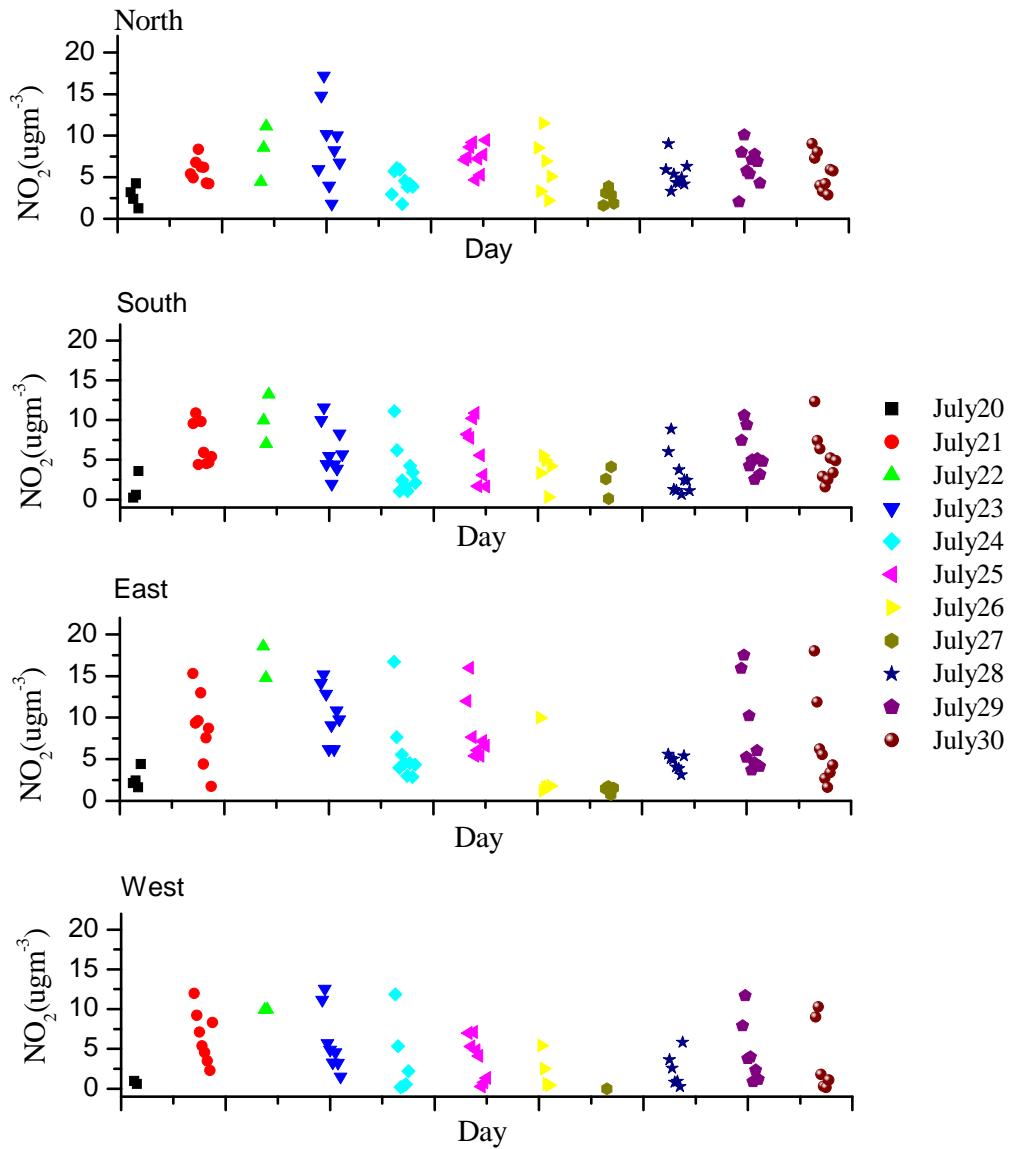


Figure 38b: Graph showing concentrations of NO₂ monitored in the north, south, east and west from July 20 to 30, 2008.

SO₂ concentration values in the north, south, east and west from 8th to 18th.

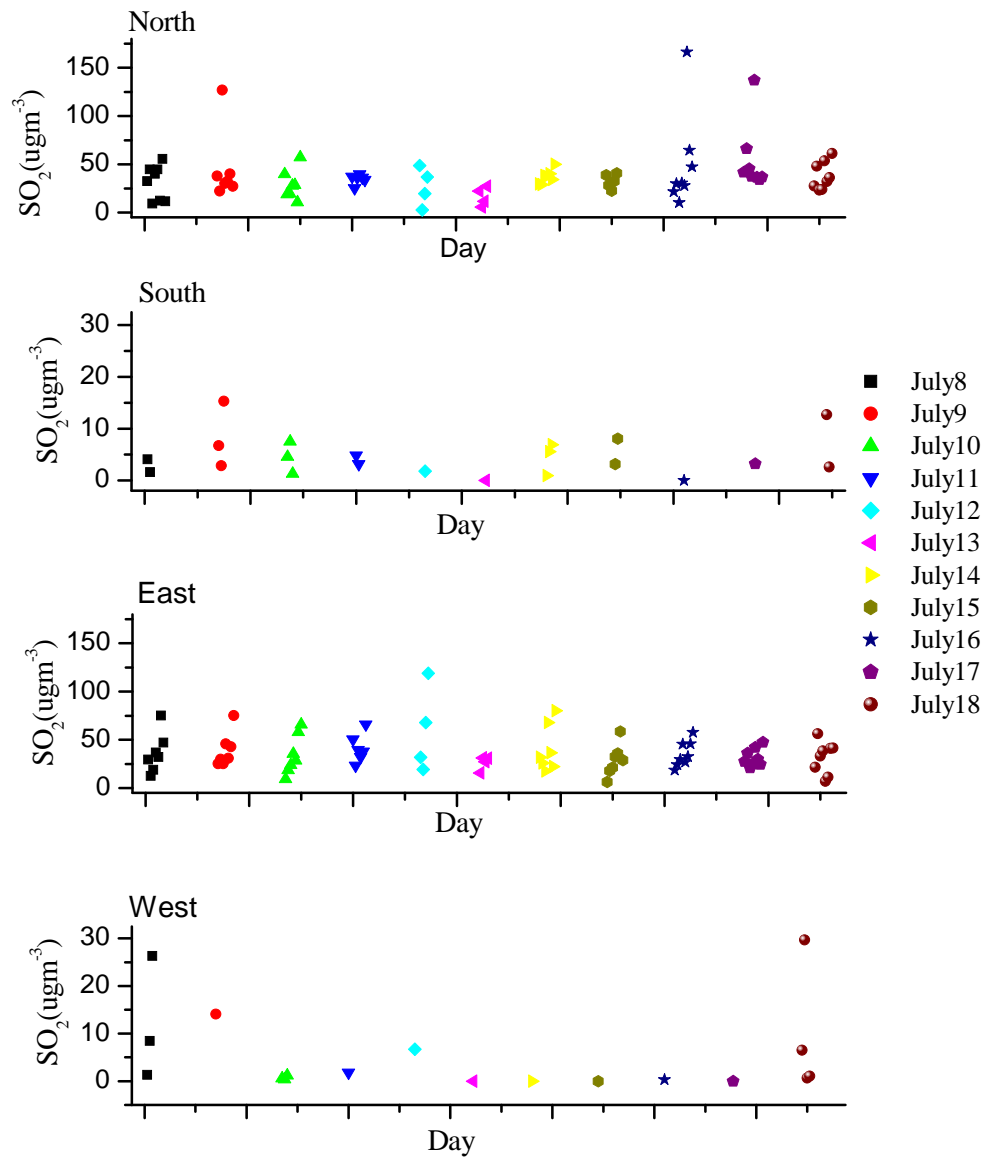


Figure 39a: Graph showing concentrations of SO₂ monitored in the north, south, east and west from July 8 to 18, 2008.

SO₂ concentration values in the north, south, east and west from 20th to 30th

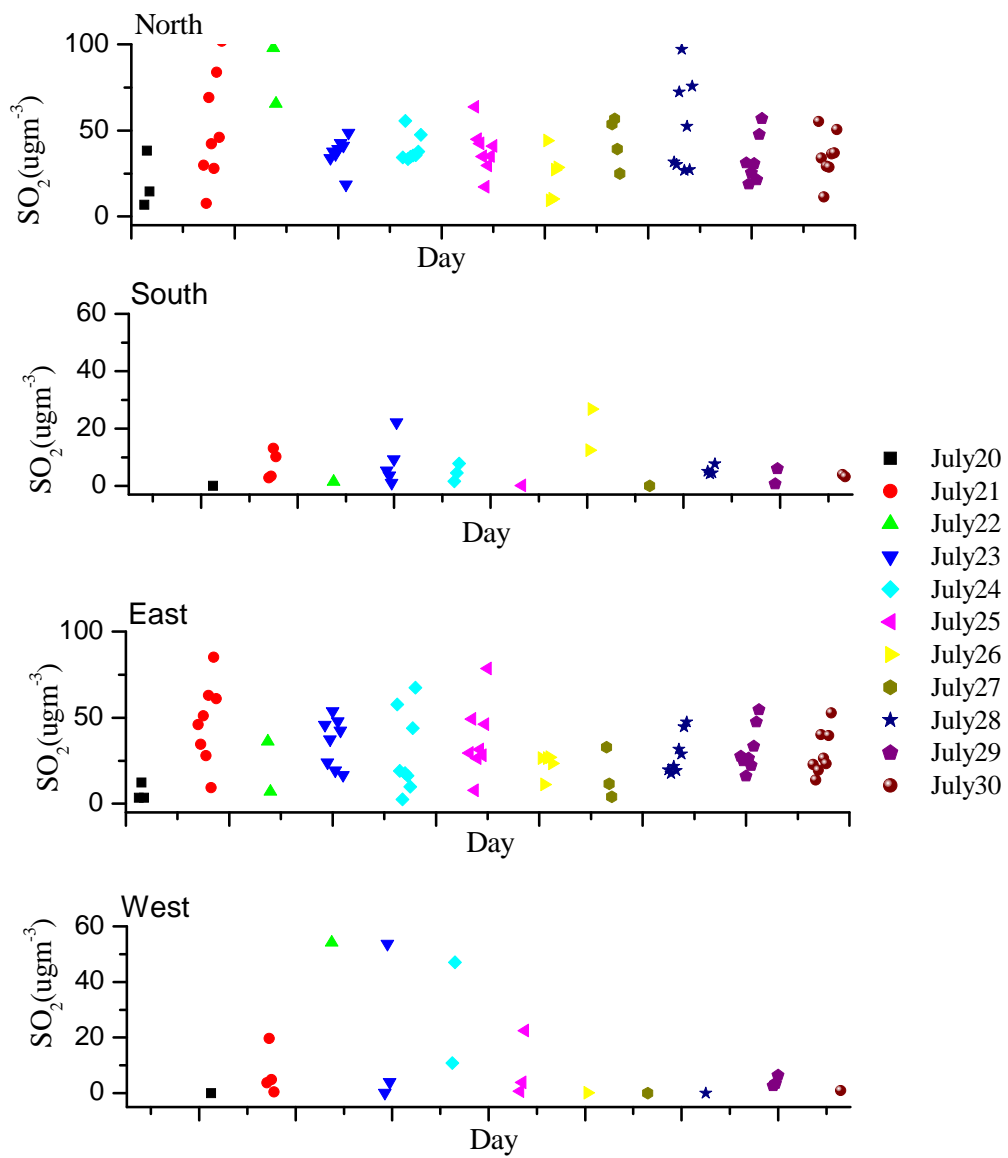


Figure 39b: Graph showing concentrations of SO₂ monitored in the north, south, east and west from July 20 to 30, 2008.

O₃ concentration values in the north, south, east and west from 8th to 18th.

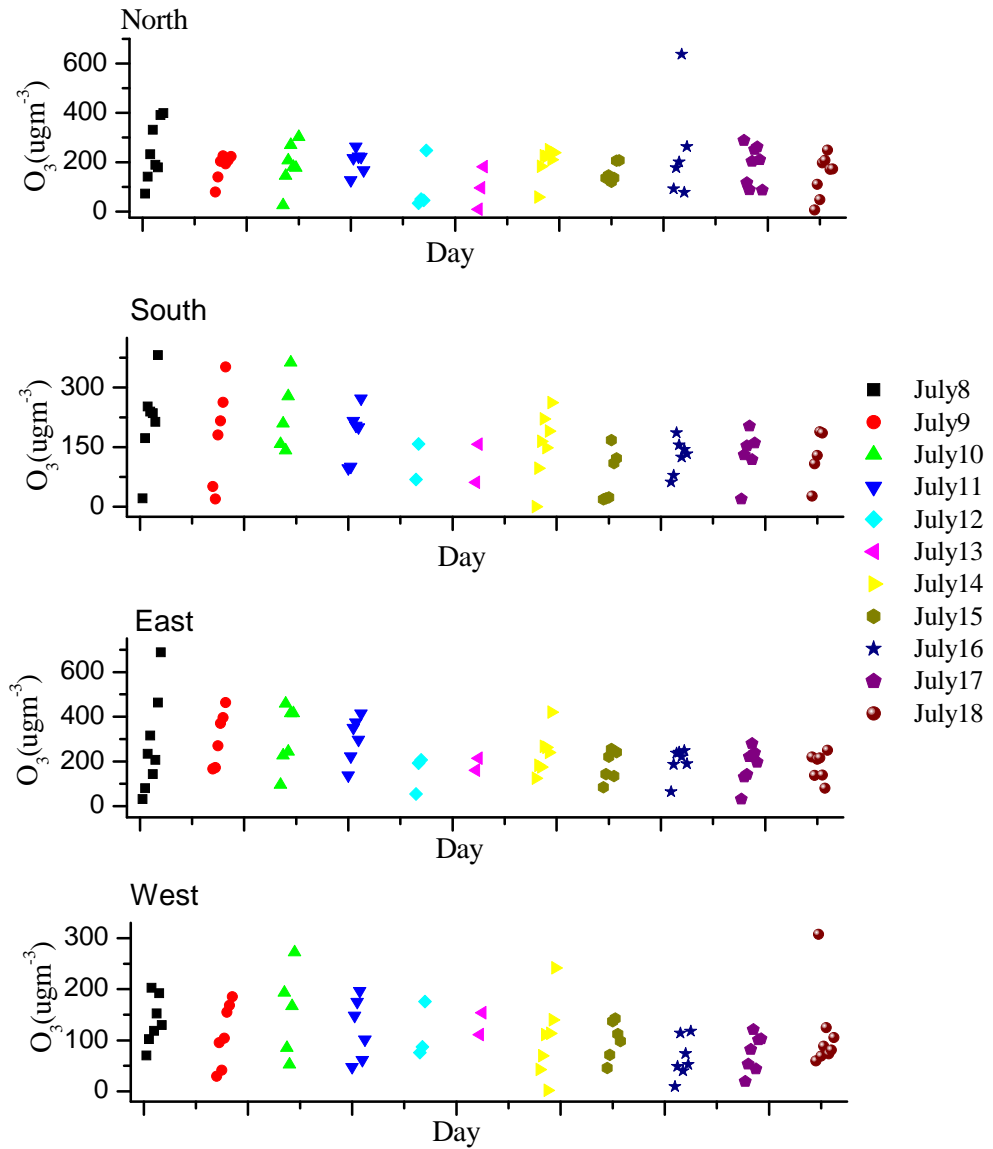


Figure 40a: Graph showing concentrations of O₃ monitored in the north, south, east and west from July 8 to 18, 2008.

O₃ concentration values in the north, south, east and west from 20th to 30th

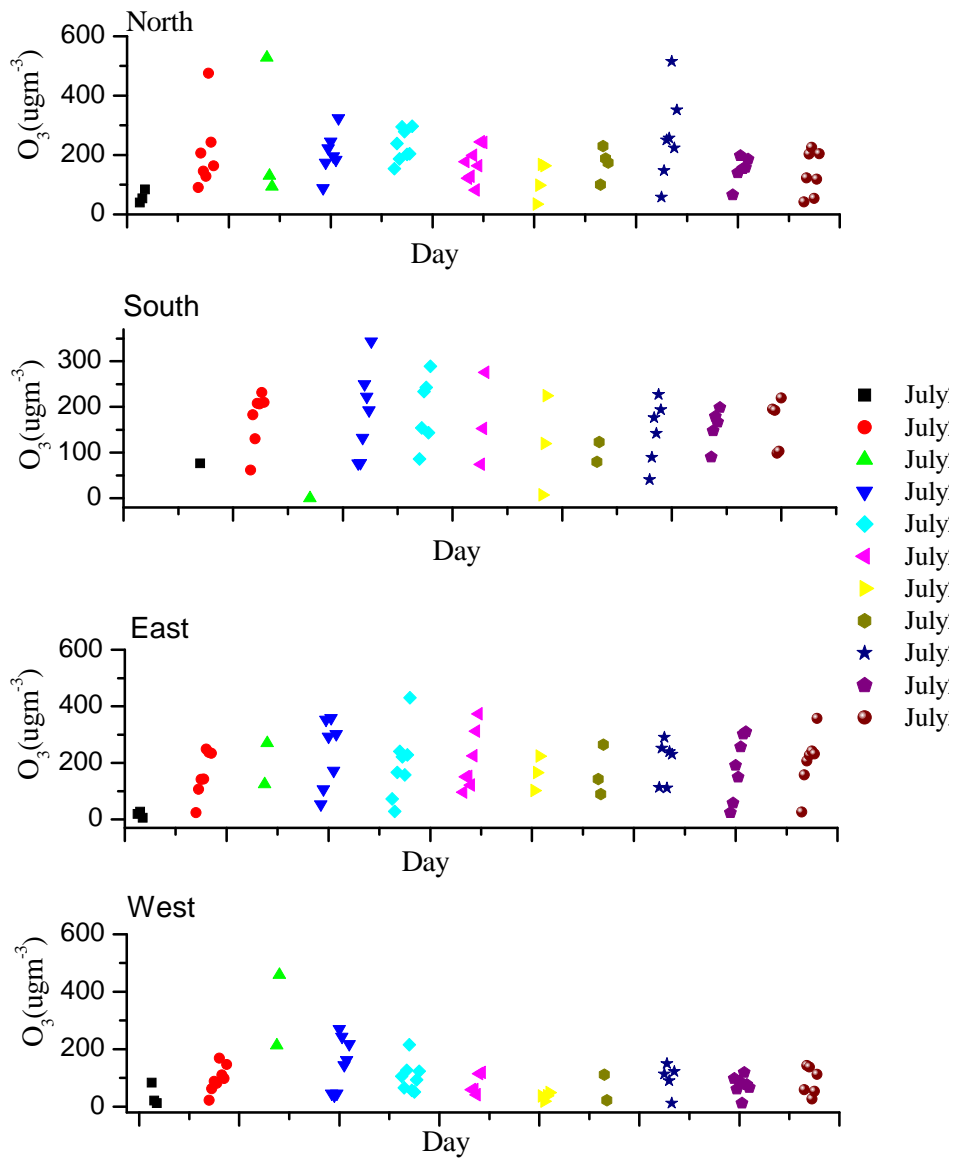


Figure 40b: Graph showing concentrations of O₃ monitored in the north, south, east and west from July 20 to 30, 2008.

Appendix 4:

Graphical representation of concentration values measured in August

2008.

NO₂ concentration values in the north, south, east and west from 1st to 14th.

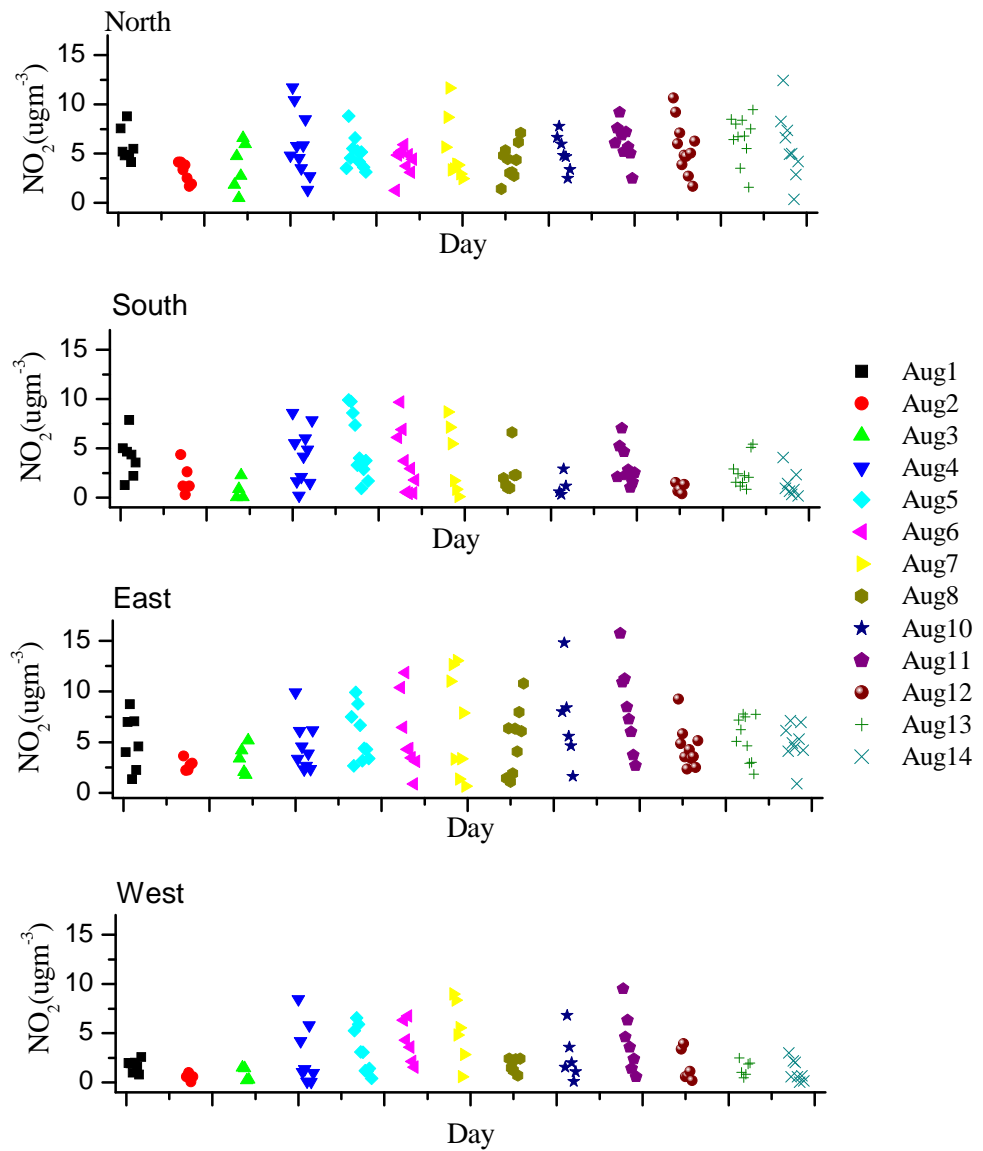


Figure 41: Graph showing concentrations of O₃ monitored in the north, south, east and west from July 20 to 30, 2008.

SO₂ concentration values in the north, south, east and west from 1st to 14th

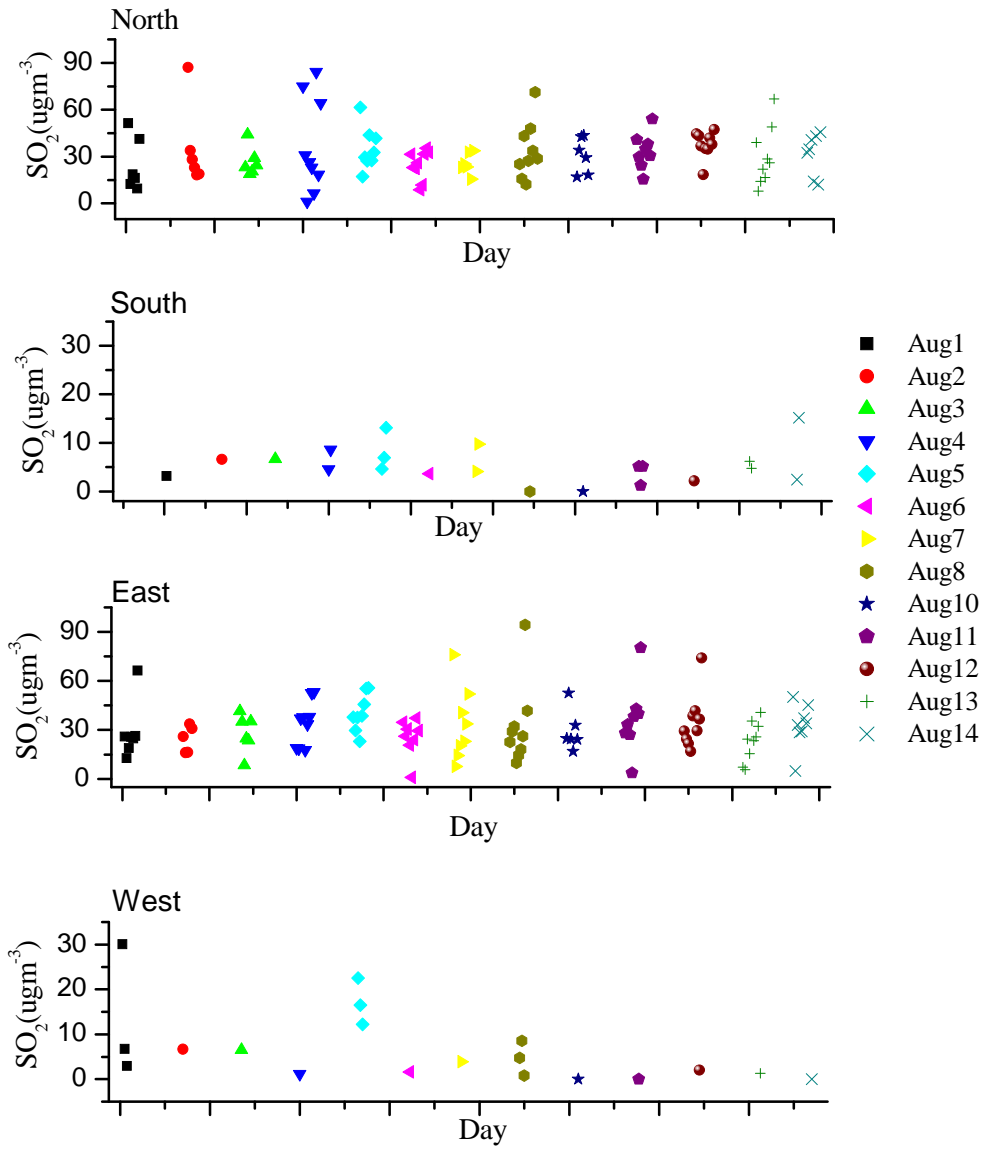


Figure 42: Graph showing concentrations of SO₂ monitored in the north, south, east and west from August 1 to 14, 2008.

O₃ concentration values in the north, south, east and west from 1st to 14th

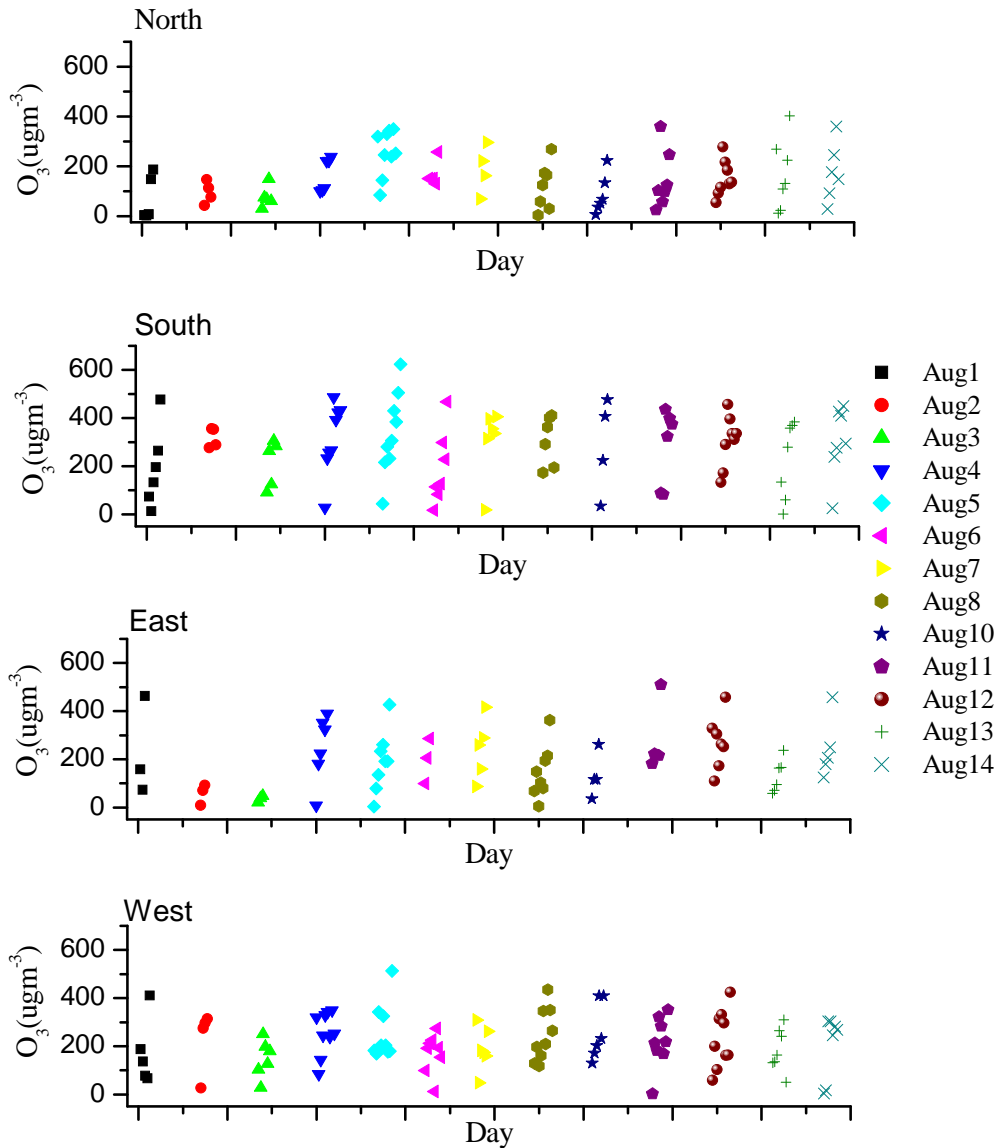


Figure 43: Graph showing concentrations of O₃ monitored in the north, south, east and west from August 1 to 14, 2008.